Ph.D. DISSERTATION

FET Gas Sensor Platform Having a Horizontal Floating Gate

수평형 Floating Gate를 갖는 FET 가스센서 플랫폼

BY

CHANG-HEE KIM

August 2015

DEPARTMENT OF ELECTRICAL ENGINEERING
AND COMPUTER SCIENCE
COLLEGE OF ENGINEERING
SEOUL NATIONAL UNIVERSITY

FET Gas Sensor Platform Having a Horizontal Floating Gate

수평형 Floating Gate를 갖는 FET 가스센서 플랫폼

指導敎授 李宗昊

이 論文을工學博士 學位論文으로 提出함

2015 년 8 월

서울大學校 大學院

電氣·컴퓨터 工學部

金 昶 憙

金昶憙의 工學博士 學位論文을 認准함

2015 년 8 월

委 員 長 : 박 영 준 (印)

副委員長 : 이 종 호 (印)

委 員 : 박 병 국 (印)

委 員 : 황 철 성 (印)

委 員 : 권 혁 인 (印)

Abstract

Today, there are numerous kinds of gases which are becoming widely used in the various industry fields. However, the harmful gases which a disease of the respiratory system are generated by industrial activity. Therefore, the demand for a gas sensor which can detect the noxious gases is expected to grow. Especially, there will be a growing interest in portable, low-cost, high reliability and low-power gas which can be applied to smart device in the future. Many kinds of gas sensors have been developed by many researcher until now: electrochemical, electrical, mass sensitive, magnetic, optical and thermometric type gas sensors. One gas sensor type of interest is that based on FET (Field Effect Transistor) has been considered as advanced gas sensor which can implant in various smart devices. However, there are many disadvantages in conventional FET type gas sensors.

In this thesis, we propose a gas sensor platform having a horizontal floating-gate (FG) to solve the problem shown in conventional FET gas sensor. We first introduce structure and fabrication process sequence of the gas sensor that we proposed. The gas sensor is based on MOSFET (Metal Oxide Semiconductor Field Effect Transistor) and have a horizontal FG and the sensing layer covers partly the control-gate (CG) formed horizontally and the passivation layer formed on the FG in the center. The gas sensor reads out work-function (WF) change in the sensing material

formed between FG and CG (control gate), when the device is exposed to a target gas. The sensing materials in our work are semi-metal or semiconductor. Next, we analysis gas sensing characteristics of the fabricated gas sensor by using various sensing materials and target gases, respectively. We measure transfer and transient curves of the device in target gases. From the measured data, we explain operating principle and show gas sensitivity, selectivity, response and recovery characteristic and Langmuir relationship of the gas sensor. We also show the various methods that various gas sensing materials are formed on the gas sensor and verify gas sensing characteristics of the device in which SnO_x (Tin Oxide), ZnO (Zinc oxide) and CNT (Carbon Nanotube) are used as a gas sensing materials by using sputtering, ALD (Atomic Layer Deposition) and ink-jet printing method. Then, we show sensor calibration of the gas sensor by CG bias. Finally, we fabricate FET gas sensor based on wide band gap material (Gallium nitride) which can operate at high temperature (T > 300 °C) and conform gas sensing characteristics of the gas sensor.

We think that the proposed gas sensor platform can be applied to various FET type device (ex TFT: Thin Film Transistor, TFET: Tunneling Field Effect Transistor) and useful in an electronic nose system.

Key Words: Gas sensor, MOSFET, horizontal, floating gate, platform, work-function, sensing material, sensing characteristic, sensor calibration

Student Number: 2012-30932

Contents

Chapter 1

Introduction

1.1 Gas sensor

Today, there are numerous kinds of chemical species, natural and artificial gases which are useful to human life. The various gases are becoming widely used in the following chemical, petrochemical, medical, manufacturing, electric power, agriculture fabrication industries. However, industrial processes to improve human life increasingly produces toxic and combustible gases causing fire, air pollution and a disease of the respiratory system. Therefore, there has been a growing interest in gas sensors to detect toxic and combustible gases. The Fig. 1(a) and (b) show gas sensor applications. The gas sensors are used for fire alarm and detector which determine the quality and freshness of food (ex pork, beef, chicken and fish) [1].

(a)

(b)

Fig.1-1. (a) Fire alarm and (b) portable electronic nose which can determine the quality and freshness of food (Peres) [1].

Recently, gas sensor technology has advanced remarkably for few decades and various gas sensors are commercially available thanks to researchers related to gas sensor. And there are a wide variety of gas sensors based on different gas sensing materials and operating on diverse gas sensing principles which can be used to gas detector. There are several types of gas sensors designed explained as shown in table 1-1 [2]. Table 1-1 show classification and operating principle of the gas sensors. And Fig. 1-2, 1-3 and 1-4 show electrochemical, electrical, mass sensitive, magnetic, optical and Thermometric type gas sensors [3]-[8].

Table 1.1 Classification and operating principle of gas sensors [2]

Class of gas sensors	Operating principle
Electrochemical	Changes in current, voltage, capacitance/impedance: : Voltammetry(including amperometry), Potentiometry : Potentiometry with solid electrolytes for gas sensing
Electrical	: Metal oxide, Organic, Electrolytic, Heterojunction (Schottky diode, FET, MOS) conductivity : Work function, Electric permittivity (capacitance)
Mass sensitive	Changes in the weight, amplitude, phase or frequency, size, shape, or position : Quartz crystal microbalance : Surface acoustic wave propagation, Cantilever
Magnetic	Changes of paramagnetic gas properties
Optical devices	Changes in light intensity, color, or emission spectra : Absorbance, Reflectance, Luminescence • Refractive index, Optothermal effect, Light scattering
Thermometric (calorimetric)	Heat effects of a specific chemical reaction. Changes in temperature, heat flow, heat content : Thermoelectric, Pyroelectric, Catalytic bead : Thermal conductivity

(a)

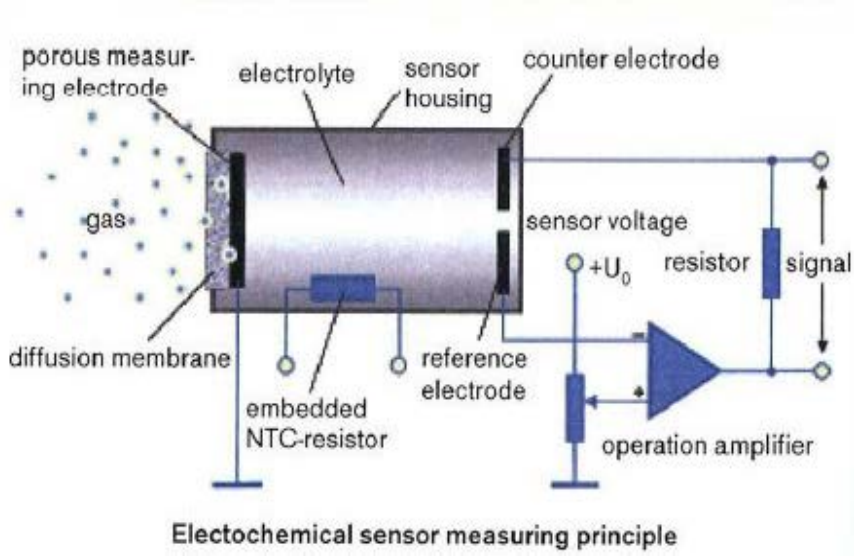

(b)

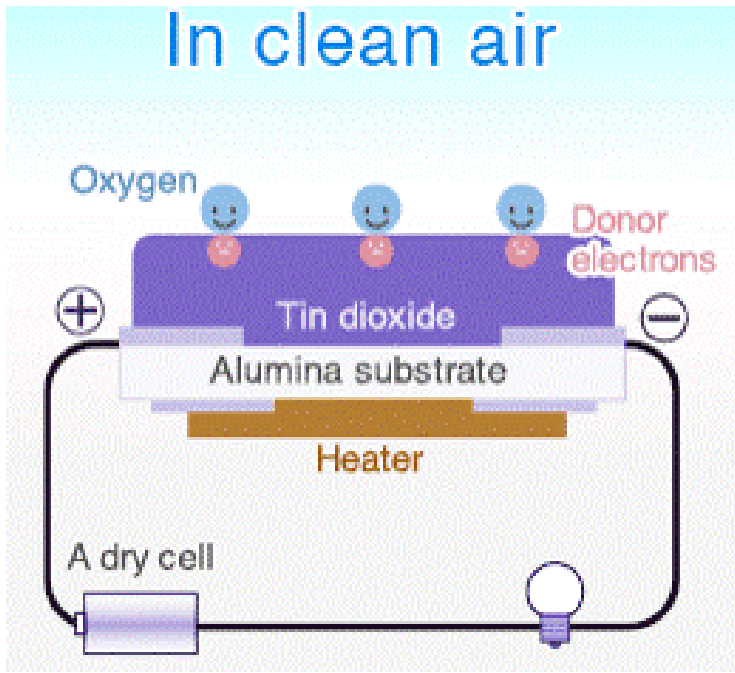

Fig.1-2. (a) electrochemical [3] and (b) electrical [4] type gas sensor (semiconductor gas sensor)

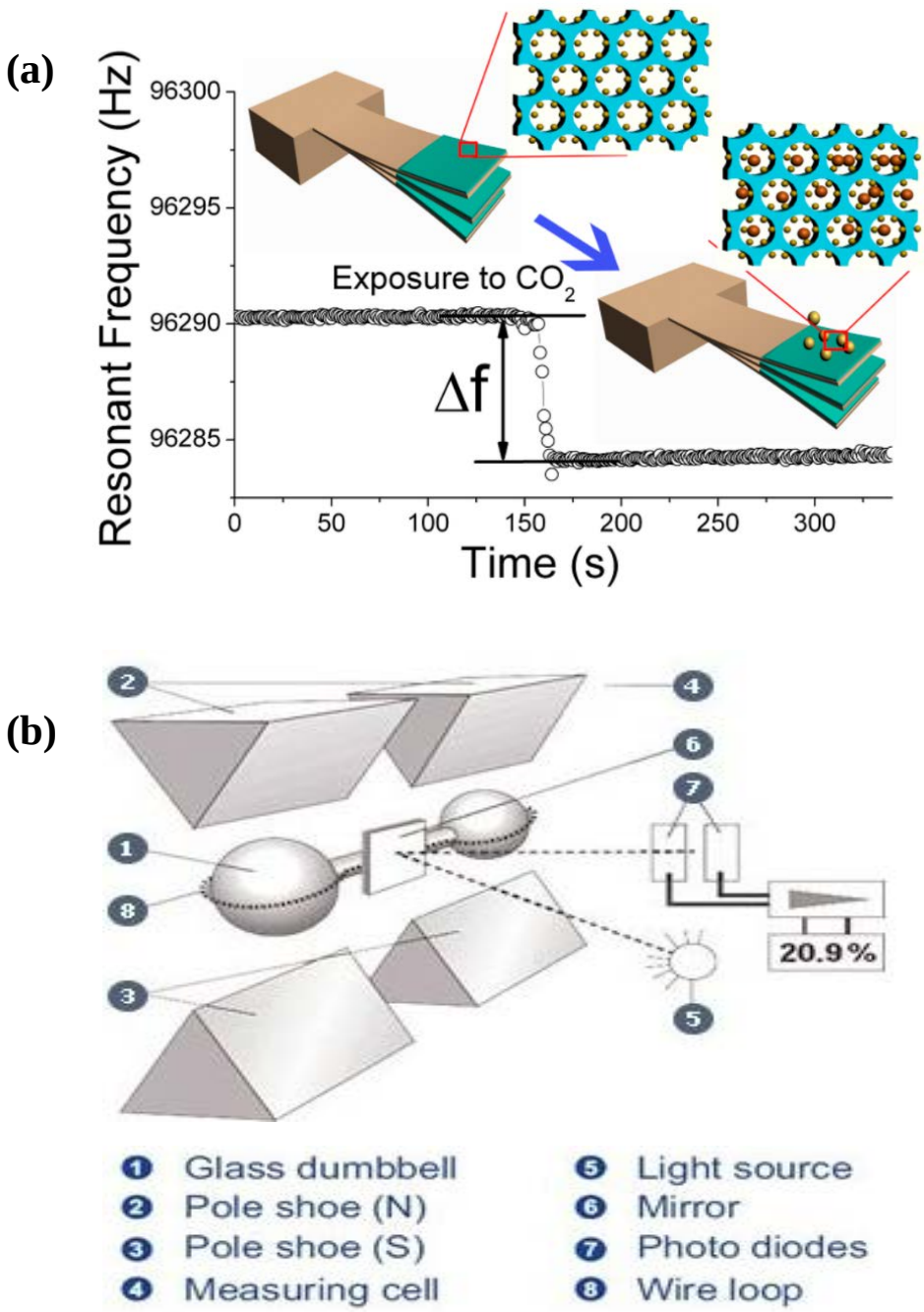

Fig.1-3. (a) mass sensitive [5] and (b) magnetic [6] type gas sensor.

(a)

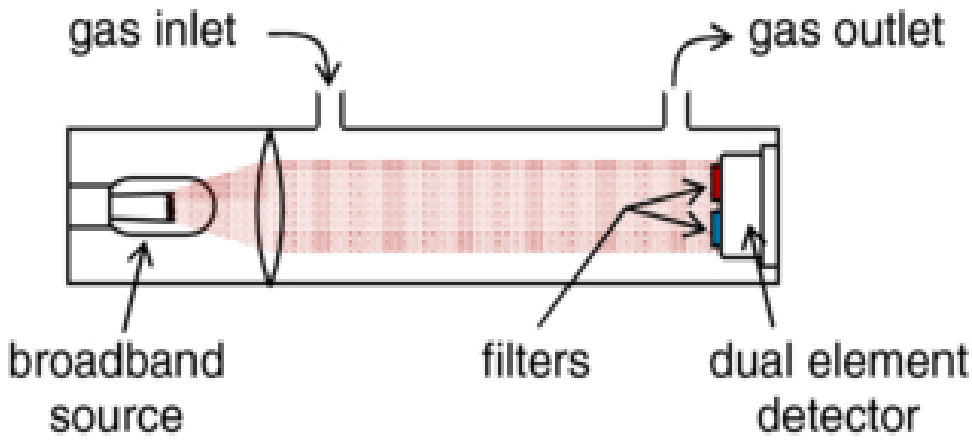

(b)

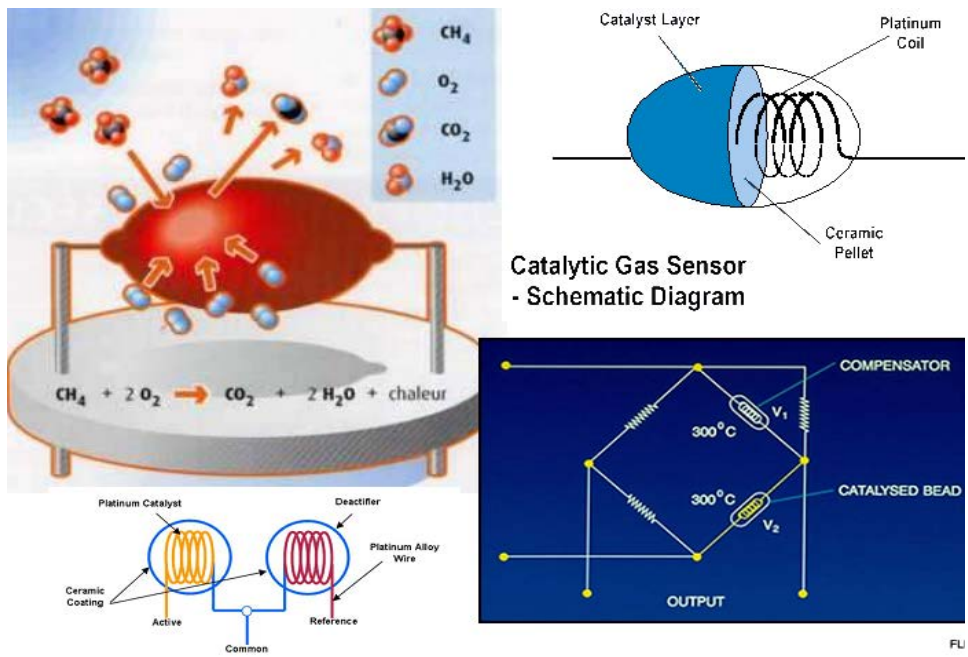

Fig.1-4. (a) optical [7] and (b) thermometric [8] type gas sensor.

1.2 FET gas sensor

Today there is an increasing need for low power, small size and low cost gas sensors for a wide range of industrial and gas sensor applications. Especially, it is required to develop gas sensor implanted into smartphone. The advantages and disadvantages of the conventional gas sensor are shown in Table 1-2 [9]. Electrochemical and optical type gas sensor are high selectivity, accuracy, low power gas sensor. However, the sensors is high cost and large size gas sensor. So, it is difficult to apply to smartphone. Owing to its unique structural, mechanical, a compatible with CMOS and electronic properties, FET (Field effect transistor) type gas sensor is considered as one of the most attractive candidates for next-generation gas sensor. The gas sensor has gas sensing gates able to provide work-function (WF) changes upon ambient atmosphere modifications. Due to their operation principle, the sensor is based on change in the channel conductance causing the change in drain current of the device by the gate potential modulation.

Table 1-2. Advantages and disadvantages of various gas sensors [9].

Major Categories of Gas Sensors				
Sensor type	**How it works**	**Example**	**Applications**	**Advantages/ disadvantages**
Conducto-metric gas sensors	Gas causes a change in the conductivity of a semiconductor	Metal oxide semi-conductor	Broad area of application for nearly all gases, e.g. blood-alcohol,	+ Robust, long life, versatile, miniaturizable - Low selectivity, high power consumption
	Gas causes a change in the conductivity of a polymer	Conductive polymers	volatile organic molecules, food testing, use in arrays as an "electronic nose"	+ Broad selectivity, high sensitivity, operation at ambi-ent temperature - Humidity inter-feres with the mea-surements, sensor could be "poisoned"
Ampero-metric gas sensors	Gas takes electrons from one electrode and passes them to the other. The current flow is a measure of the gas concentration	Electro-chemical cells	Applications: For example, monitoring the presence of toxic gases at the workplace, mea-surement of numer-ous inorganic and organic molecules	+ Versatile - Average level of selectivity, low life-span, sensitive to high humidity and extreme temperatures
Potentio-metric gas sensors	Electrical charge on an ion-conducting membrane	Lambda sensors	Measurement of oxygen content in vehicle exhaust or in metallurgical processes	+ Functions at high temperatures
Optical gas sensors	Gas absorbs light	Laser diode spectro-meter	Simple gases such as O_2, CO_2, CH_4, HCl, HF	+ Very precise, selective - Gases require sharp absorption lines in the near IR, unsuitable for complex molecules
	Gas alters the transmission of light through a polymer layer	Optode	Fire detector	+ Miniaturizable, low power consumption
FET gas sensors	Gas is adsorbed on the surface, a voltage is generated		Still under development	+ Inexpensive, par-tially miniaturizable, rapid reaction, sensitive, selective

The first FET type gas sensor detecting hydrogen (H_2) was developed by Lundström [10] as shown in Fig. 1-5. The FET gas sensor has a heated palladium gate as a sensing layer. The H_2 gas diffuses through the sensing layer to the interface between the gate oxide and the channel, which to work-function (WF) change in the gate. As a result, the channel conductance of the gas senor is modulated [11]. However, the FET gas sensor usually cannot detect large gas molecules due to the lack of electronic conductors having the required gas permeability [11].

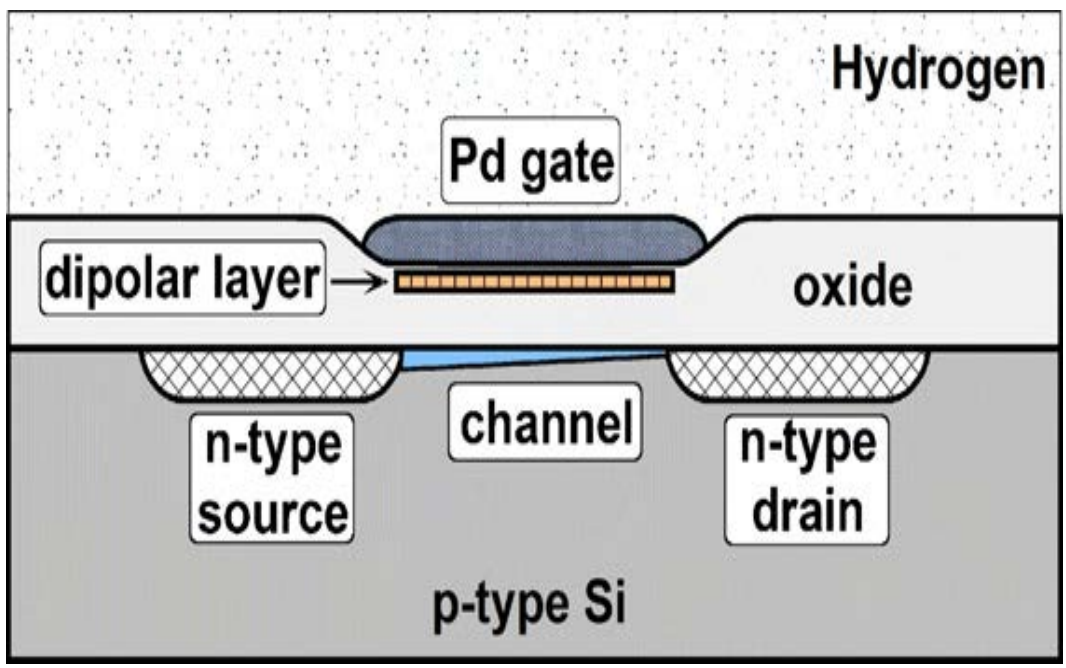

Fig.1-5. Schematic view of the Lundström hydrogen FET [10].

In order to solve this problem, a gas sensor based on suspended gate (SG) FET is developed [12] as shown in Fig. 1-6. In [12], the gate was coated with various gas sensing materials and separated from channel by forming an air gap between the gate and channel for eliminating gas diffusion process. But the target gas has still to diffuse through this air gap so that larger air gaps to improve response and recovery times of the sensor. As a result, the increase of the air gap lead to decrease of the trans-conductance of the FET gas sensor. The trans-conductance is related to sensitivity of the sensor

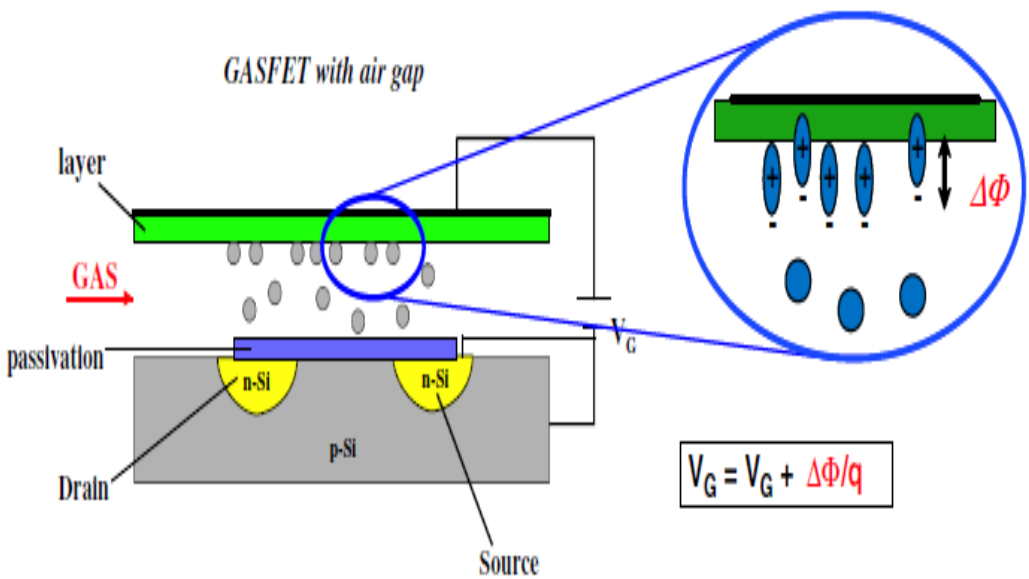

Fig.1-6. Schematic view of SG-FET gas sensor [12].

To improve of performance of the suspended gate FET gas sensor capacitive (charge) coupled FET (CC-FET) type gas sensor was developed [13] as shown in Fig 1-7. A floating gate is formed over the channel in CC-FET. This device can improve the controllability of the suspended gate. As a result, CC-FET gas sensor had higher gas sensitivity than [13]. This design also ensures a better protection of the FET gas sensor against corrosive gases.

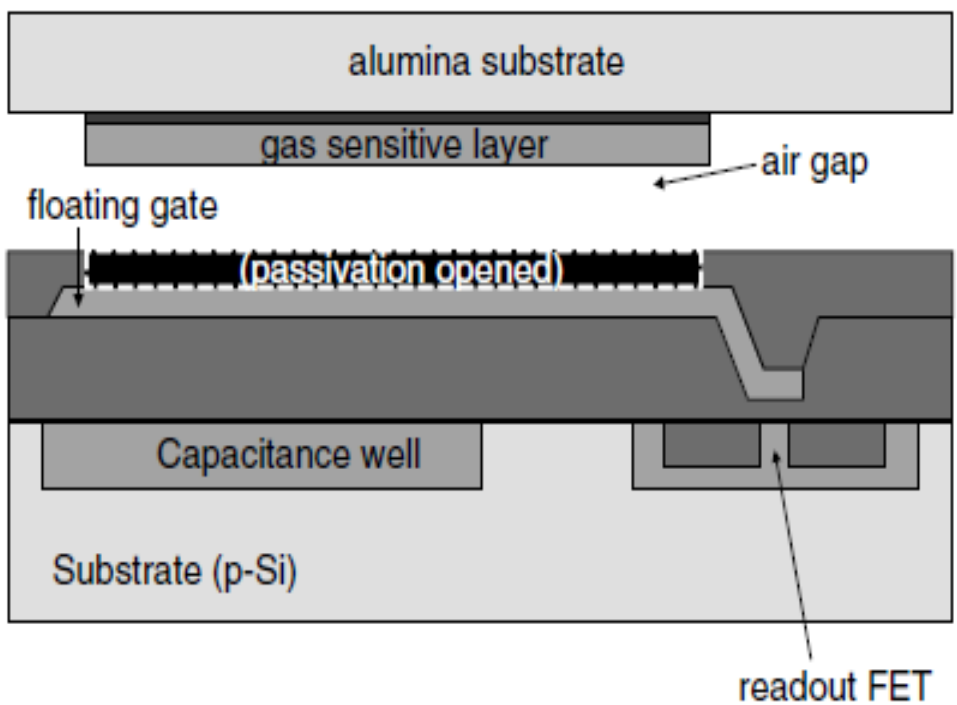

Fig.1-7. Schematic view of CC-FET gas sensor [13].

1.3 Work function change of sensing materials

Conventional FET gas sensor is based on work-function (WF) change of the gas sensing layer as act on gate of the FET device. An amount of the WF change of the sensing layer is measured by Kelvin method which measure surface potential of a thin film [14]. Fig. 1-8 shows schematic view of the scanning Kelvin probe system (Model: SKP 5050) [15], [16].

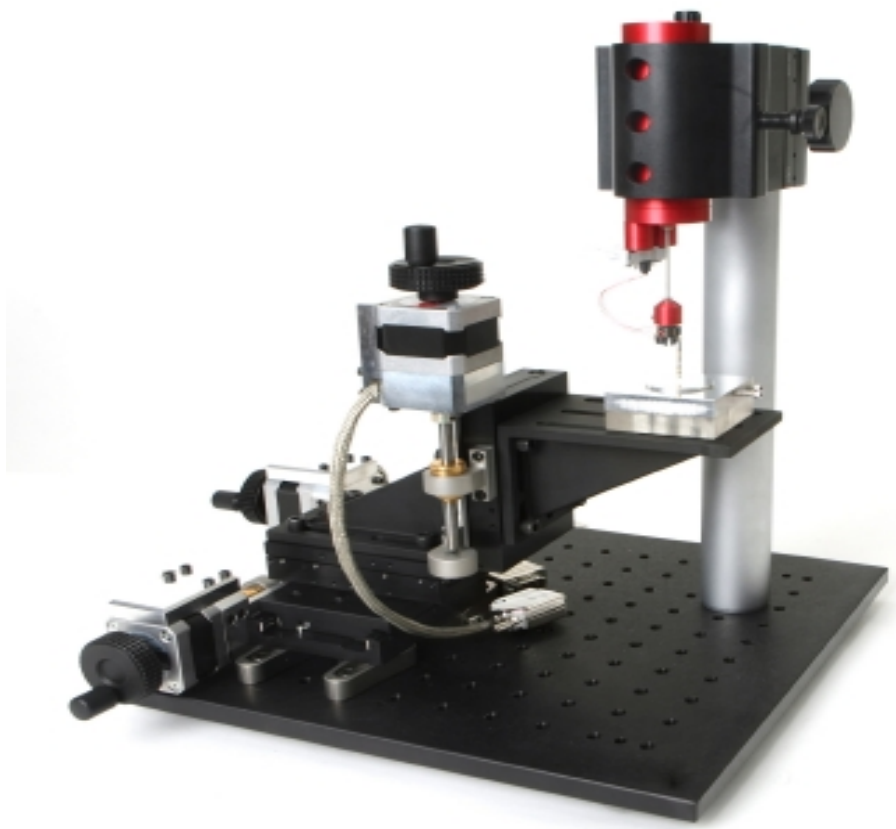

Fig. 1-8. Schematic view of the scanning Kelvin probe system [16]

The detection mechanism of change in WF of the sensing layer based on semiconductor is still controversial. Commonly it is assumed that the target gases are chemisorbed on the sensing layer surface. Fig. 1-9 (n-type semiconductor) and 1-10 (p-type semiconductor) show gas sensing mechanism of the work function change of the sensing layer. As shown in the figures (Fig. 1-9 and 1-10), target gases extract charge (electrons or holes) from the conductance (electrons) or valence (holes) band and trap them on the surface in form of ions having positive or negative charge. It causes a band bending in the sensing layer and traps the electrons (or holes) at the surface of the sensing layer in the form of ions. The trapping of the charges will be continued until a thermodynamic equilibrium is achieved. As a result of the transfer of charge, dipole layers are formed on the surface of the sensing layer causing potential difference across the surface. This potential difference lead to change in WF of the sensing layer. The surface dipole determines the amount of work-function shift [11], [15].

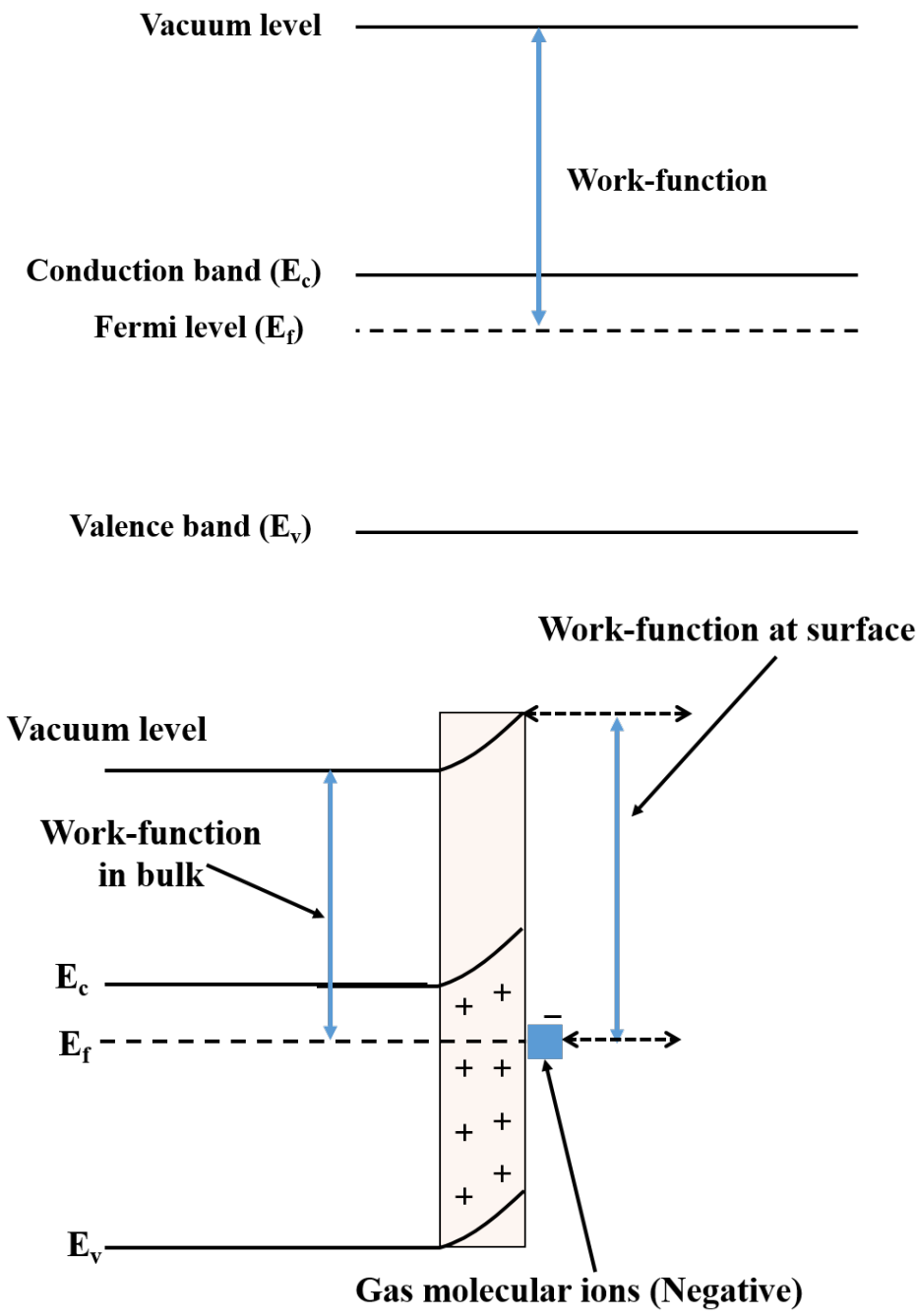

Fig. 1-9. Gas sensing mechanism of the work function change of the sensing layer (n-type semiconductor).

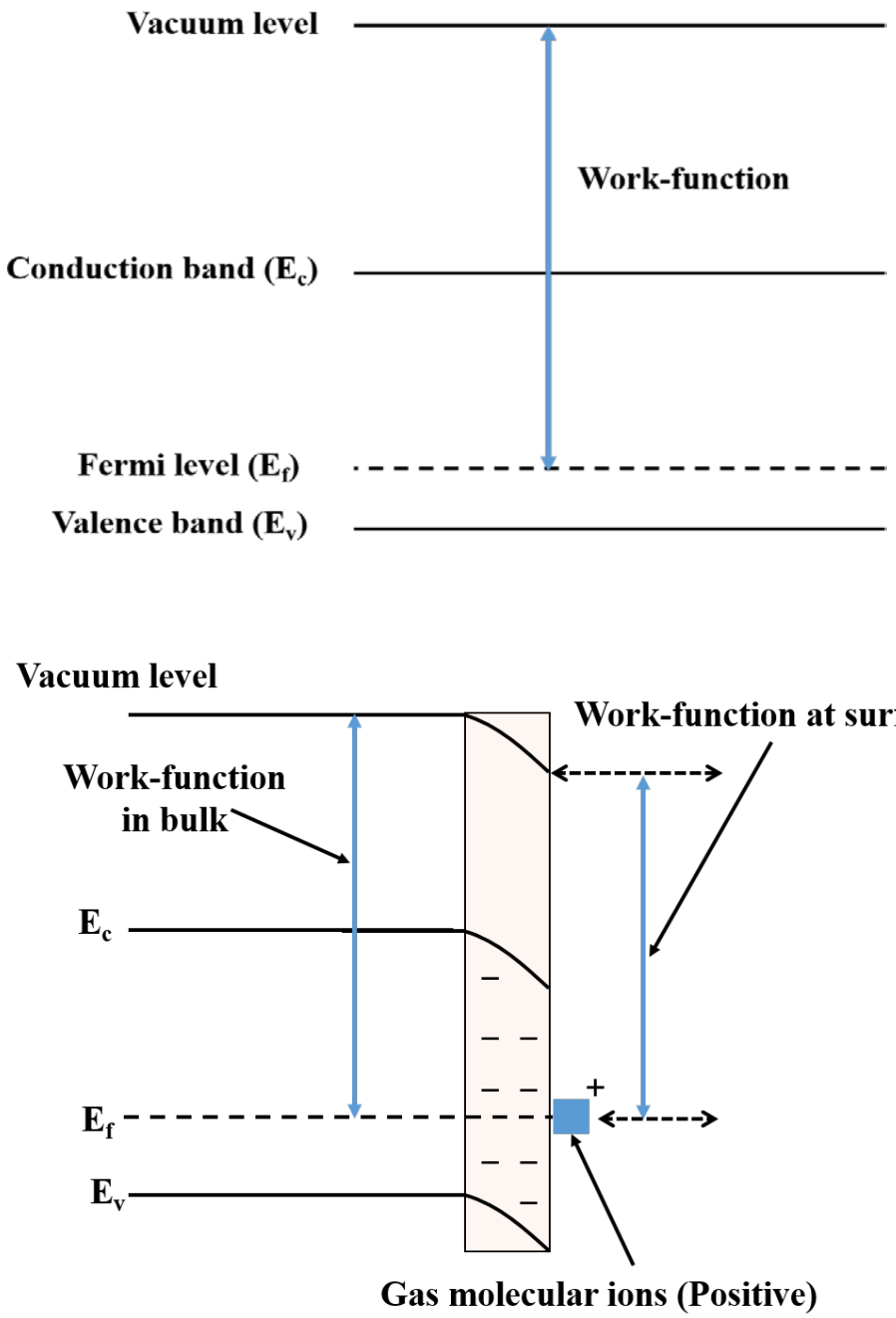

Fig. 1-10. Gas sensing mechanism of the work function change of the sensing layer (p-type semiconductor).

Chapter 2

MOSFET gas sensor having a horizontal floating gate

2.1 Introduction

Recently, there has been a growing interest in gas sensors to detect air contaminants causing smog and lung diseases such as asthma [17]. One gas sensor type of interest is that based on Si MOSFET has been considered as low cost and portable gas sensor. Various MOSFET gas sensors are developed [10], [12] and [13]. However, there are many disadvantage of the conventional gas sensors: low gas sensitivity, complex fabrication process and device size. Thus, it becomes increasingly important to develop high sensitivity and low cost the FET type gas sensor detecting various gases. In this letter, we propose a new gas sensor based on MOSFET having a horizontal floating-gate (FG) [18]. First, we introduce structure and key fabrication process steps of the gas sensor. Then we confirm gas sensing characteristics of the device by using tin oxide (SnO_x) as a sensing layer and target gases, respectively.

2.2 Device structure and fabrication

Fig. 2-1 (a) and (b) show the SEM image and 2D cross sectional views of the fabricated gas sensor having a horizontal floating gate (FG), respectively. In the gas senor, materials of the FG, metal, sensing layer and passivation layer are used to highly doped poly silicon, titanium/nickel, tin oxide (SnO_x) and silicon nitride on silicon substrate respectively. In Fig. 1 (a), source and drain are formed on the left and right, respectively. In Fig. 1 (b), the SnO_x covers partly the control-gate (CG) formed horizontally and the passivation layer formed on the FG in the center. The gas sensor reads out work-function (WF) change in the sensing layer butted to the CG, when the device is exposed to a target gas. The SnO_x in our work is an n-type semiconductor.

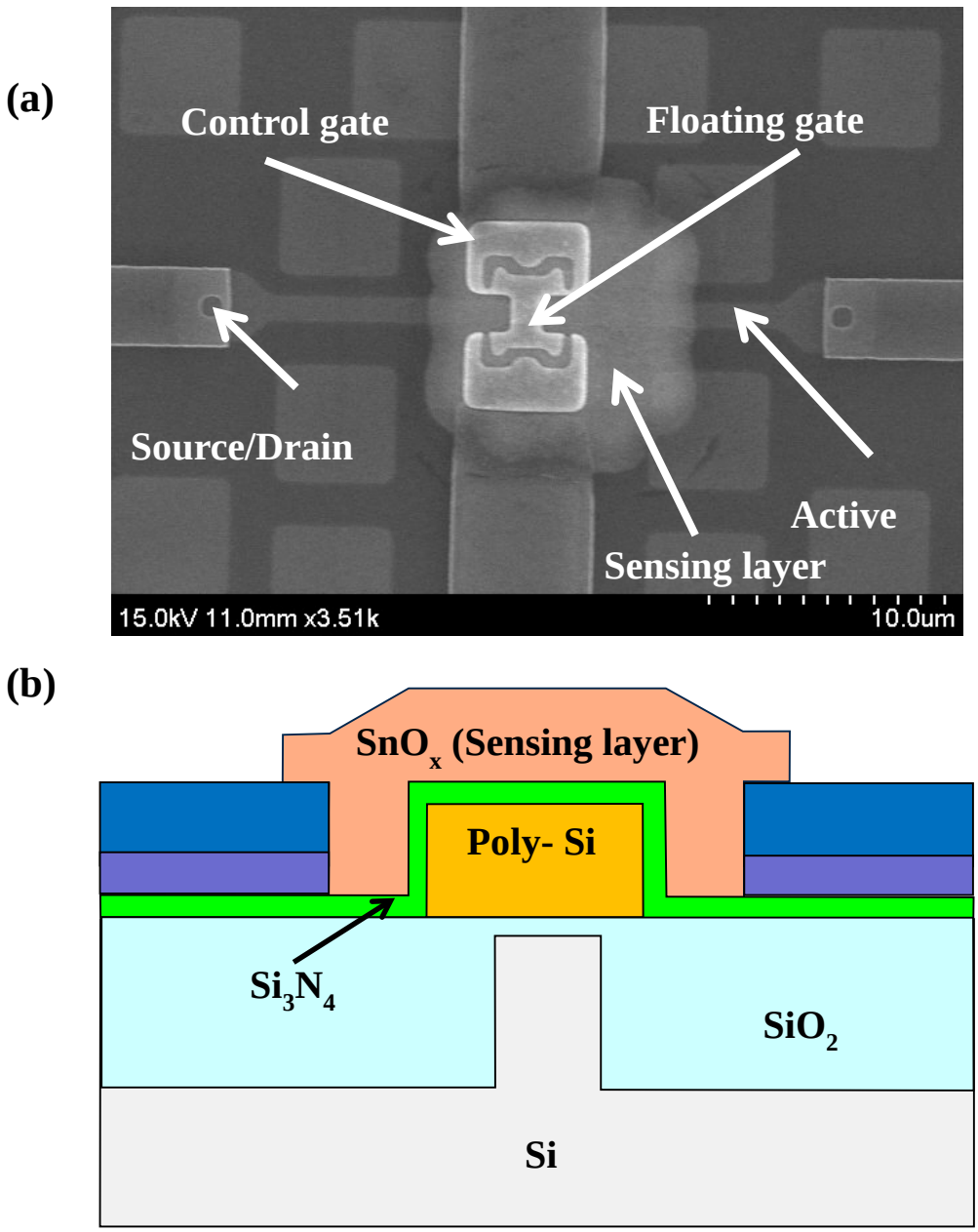

Fig.2-1. (a) SEM image and (b) 2D cross-sectional view of the gas sensor cut along A–A'.

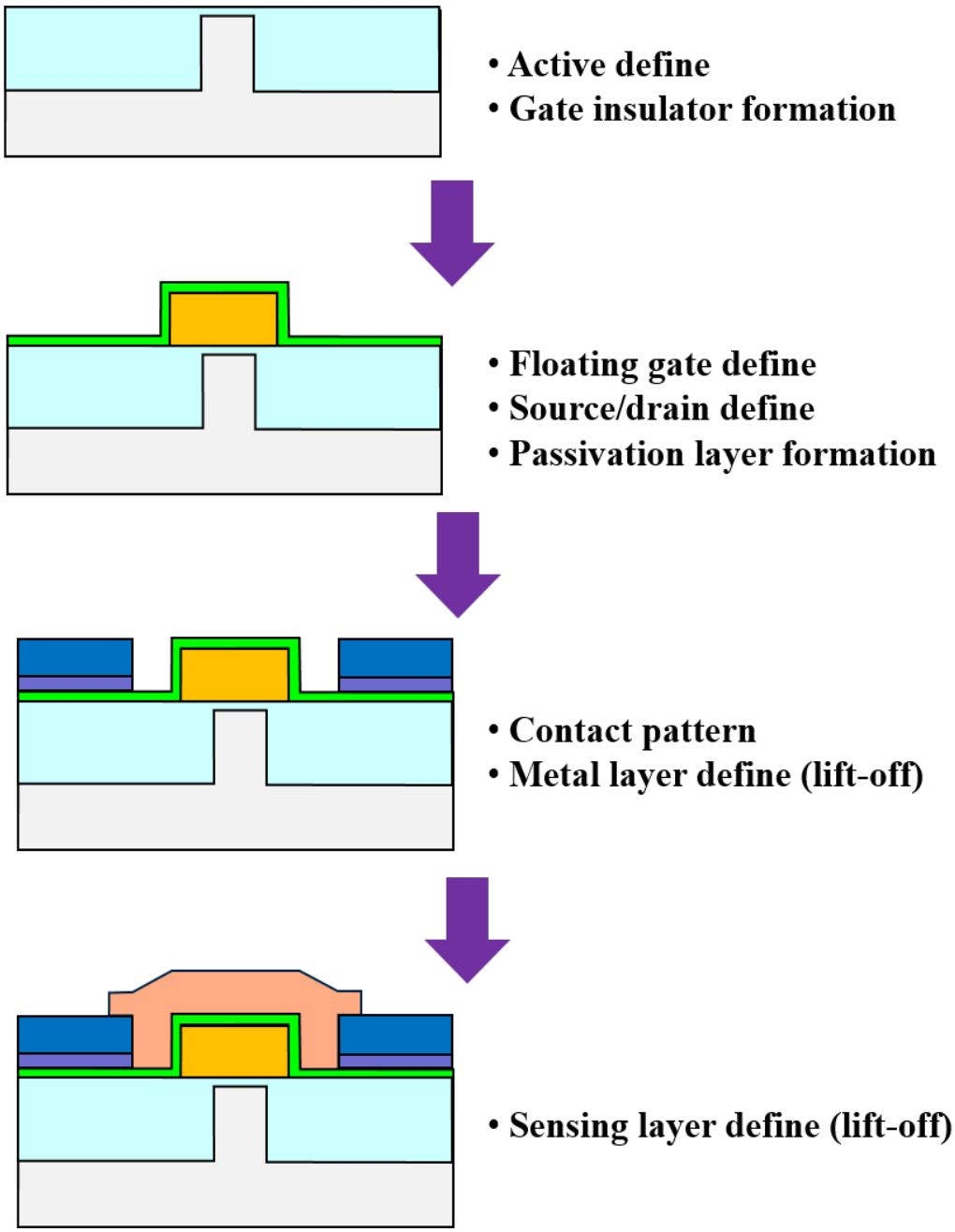

Fig.2-2. Fabrication process flow and steps of the fabricated gas sensor.

Key fabrication process flow and steps of the fabricated gas sensor are shown in Fig 2-2 and explained as follows. STI (Shallow Trench Isolation) technique is used for device isolation. A Silicon dioxide (SiO_2) and Silicon nitride (Si_3N_4) layers are grown and deposited by thermal oxidation and low pressure chemical vapor deposition (LPCVD) on 150 mm Si wafer. These layers are act as a stop layer of chemical mechanical polishing (CMP) and the thickness of the layers 10 nm and 100 nm, respectively. After photolithography process for active patterns, the stop layer and underlying Si are etched by dry etching process as shown in Fig. 2-3.

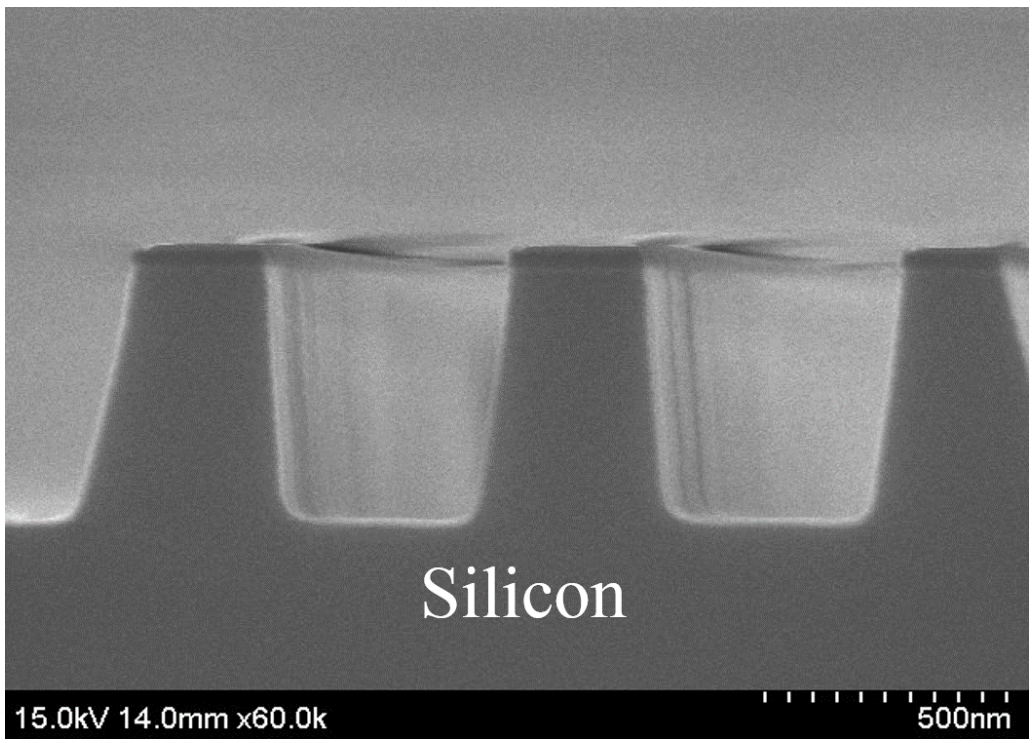

Fig. 2-3. Cross-sectional SEM image of the silicon trench formation

.

The isolation oxide is formed by high density plasma chemical vapor deposition (HDPCVD) and followed by CMP until the Si_3N_4 layer is exposed as shown in Fig. 2-4. The Si_3N_4 and SiO_2 layers are removed in a phosphoric acid solution at 160 °C and HF.

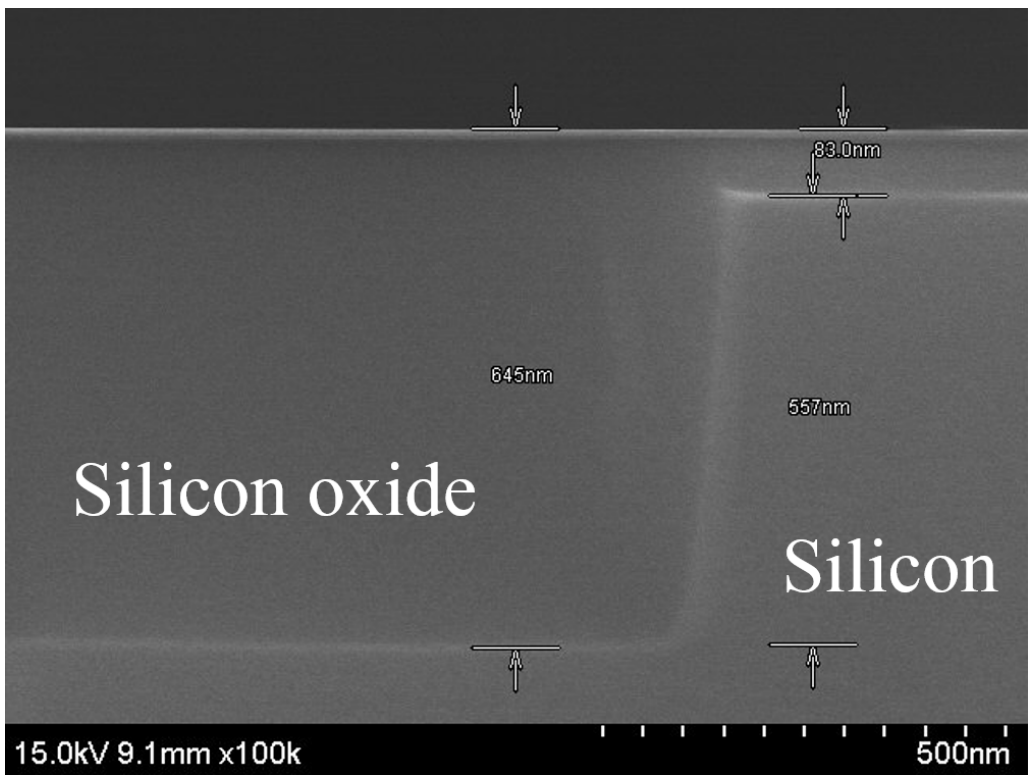

Fig. 2-4. Cross-sectional SEM image of STI structure with CMP process.

Thermal oxidation with the thickness of 10 nm is carried out. Then an in-situ phosphorous doped poly-Si layer is deposited to form the FG. The poly-Si is patterned by photolithography and dry etching process as shown in Fig. 2-5.

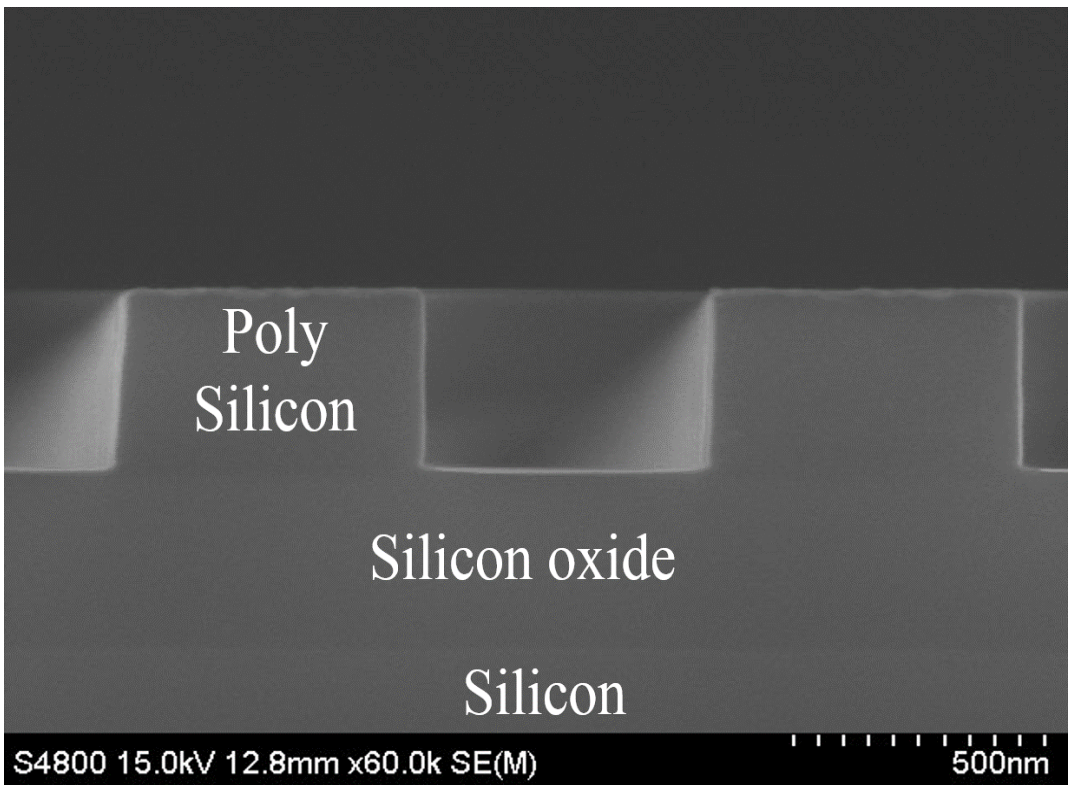

Fig.2-5. Cross-sectional SEM image of floating gate patterning with dry etch process.

After ion implantation and annealing process are performed to form source and drain regions, a 50 nm thick Si_3N_4 layer is deposited to be used for a passivation layer. Then, photolithography process for contact patterns are etched by dry etching process. Then, the CG (Ni/Ti) and sensing layer (SnO_x) are formed by e-beam evaporation and sputtering processes, respectively. They are patterned by lift-off process. Thicknesses of Ni, Ti and SnO_x are 180 nm, 20 nm and 200 nm, respectively. Because the sensing layer is formed in final process step, various gas sensing layers can be formed by various methods. This means that the proposed gas sensor can detect various gases.

2.3 Electrical characteristic

Fig. 2-6 (a) shows transfer curve of fabricated gas sensor based on p-type MOSFET at 25 ^{o}C. We adopted p-type MOSFET because it gives less 1/f noise than n-type MOSFET [19]. Both of the channel length and width of the gas sensor are 1 μm, respectively. Fig. 2-6 (b) shows the equivalent circuit diagram of the gas sensor. Sensitivity of the device depends on coupling ratio (γ) between the CG and FG [20]. The γ is defined as

$$\gamma = \frac{(C_s // C_{pass})}{(C_s // C_{pass}) + C_p + C_{fg}} \quad (1)$$

where C_s and C_{pass} represent the capacitances for the sensing layer and the passivation layer, respectively. C_p and C_{fg} are a parasitic capacitance between the FG and Si substrate, and the FG capacitance considering the gate oxide and Si capacitance, respectively. Here, the capacitances between the FG and source and drain are neglected. To obtain high sensitivity, the γ needs to be close to 1, which means $C_s//C_{pass}$ has to be larger than C_p+C_{fg}. Because the CG and FG has interdigitated pattern (for example, two fingers of FG in Fig. 2-1 (a)), the γ in this work is higher than in conventional gas sensor having air gap between the CG and FG [11].

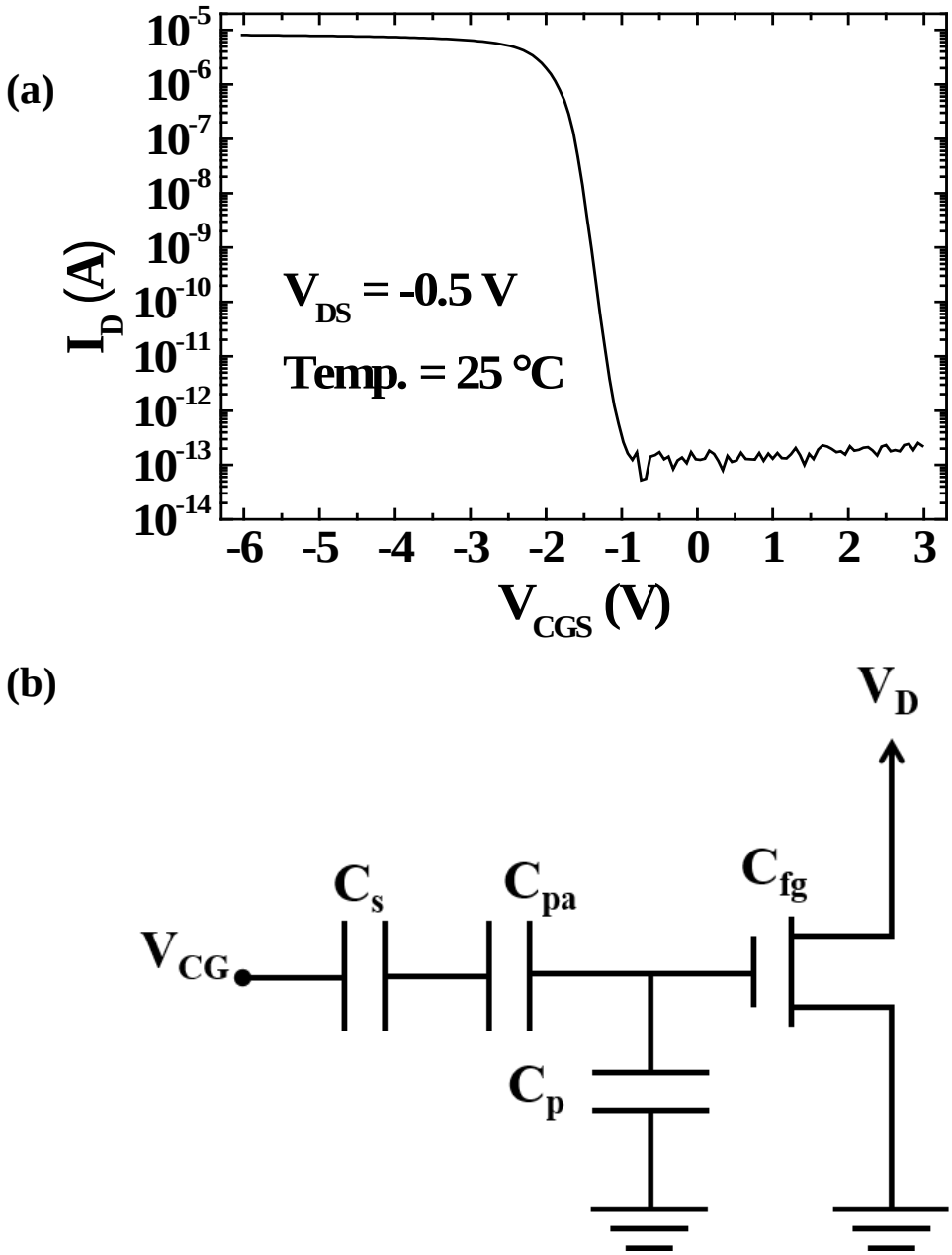

Fig.2-6. (a) Transfer (I_D-V_{CGS}) curve at 25 °C and (b) equivalent circuit diagram of the fabricated gas sensor.

Chapter 3

Gas sensing characteristic

3.1 Gas sensor measurement system

To measure gas sensing characteristics of the fabricated gas sensor, we use gas sensor measurement system as shown in Fig. 3-1, 3-2, 3-3 (a) and (b). The system is consist of hood, mass flow controller (MFC), gas cabinet, vacuum chamber probe station, hot chuck, gas calibrator, and electrical instrument. The fabricated gas sensor is placed inside the sealed vacuum chamber where gas supply and pump lines are available by MFC. Electrical measurements are carried out using a Keithley 4200-SCS. Calibrated commercial gas intermixing with nitrogen is used to check the response of a target gases (NO_2, H_2S...). The target gas concentration is controlled with a MFC.

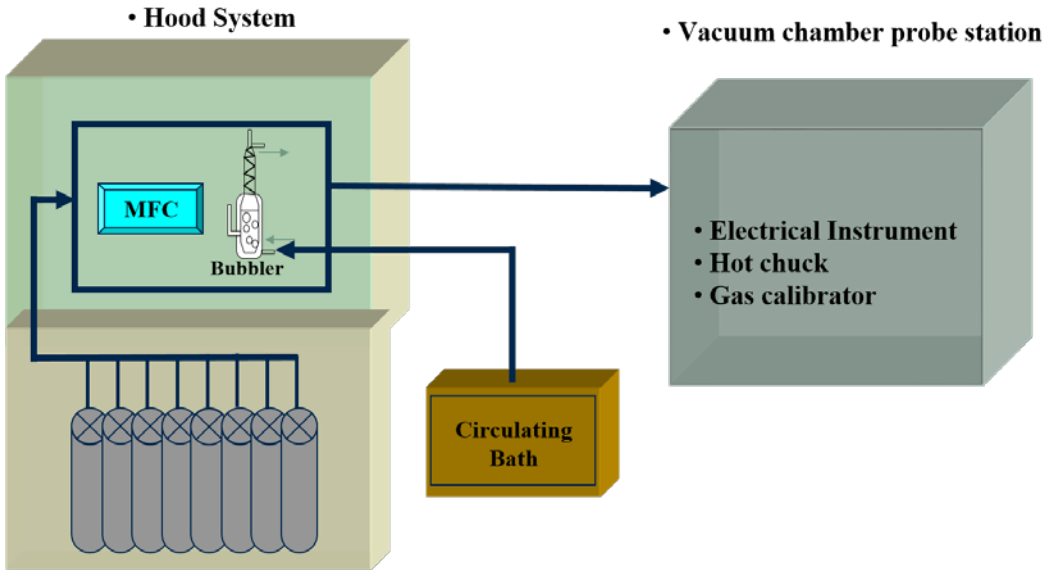

Fig.3-1. Schematic view of gas sensor measurement system.

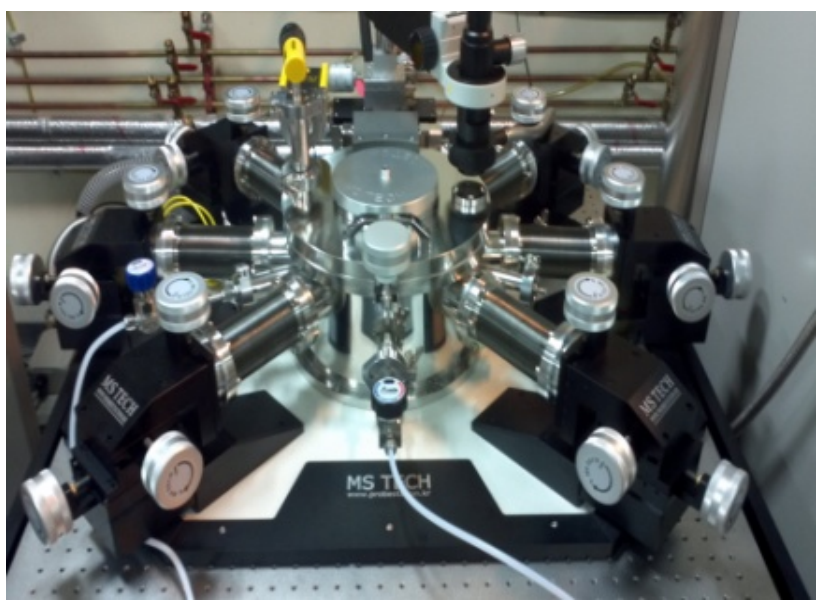

Fig.3-2. View of vacuum chamber probe station.

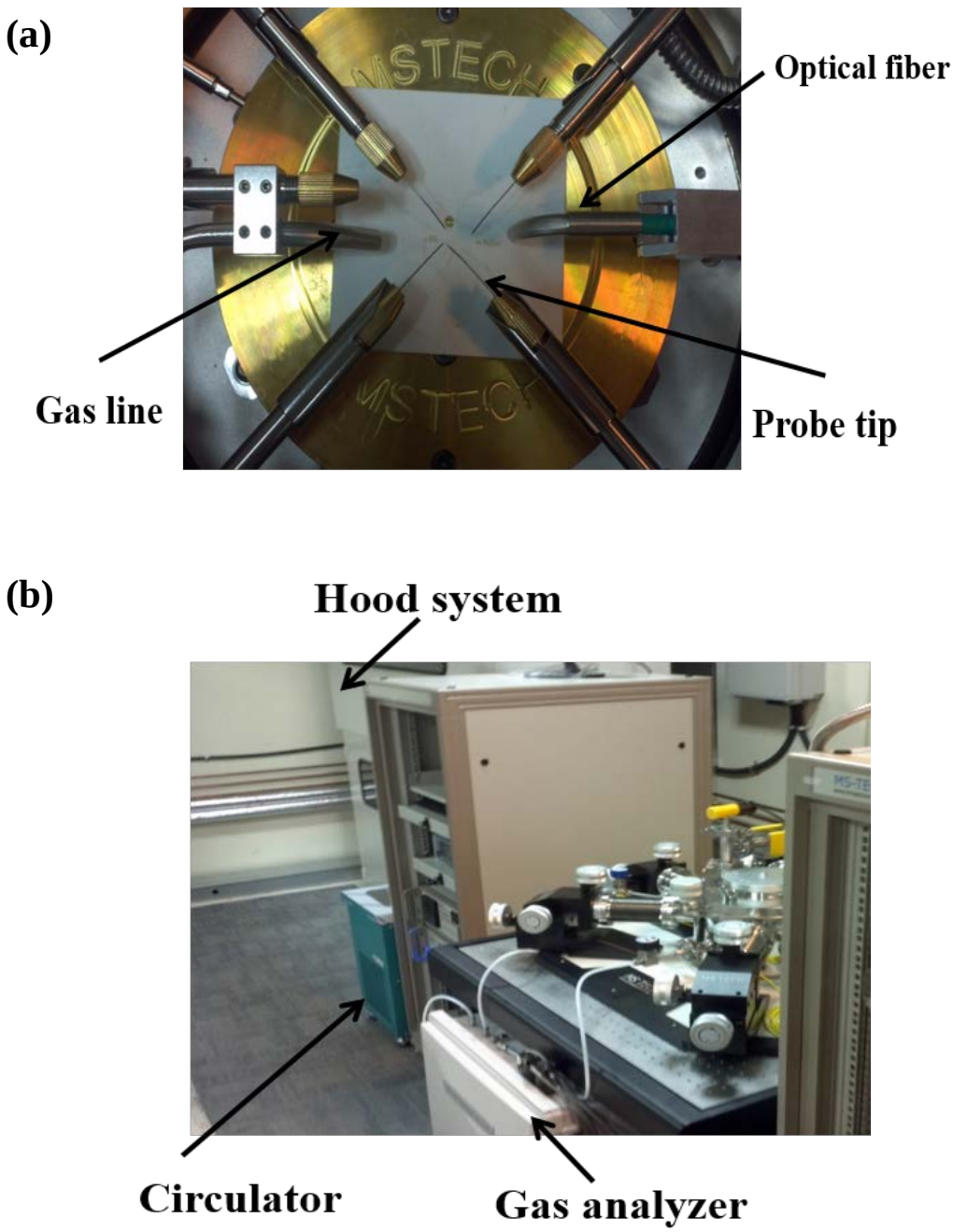

Fig.3-3. View of (a) The inside of vacuum chamber probe station and (b) hood system, circulator and gas calibrator.

Transfer (drain current–control gate voltage) characteristic of the gas sensor is obtained at one atmospheric pressure after exposing the device to a target gas for 30 min (saturation state) in the chamber. Here, the measurement is performed at 180 ^{o}C which is the working temperature for sensing layer (SnO_x) in target gases [21]. As a control drain current (I_D)-control gate voltage (V_{CGS}) curve, I_D-V_{CGS} curve in air is measured. Then threshold voltage change (ΔV_{th}) and drain current change (ΔI_D) with target gases concentrations are measured. The ΔV_{th} and ΔI_D are defined as

$$\Delta V_{th} = V_{CGS} - V_{CGS0} \quad (2)$$

$$\Delta I_D = |[(I_D/I_{D0}) - 1]| \times 100\ (\%) \quad (3)$$

where V_{CGS} in (2) and I_D in (3) are a gate voltage at I_D = 0.56 μA and drain current at V_{CGS} = -1.2 V, respectively, with different target gas concentrations (1 - 50 ppm). The V_{CGS0} in (2) and I_{D0} in (3) are the V_{CGS} (at I_D = 0.56 μA) and I_D (at V_{CGS} = -1.2 V) in air.

3.2 Results and discussion

Fig. 3-4 show transfer curves of the fabricated gas sensor as a parameter of NO_2 concentration. In this measurement, the I_D is changed with different NO_2 concentrations (0–50 ppm). As the NO_2 concentration increases, the I_D increases. To explain the phenomena, the I_D in linear (4) and sub-threshold (5) regions of the gas sensor are obtained by modifying I_D of conventional MOSFET. The I_Ds are written by [22], [23].

$$I_D = -\mu C_{fg}\frac{W}{L}\left(|\gamma V_{GS} - V_{th}| + \frac{m}{2}V_{DS}\right)V_{DS} \qquad (4)$$

$$I_D = \mu C_{fg}\frac{W}{L}\sqrt{\frac{\epsilon_{si} q N_d}{4\psi_B}}\left(\frac{kT}{q}\right)e^{-q(|\gamma V_{GS} - V_{th}|)/mkT} \qquad (5)$$

where N_d, ψ_B, and m represent the donor concentration in the channel, Fermi potential, and body effect coefficient. In (5), it is assumed that $e^{qV_{DS}/kT}$ is close to 0.

When the gas sensor is exposed to NO_2 gas, the gas diffuses through the sensing layer to its interface with the passivation layer [11]. The NO_2 at the interface increases WF and decreases the C_s of the SnO_x due to the formation of depletion layer by transferring charges between the NO_2 and SnO_x as shown in Fig. 3-5 [11], [24]. The increased WF shifts V_{th} into the positive bias direction [22], [25]. Finally, the I_D depends on the value of $|\gamma V_{GS}-V_{th}|$. As shown in Fig. 3-4, $|V_{th}|$ is decreased more significantly than $|\gamma V_{GS}|$ with increasing NO_2 concentration, resulting in the increase of I_D.

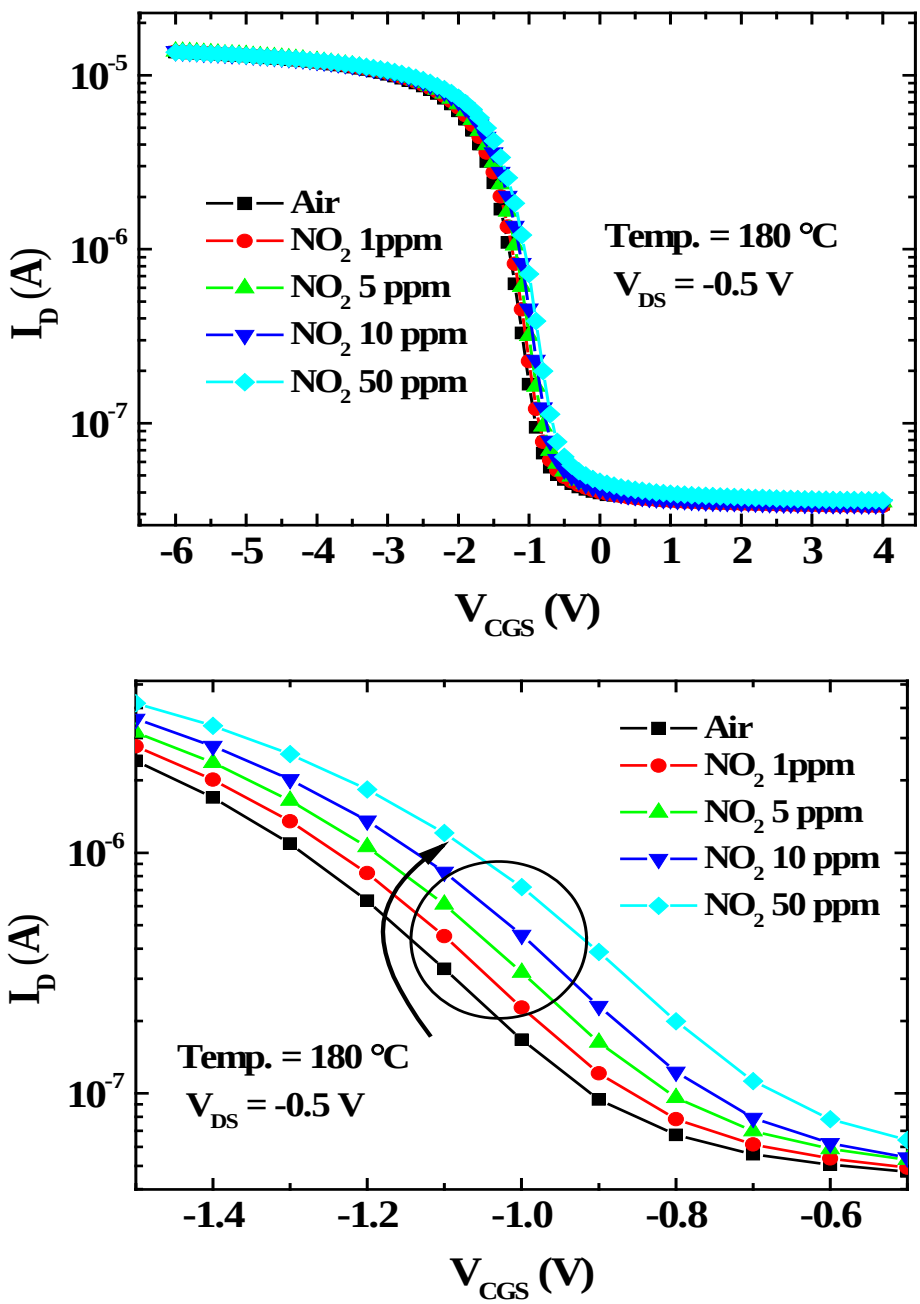

Fig.3-4. Transfer (I_D-V_{CGS}) curves for the fabricated gas sensor exposed to different NO_2 concentrations.

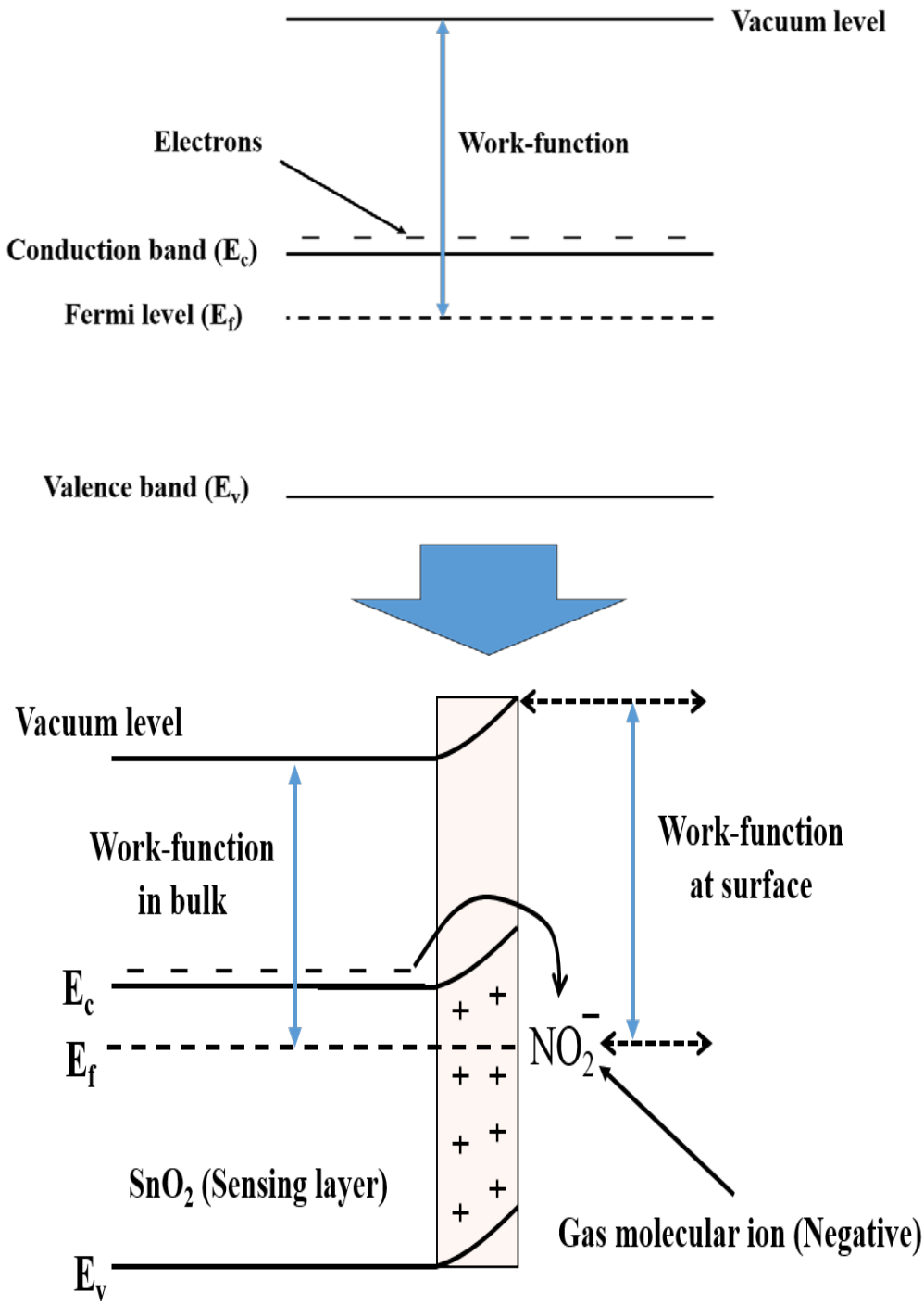

Fig.3-5. Gas reaction change between a target gas (NO_2) and sensing layer (SnO_x).

As shown in Fig. 3-6, ΔV_{th} and ΔI_D are increased with increasing NO_2 concentrations. They show about 0.24 V of ΔV_{th} and 195 % of ΔI_D by increasing NO_2 concentration to 50 ppm.

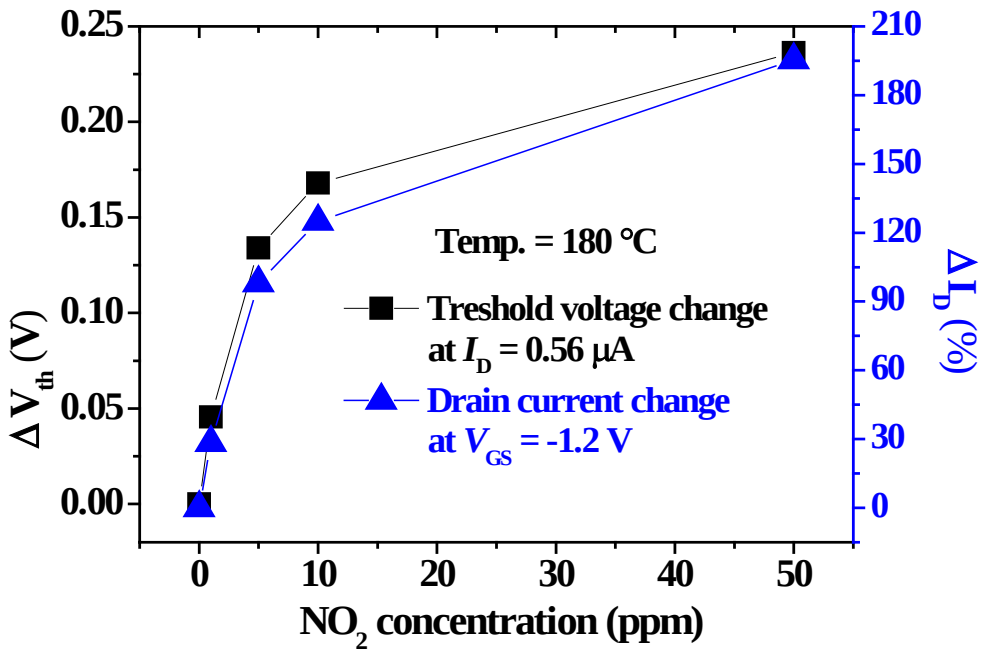

Fig.3-6. Threshold voltage and drain current change for the fabricated gas sensor exposed to different NO_2 concentrations.

We investigate the Langmuir isotherm in the fabricated gas sensor for target gas [26], [27]. Fig. 3-7 shows relationship between gas concentration and the threshold voltage change of the gas sensor [26], [28]. The $|\Delta V_{th}|$ is defined as

$$|\Delta V_{th}| = \Delta V_{max} \frac{\alpha C}{1 + \alpha C} \qquad (6)$$

where C is target gas concentration and ΔV_{max} and α are empirical parameters. As shown in Fig. 3-7, the ΔV_{max} and α are 0.26 V and 0.18 ppm^{-1} in the gas sensor where the target gas and sensing layer are NO_2 and SnO_x, respectively.

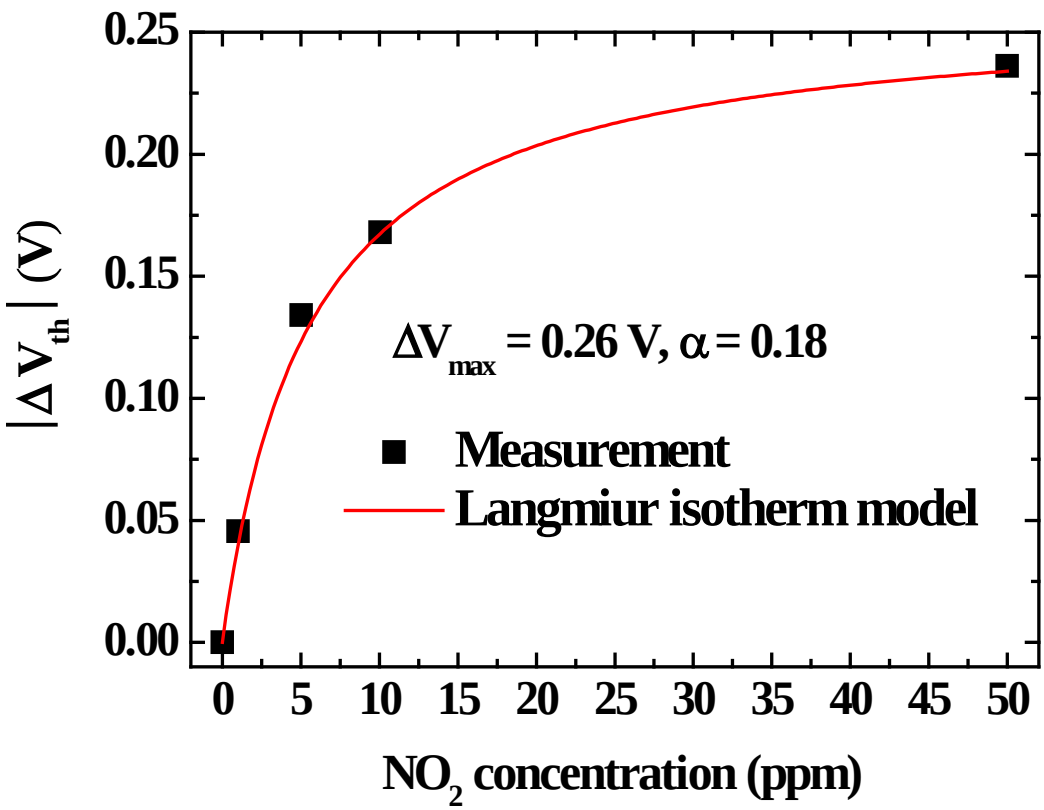

Fig. 3-7. The Langmuir relationship of the gas sensor by using SnO_x as a sensing layer at NO_2 (ΔV_{max} = 0.26 V and α = 0.18 ppm^{-1})

Fig. 3-8 shows transient response of the fabricated gas sensor by changing chamber ambient (air and 50 ppm NO_2) at 180 ^oC. The applied V_{CGS} and V_{DS} are fixed at -1.2 V and -0.5 V, respectively. We define sensing and recovery times which are specified in terms of the time to reach 90 percent (T_{90}) of its final reading from initial reading when the ambient is changed (air or NO_2). The reference drain currents in the air and NO_2 ambient are 0.56 μA and 1.80 μA, respectively. The sensing (air => NO_2) and recovery (NO_2 => air) times are about 50s and 300 s, respectively.

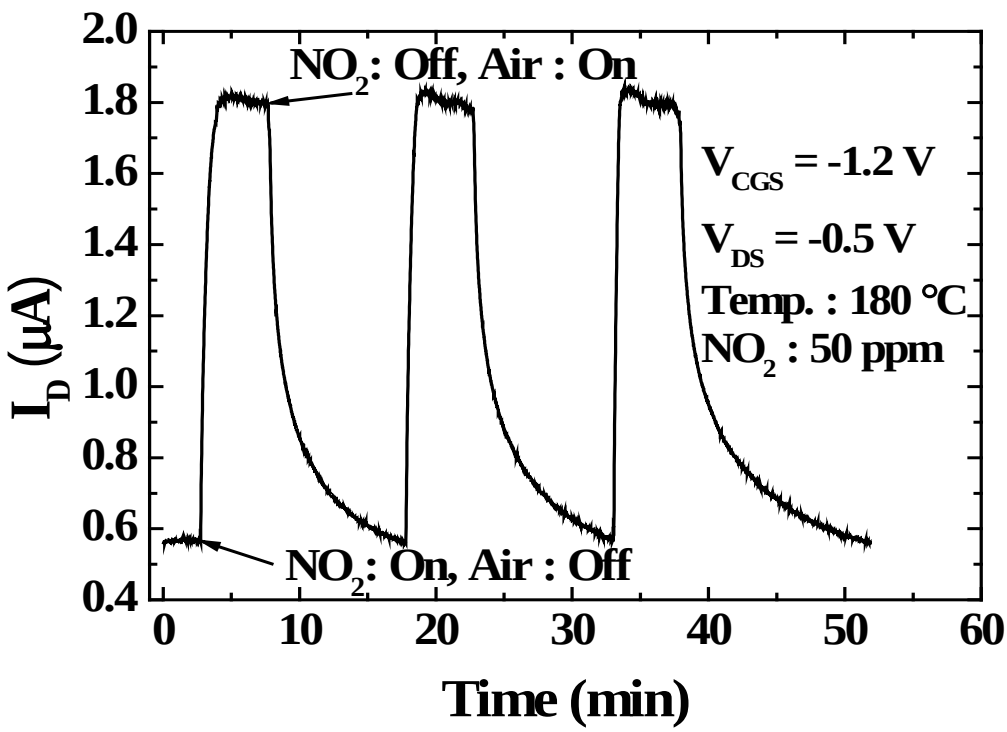

Fig. 3-8. Transient response of the fabricated gas senor in alternate ambient of NO_2 and air.

We also investigate gas sensitivity of the gas sensor for H_2S. Fig. 3-9 shows transfer curve for the gas sensor as a parameter of H_2S concentration. As a concentration of the gases increases, the drain current of the gas sensor decreases in H_2S. The transfer curve shifts V_{th} into the negative bias direction with in the increase in H_2S concentration. When the gas sensor is exposed to O_2, the gases extract electrons from SnO_x in the form of ions. They increase the WF of the SnO_x [11]. The increased WF shifts threshold voltage (V_{th}) of the gas sensor into the positive bias direction and increases the I_D. The V_{th} moves into the opposite direction in H_2S because the gas releases electrons back to the SnO_x by reacting on the adsorbed O_2 ions in air as shown in Fig. 3-10 [29].

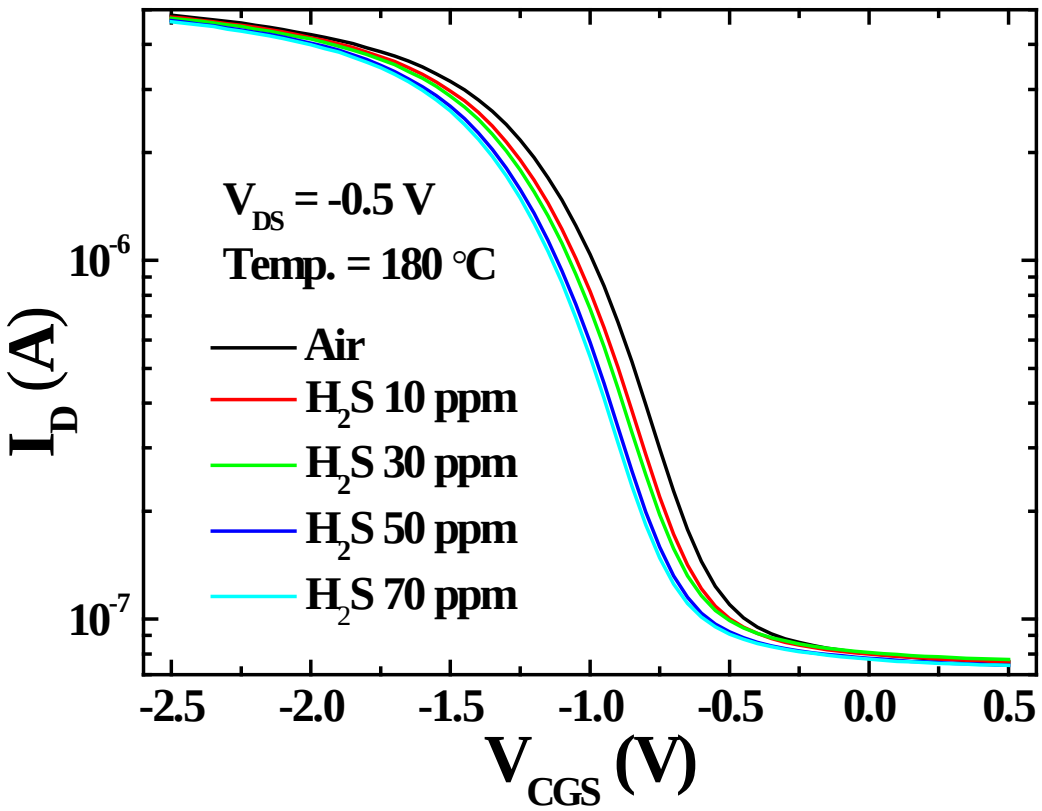

Fig.3-9. Transfer curve for the fabricated gas sensor exposed to different H_2S concentrations.

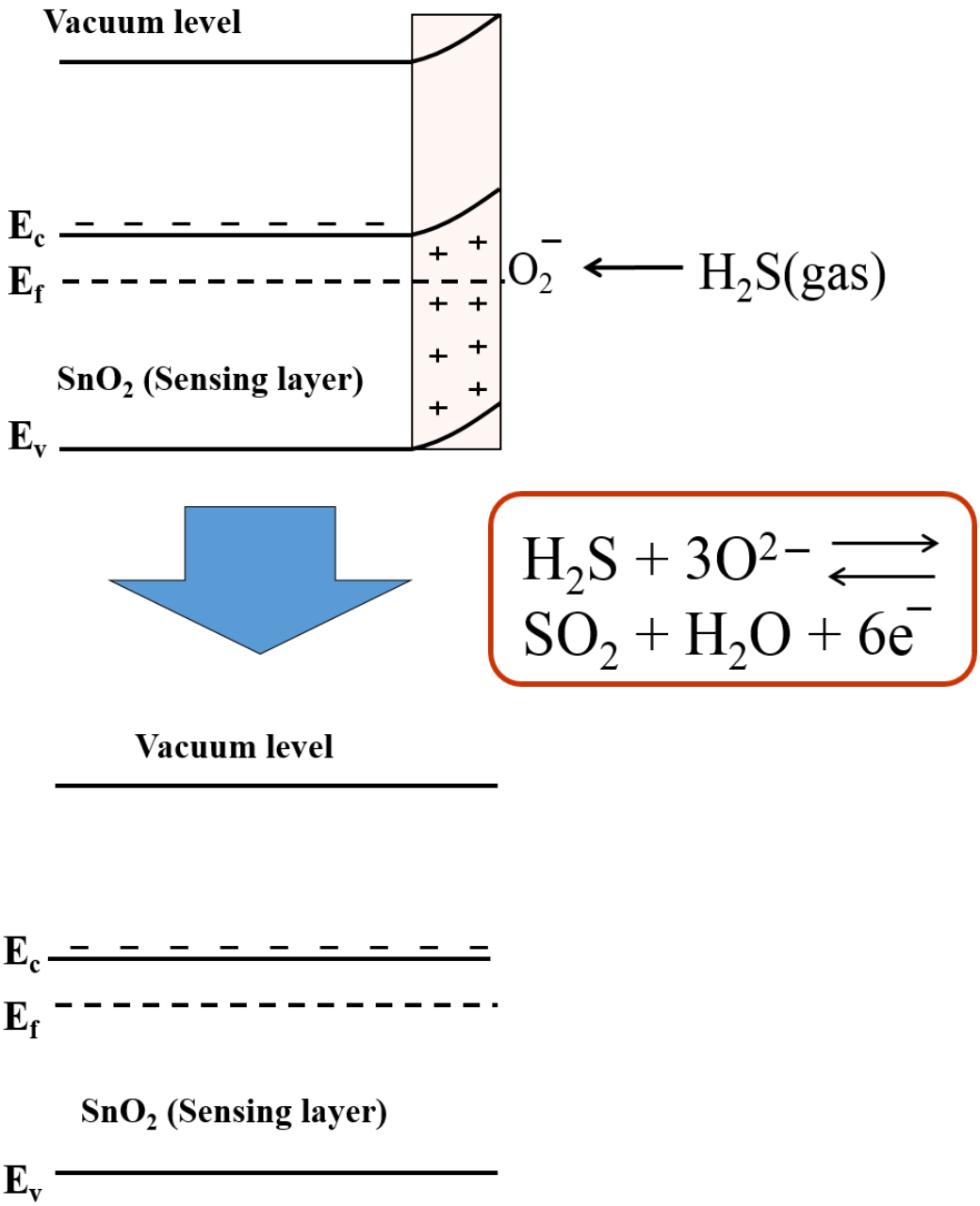

Fig.3-10. Gas reaction change between a target gas (H_2S) and sensing layer (SnO_x).

As shown in Fig. 3-11, ΔV_{th} at I_D = 0.50 μA and ΔI_D at V_{CGS} = -0.84 V are increased with increasing H_2S concentrations. They show about -0.14 V of ΔV_{th} and 55 % of ΔI_D by increasing H_2S concentration to 70 ppm.

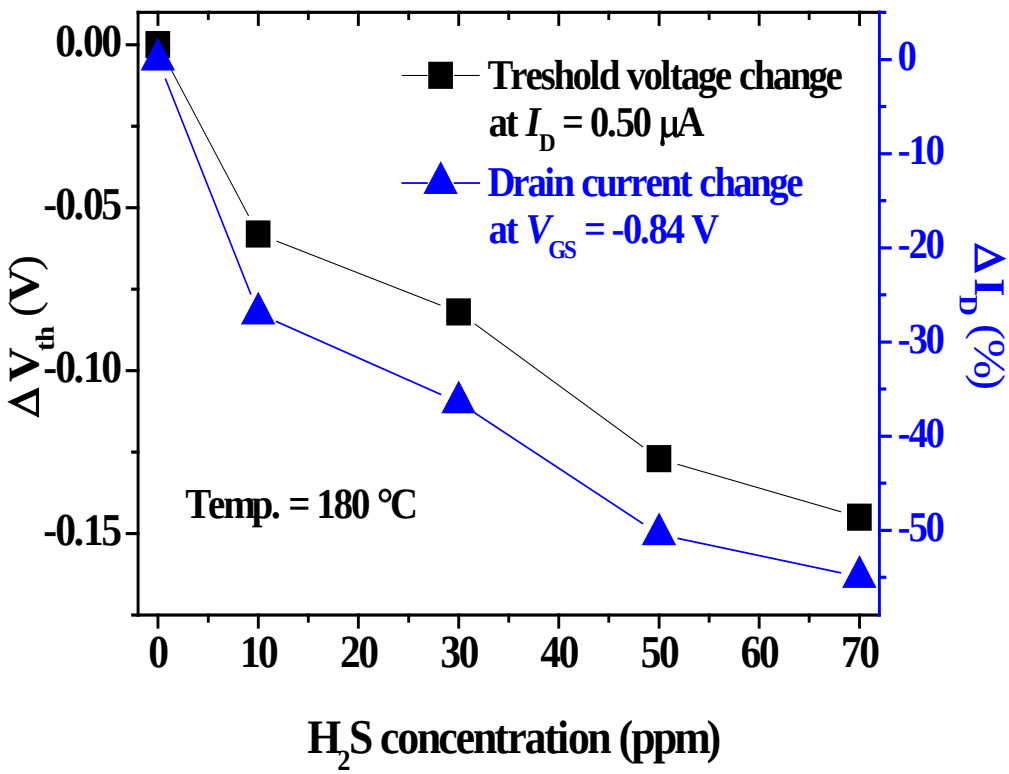

Fig.3-11. Threshold voltage and drain current change for the fabricated gas sensor exposed to different H_2S concentrations.

Fig. 3-12 shows the Langmuir relationship between H_2S concentration and the threshold voltage change of the gas sensor. The ΔV_{max} and α of the gas sensor are 0.156 V and 0.28 ppm^{-1}, respectively.

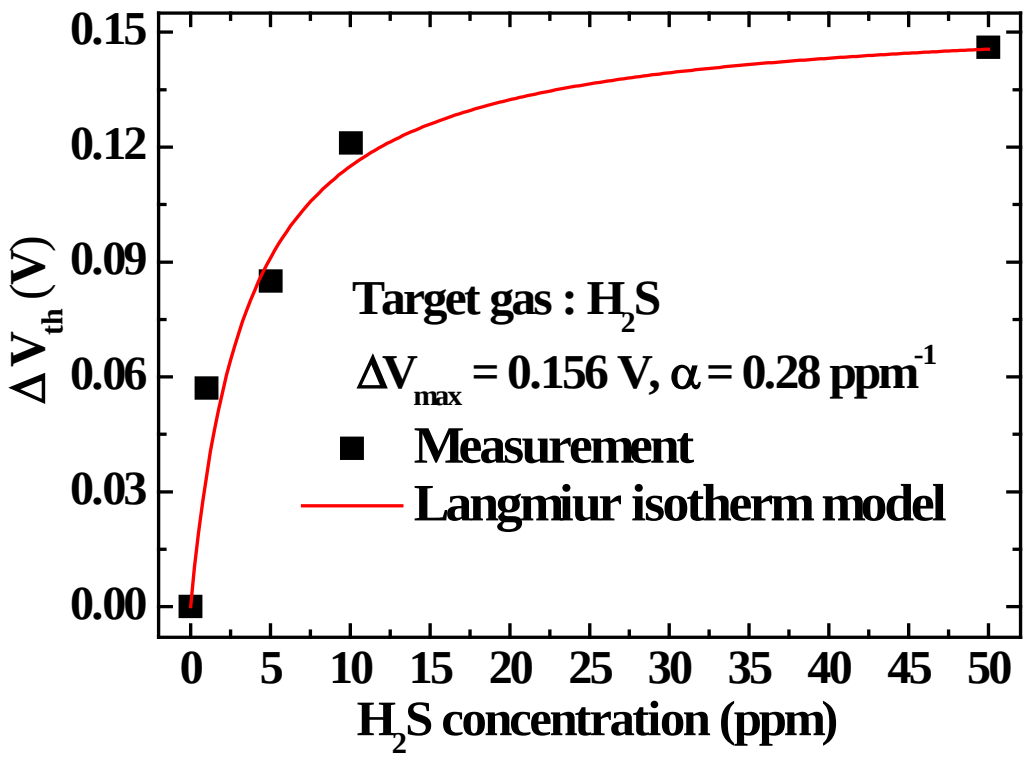

Fig.3-12. The Langmuir relationship of the gas sensor by using SnO_x as a sensing layer at H_2S (ΔV_{max} = 0.156 V and α = 0.28 ppm^{-1})

Fig. 3-13 shows transient response of the fabricated gas sensor by changing chamber ambient (air and 50 ppm H_2S) at 180 ^oC. The applied V_{CGS} and V_{DS} are fixed at -0.9 V and -0.5 V, respectively. We define sensing and recovery times which are specified in terms of the time to reach 90 percent (T_{90}) of its final reading from initial reading when the ambient is changed (air or H_2S). The reference drain currents in the air and H_2S ambient are 0.49 μA and 0.31 μA, respectively. The sensing (air => H_2S) and recovery (H_2S => air) times are about 75 s and 400 s, respectively.

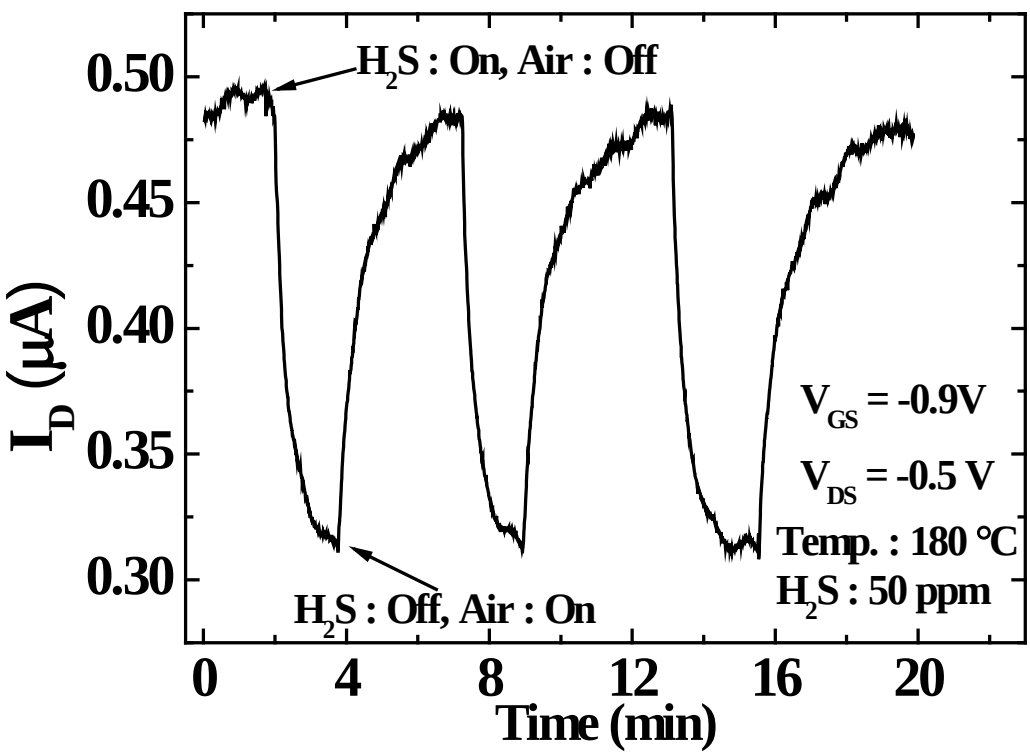

Fig.3-13. Transient response of the fabricated gas senor in alternate ambient of H_2S and air.

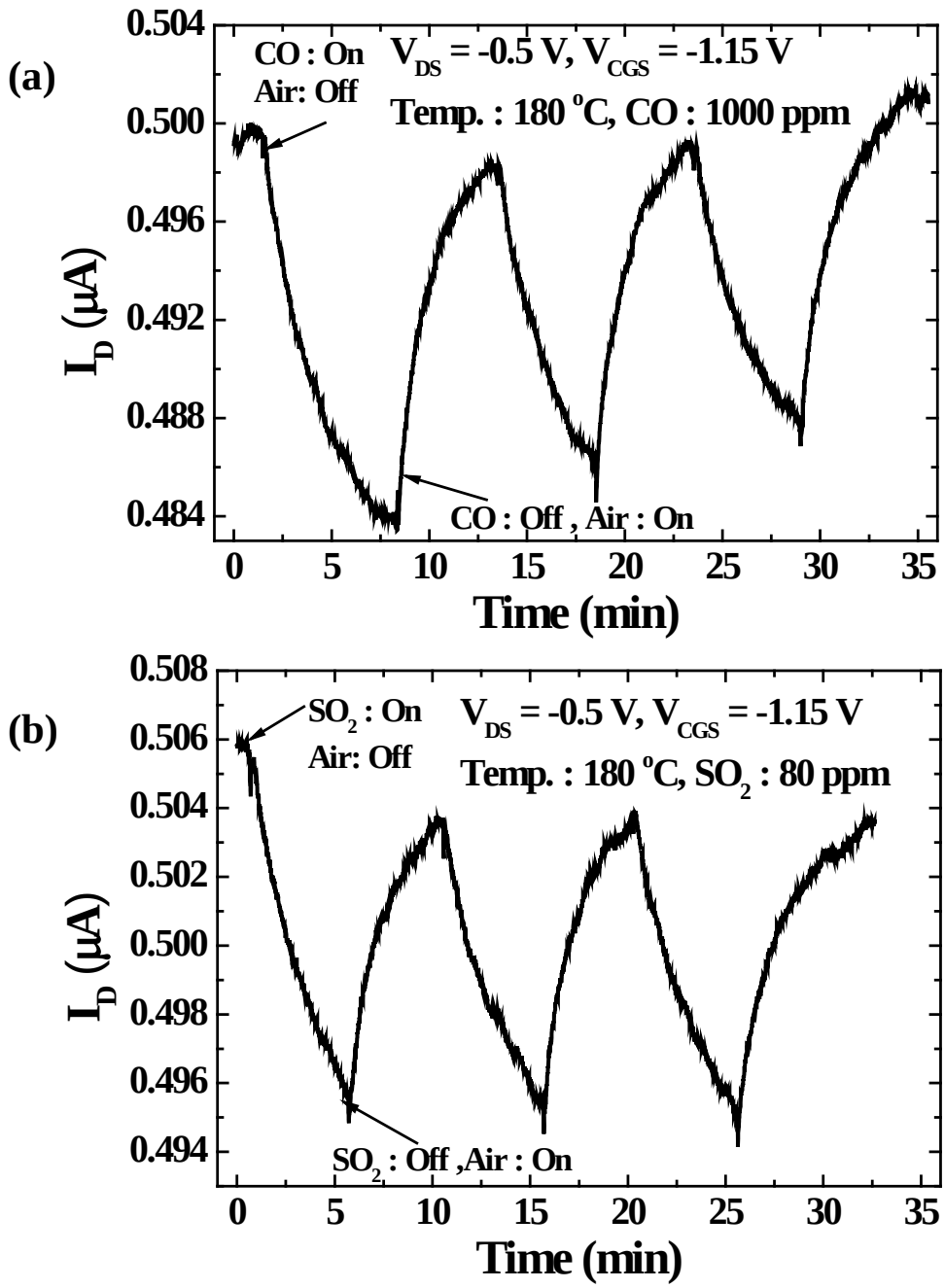

Fig.3-14. Transient curves for the fabricated gas sensor exposed to air, (a) 1000 ppm CO and (b) 80 ppm SO_2.

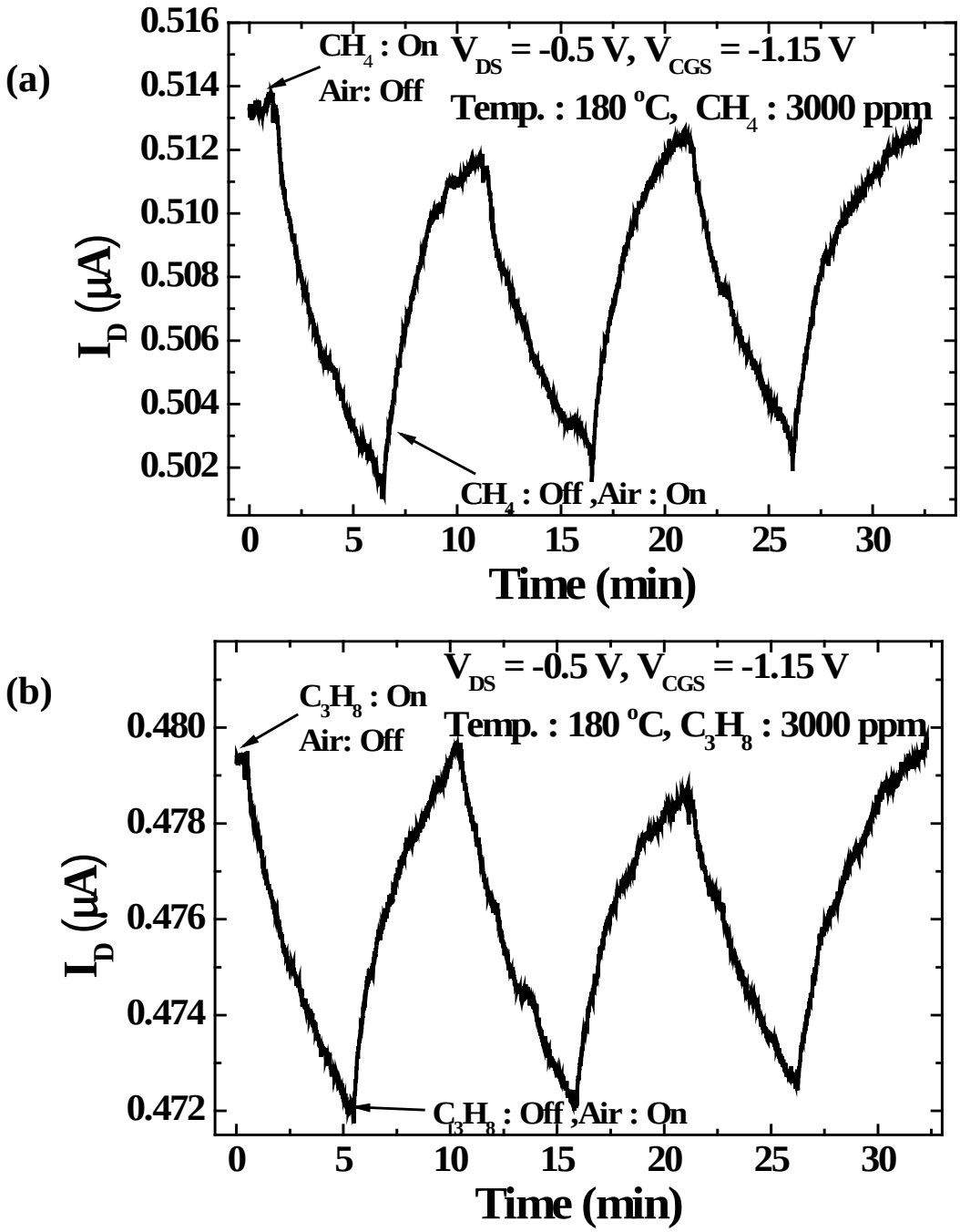

Fig.3-15. Transient curves for the fabricated gas sensor exposed to air, (a) 3000 ppm CH_4 and (b) 3000 ppm C_3H_8.

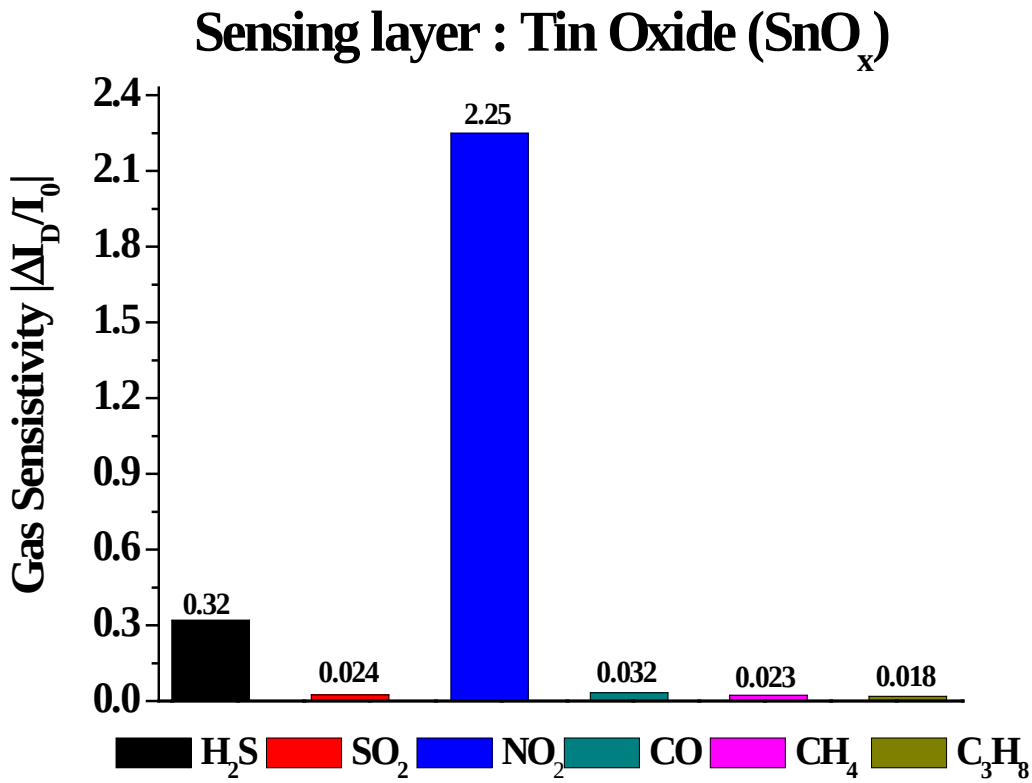

Fig.3-16. Gas sensitivity of the fabricated gas sensor for various gases.

We also investigate gas selectivity of the gas sensor having SnO_x as a sensing layer. We extract a gas sensitivity ($|\Delta I_D/I_{D0}|$) from transient curves for the target gases. The gas sensitivity is defined as $|\Delta I_D/I_{D0}| = [(I_D/I_{D0}) - 1]$ (7) where I_D and I_{D0} are drain current in target gas and air at constant CG and drain voltage. Fig. 3-14, 3-15 and 3-16 show transient curves and gas selectivity of the gas sensor for various gases. The gas sensor has higher sensitivity for NO_2 and H_2S than the others (SO_2, CO, CH_4 and C_3H_8) as shown in Fig. 3-16.

3.3 Zinc oxide sensing layer with ALD method

In this work, we propose a Si MOSFET type gas sensor having a horizontal FG which use a 10 nm thick ZnO (n-type semiconductor) formed by atomic layer deposition (ALD) as a sensing layer and show gas sensing property of the device for target gases. Fig. 3-17 (a) and (b) the Top and 2D cross sectional views of the fabricated gas sensor based on p-type MOSFET, respectively. In Fig. 3-17 (b), the ZnO covers partly the control-gate (CG) formed horizontally and the passivation layer formed on the FG in the center. The device reads out work-function (WF) change in the sensing layer butted to the CG, when the device is exposed to a target gas.

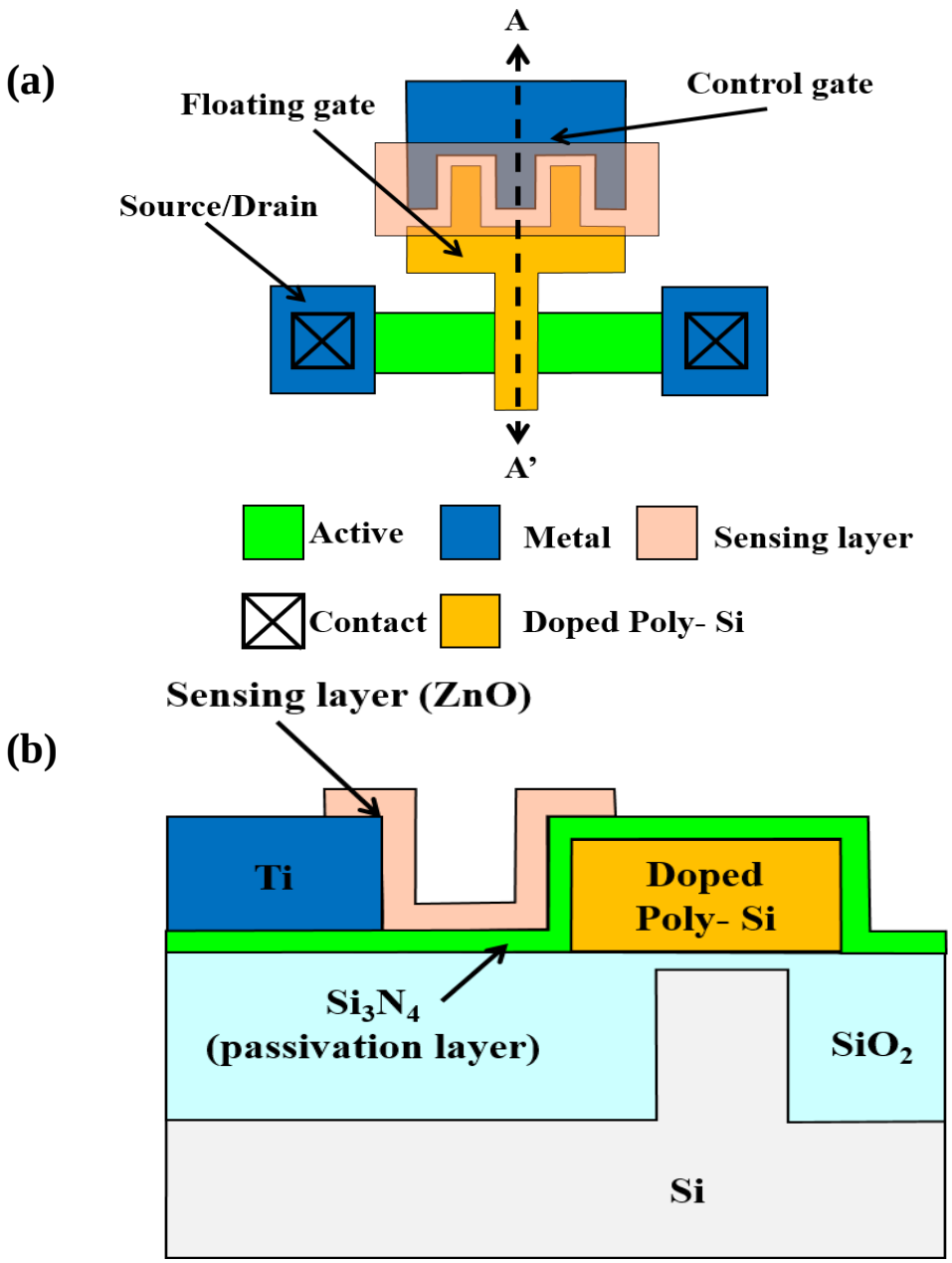

Fig.3-17. (a) Top and (b) 2D cross sectional views of the fabricated gas sensor cut along A–A'.

Key fabrication process steps of the fabricated gas sensor are shown in Fig. 3-18 and explained as follows. A Si_3N_4 layer is deposited by LPCVD on 150 mm Si wafer. This layer acts as a stop layer of CMP. After photolithography process for active patterns, the stop layer and underlying Si are etched. Then isolation oxide is formed by HDPCVD and followed by CMP until the Si_3N_4 layer is exposed. The Si_3N_4 layer is removed in a phosphoric acid solution at 160 °C. Thermal oxidation with the thickness of 10 nm is carried out. Then an *in-situ* phosphorous doped poly-Si layer with a thickness of 200 nm is deposited to form the FG. The poly-Si is patterned by photolithography. After ion implantation is performed to form source and drain regions, a 10 nm thick SiO_2 and 30 nm thick Si_3N_4 layers are grown and deposited to be used for a passivation layer. Then, the CG (Ti) and sensing layer (ZnO) are formed by e-beam evaporation and ALD processes, respectively. They are patterned by lift-off and wet etch process. Thicknesses of Ti and ZnO are 100 nm and 10 nm, respectively

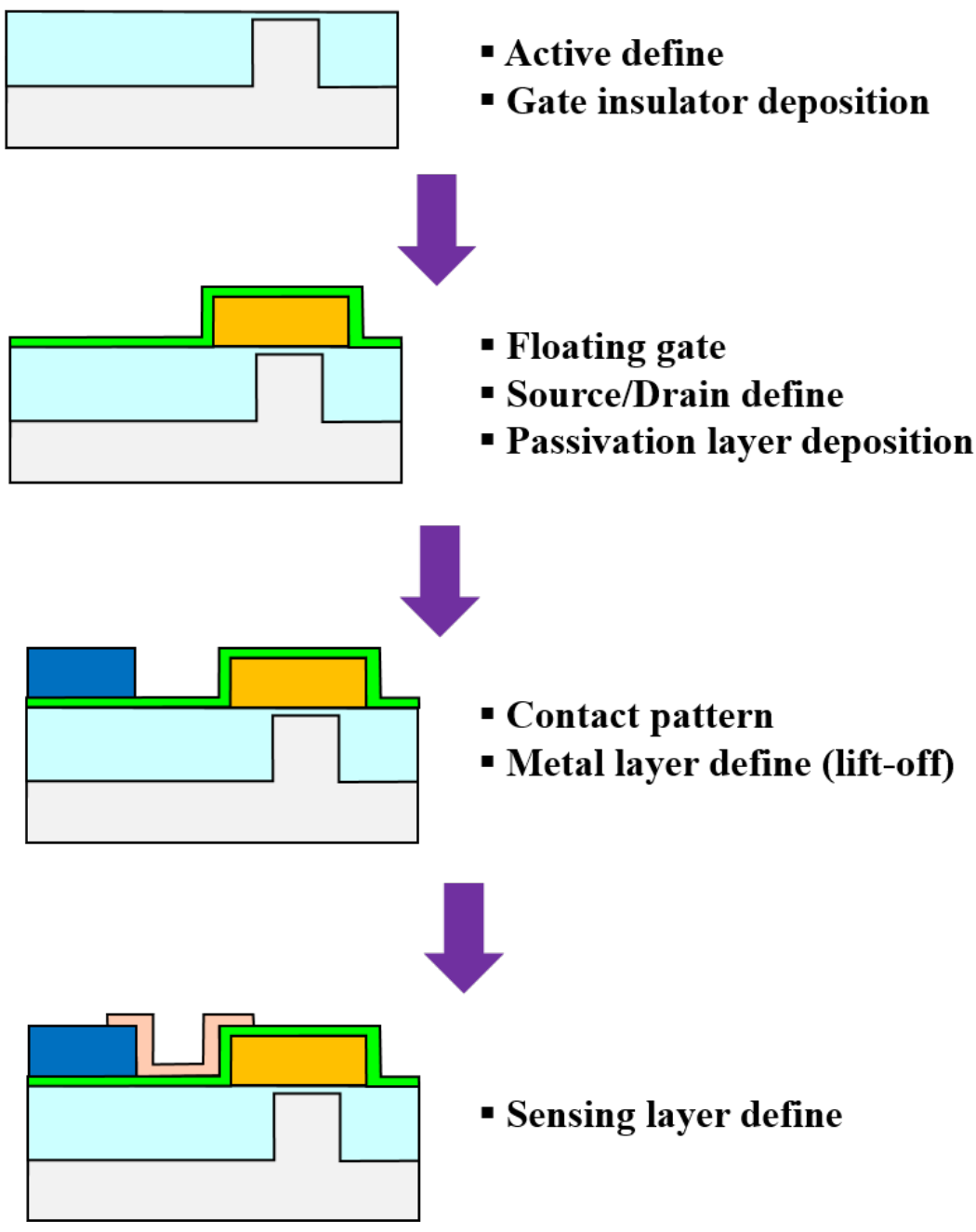

Fig.3-18. Fabrication process flow and steps of the fabricated gas sensor with ZnO sensing layer.

Fig. 3-19 (a) and (b) show transfer and transient curves for the fabricated gas sensor exposed to N_2 gas ambient as a reference and in NO_2 gas ambient with a concentration of 50 ppm. Transient response of the fabricated gas sensor is measured by changing chamber ambient (air and 50 ppm NO_2) at 180 ^oC. The applied V_{CGS} and V_{DS} are fixed at -1.4 V and -0.5 V, respectively. As shown in Fig. 3-19 (b), the I_D increases from 0.11 μA in the air to 0.26 μA in the NO_2 ambient. Response and recovery times of the gas sensor are about 80 s and 240 s, respectively. In this work, an I_D of the gas sensor decreases when the device is exposed to NO_2. The NO_2 is an acceptor-type gas on the ZnO [30]. When the gas sensor is exposed to NO_2 gases, the gases diffusing through the ZnO extract electrons from the ZnO and become negatively charged ions at surface of ZnO. It creates a positive space-charge (depletion) region in the ZnO. The region increases WF of the ZnO. The increased WF shifts threshold voltage of the gas sensor into the positive bias direction and increases sensing current [11].

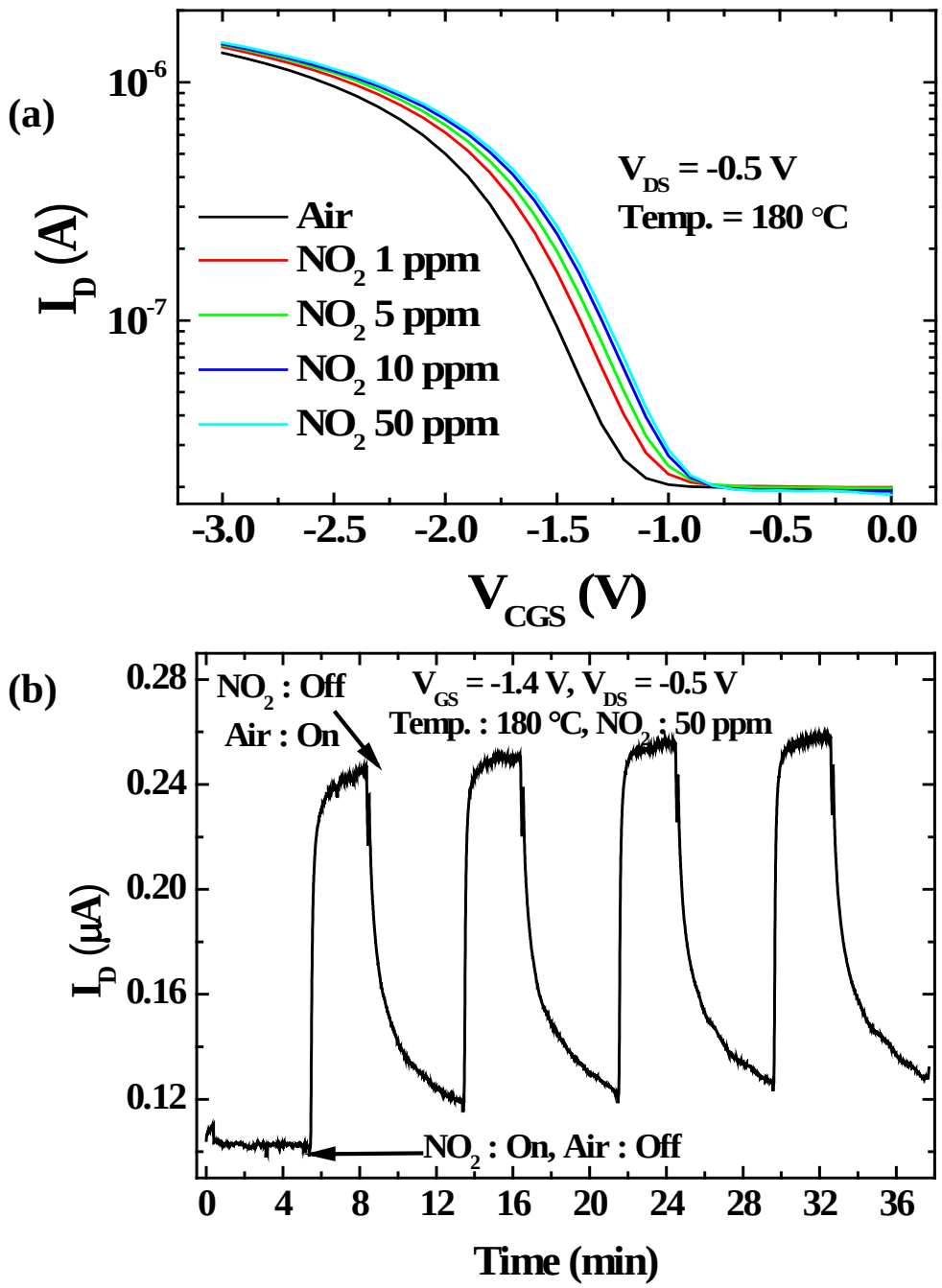

Fig. 3-19. (a) transfer and (b) transient curves for the fabricated gas sensor exposed to air and 50 ppm NO_2.

Fig. 3-20 shows the Langmuir relationship between NO_2 concentration and the threshold voltage change of the gas sensor where the sensing layer is ZnO. The ΔV_{max} and α of the gas sensor are 0.245 V and 0.57 ppm^{-1}, respectively.

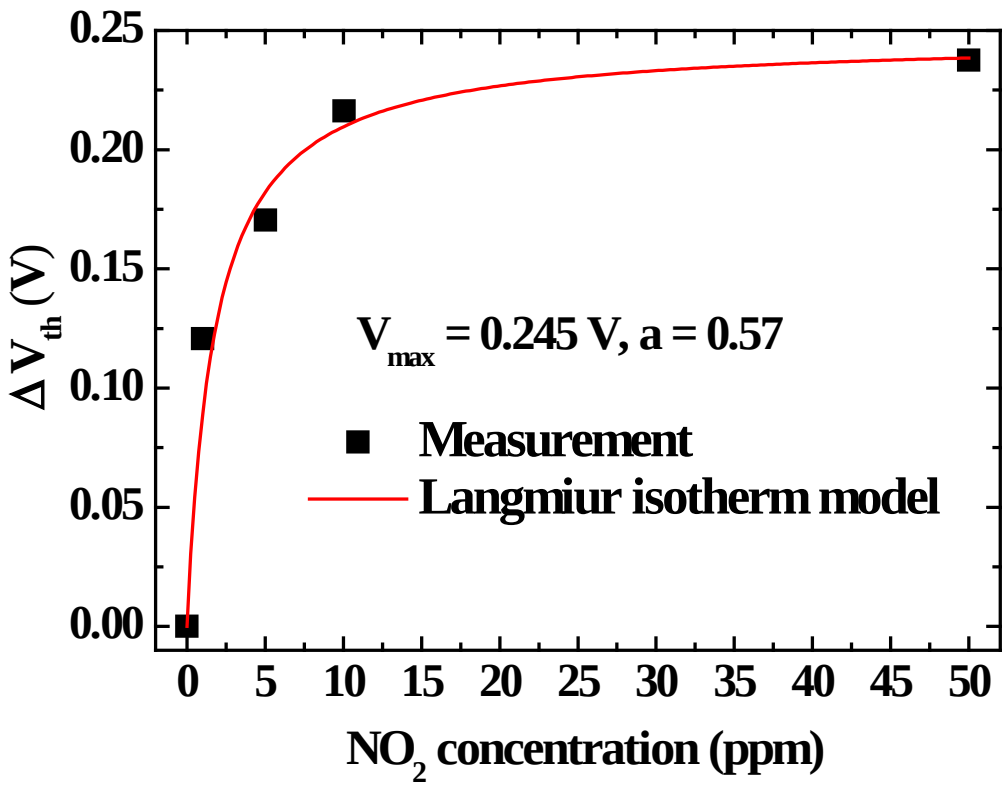

Fig. 3-20. The Langmuir relationship of the gas sensor by using ZnO as a sensing layer at NO_2 (ΔV_{max} = 0.245 V and α = 0.57 ppm^{-1}).

We investigate gas sensitivity of the fabricated gas sensor for various target gases. As a transfer curves, I_D-V_{CGS} curve in air and target gases is measured. The applied V_{CGS} and V_{DS} are fixed at -1.7 V and -0.5 V, respectively. As shown in Fig. 3-21, the I_D increases from 0.11 μA in the air to 0.26 μA in the H_2S ambient [31]. Response and recovery times of the gas sensor are about 110 s and 400 s, respectively. Then we investigate a gas sensitivity having ZnO as a sensing layer. . Fig. 3-22, 3-23, 3-24 and 3-25 show transient curves and gas selectivity of the gas sensor for various gases. The gas sensor has higher sensitivity for NO_2 and H_2S than the others (NH_3, SO_2, CO_2, CH_4 and C_3H_8) as shown in Fig. 3-25.

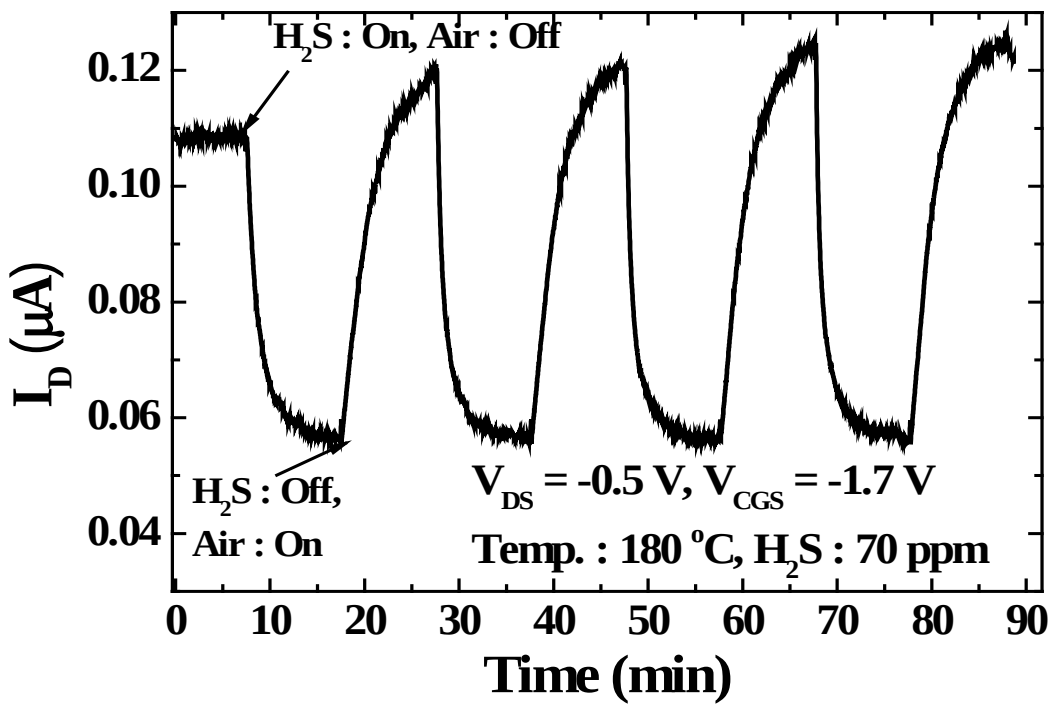

Fig. 3-21. Transient curve for the fabricated gas sensor exposed to air and 70 ppm H_2S.

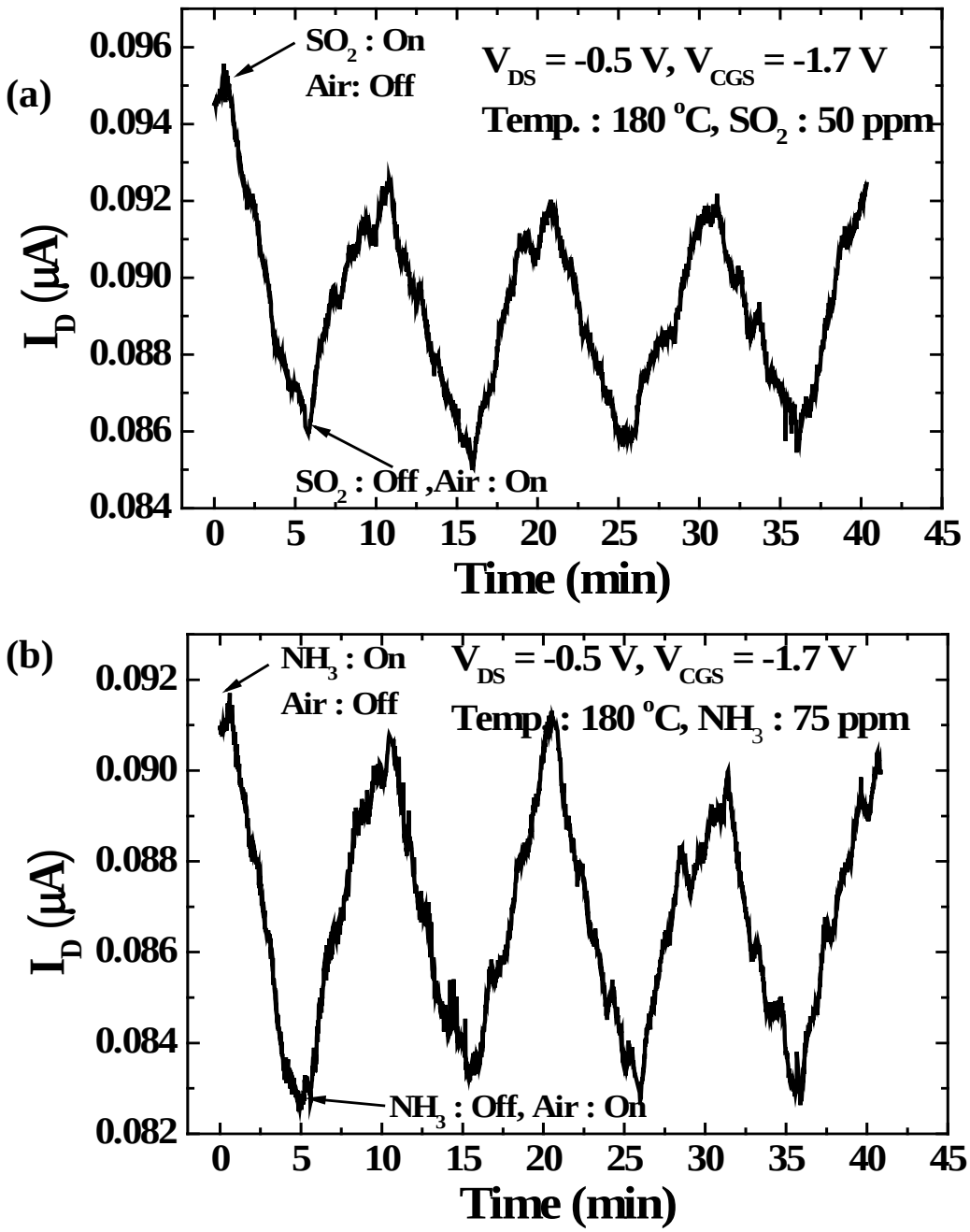

Fig. 3-22. Transient curves for the fabricated gas sensor exposed to air, (a) 50 ppm SO_2 and (b) 75 ppm NH_3.

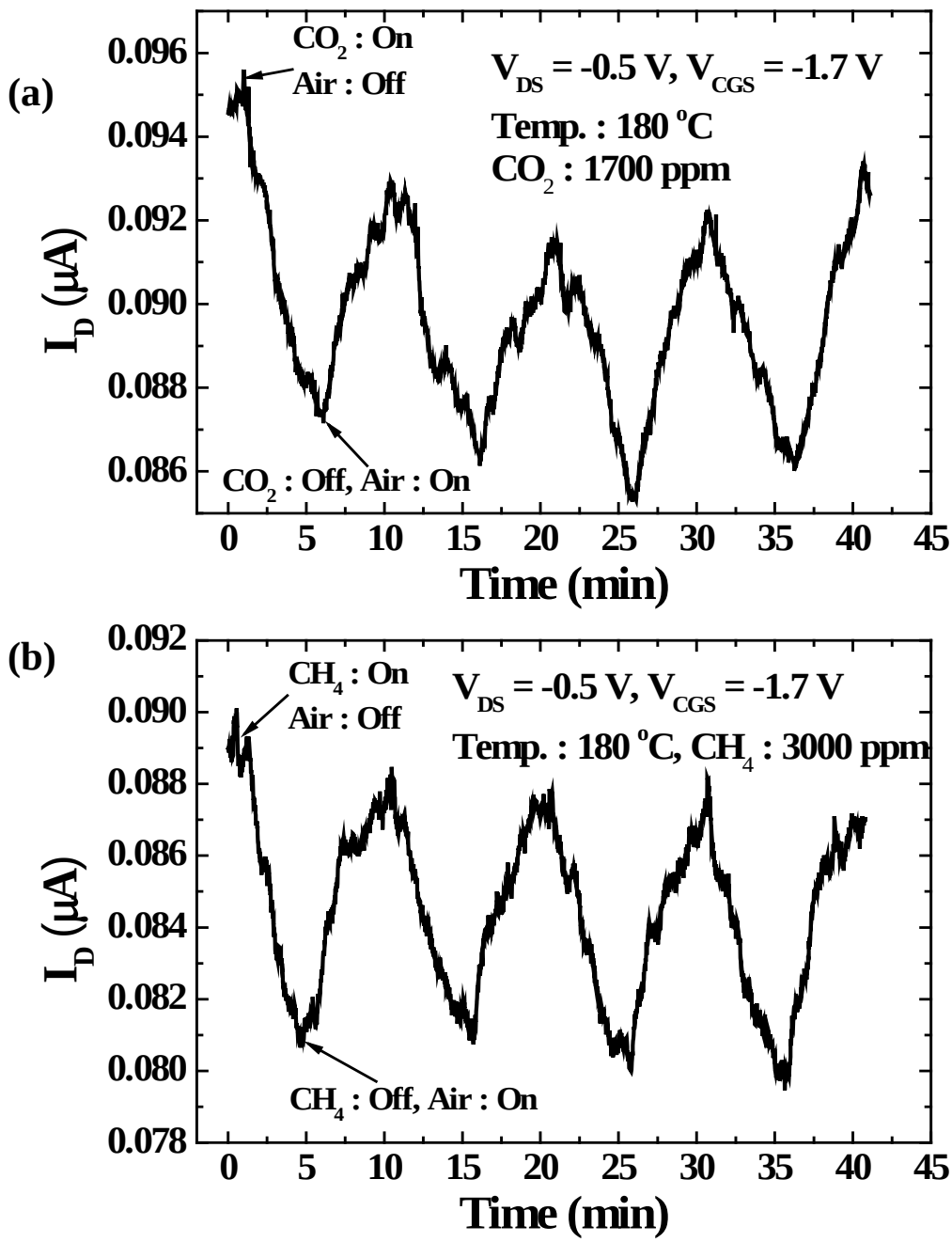

Fig. 3-23. Transient curves for the fabricated gas sensor exposed to air, (a) 1700 ppm CO_2 and (b) 3000 ppm CH_4.

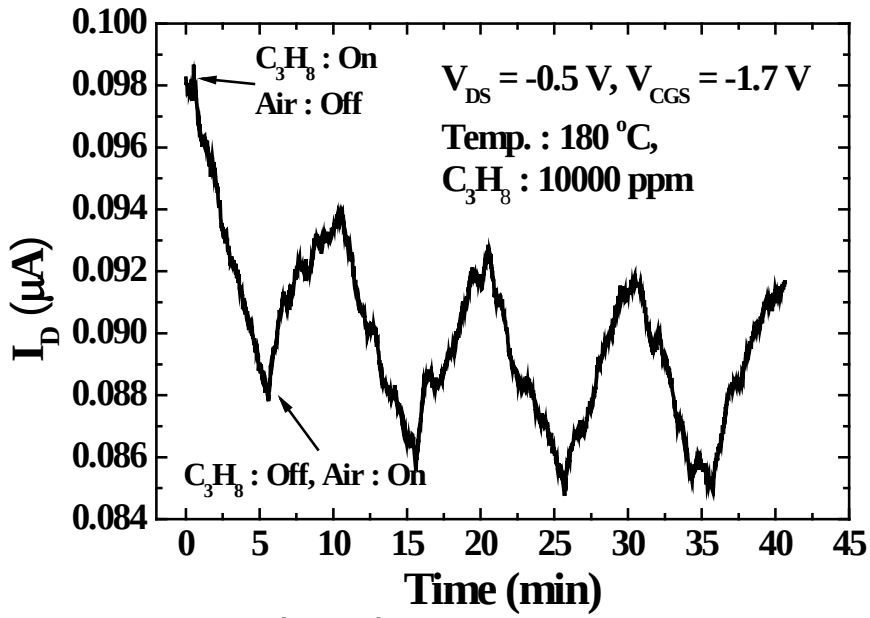

Fig. 3-24. Transient curves for the fabricated gas sensor exposed to air and 10000 ppm C_3H_8.

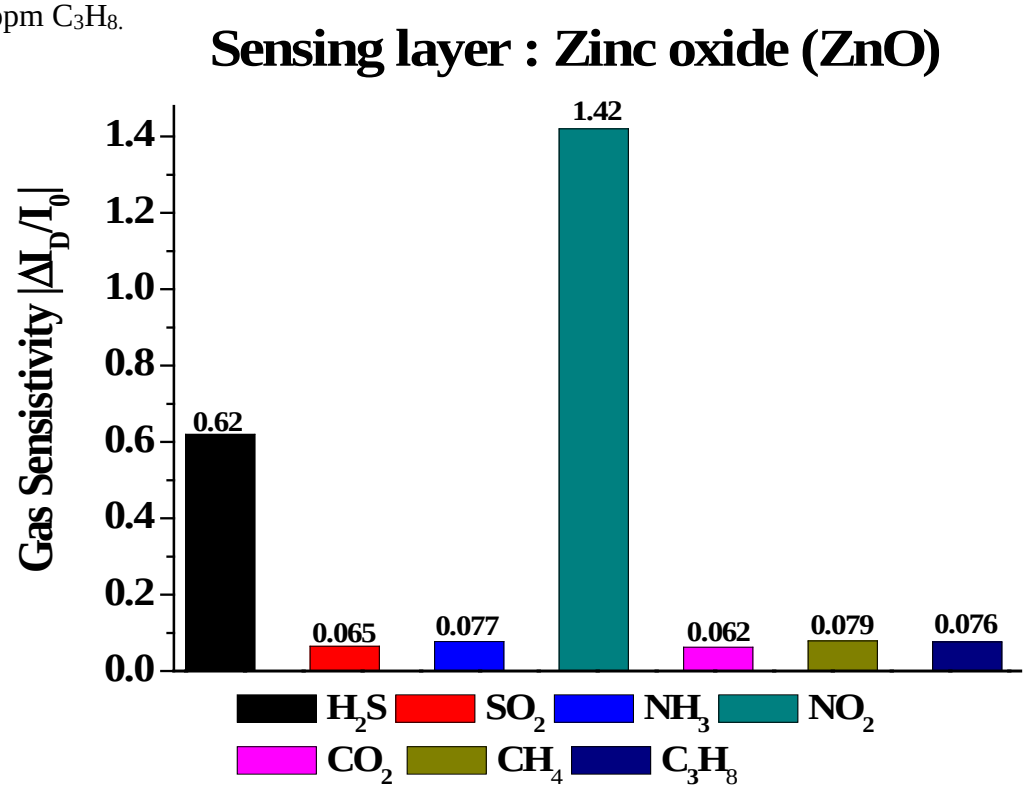

Fig. 3-25. Gas sensitivity of the fabricated gas sensor for various gases.

3.4 Carbon nanotube sensing layer with ink-jet printing method.

In this work, we propose a Si MOSFET type gas sensor having a horizontal FG which use a carbon nanotube (CNT) formed by ink-jet printing as a sensing layer and show gas sensing property of the device for target gases. Fig. 3-26 shows cross sectional view of the fabricated gas sensor based on p-type MOSFET, respectively. In Fig. 3-26, the CNT which is p-type semiconductor formed between the control-gate (CG) and the FG. The SU-8 is formed for isolating between metal layers.

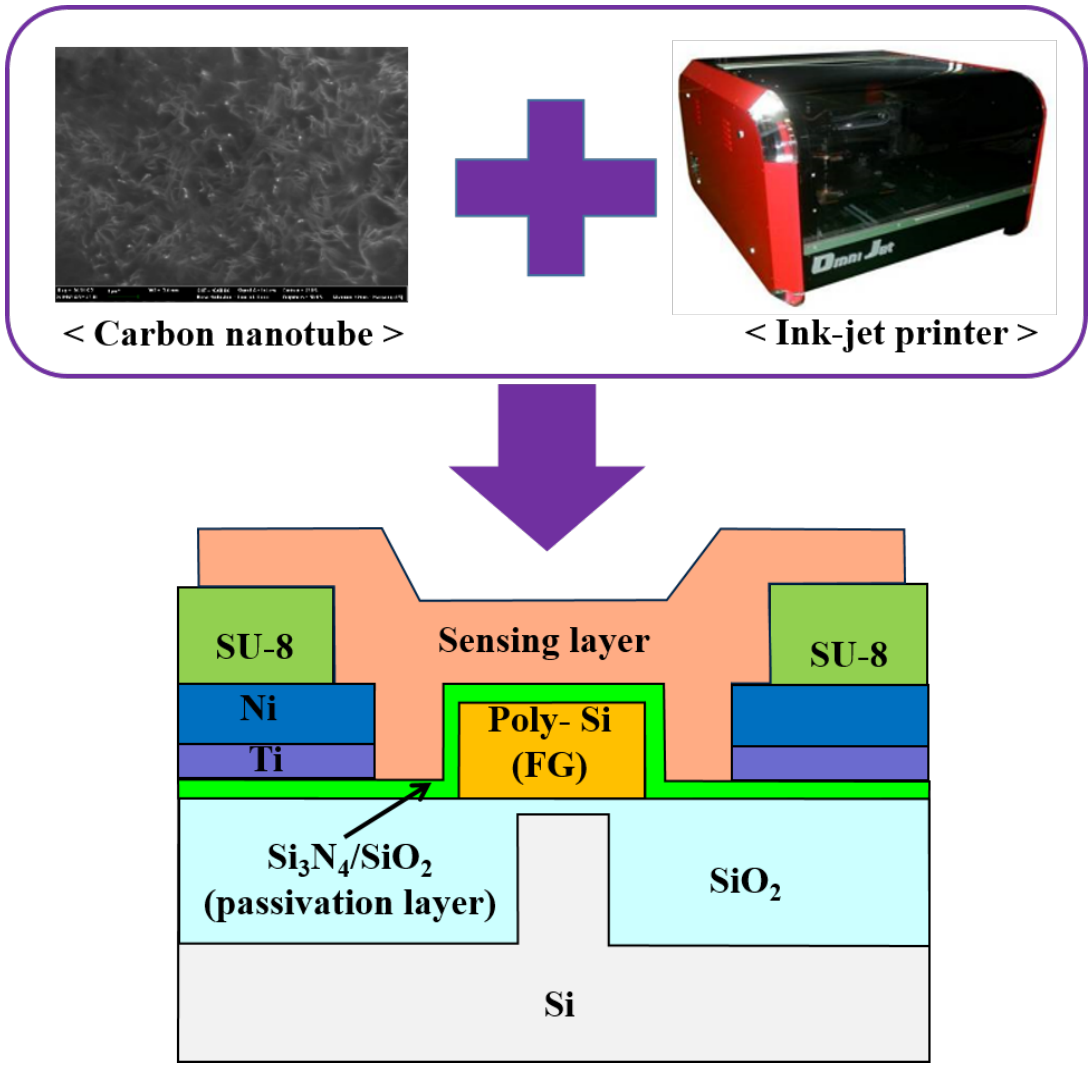

Fig.3-26. Cross sectional view of the fabricated gas sensor with ink-jet printing method.

Key fabrication process steps of the fabricated gas sensor are shown in Fig. 3-27 and explained as follows. A Si_3N_4 layer is deposited by LPCVD on 150 mm Si wafer. This layer acts as a stop layer of CMP. After photolithography process for active patterns, the stop layer and underlying Si are etched. Then isolation oxide is formed by HDPCVD and followed by CMP until the Si_3N_4 layer is exposed. The Si_3N_4 layer is removed in a phosphoric acid solution at 160 °C. Thermal oxidation with the thickness of 10 nm is carried out. Then an *in-situ* phosphorous doped poly-Si layer with a thickness of 200 nm is deposited to form the FG. The poly-Si is patterned by photolithography. After ion implantation is performed to form source and drain regions, a 10 nm thick SiO_2 and 50 nm thick Si_3N_4 layers are grown and deposited to be used for a passivation layer. Then, the CG (Cr/Au) formed by e-beam evaporation. Thicknesses of Cr and Au are 70 nm and 30 nm, respectively. They are patterned by lift-off process. The Su-8 is patterned by photolithography. The sensing layer (CNT) are pattered by ink-jet printing. Then, vacuum annealing process is carried out at 250 °C to remove surfactant in CNT.

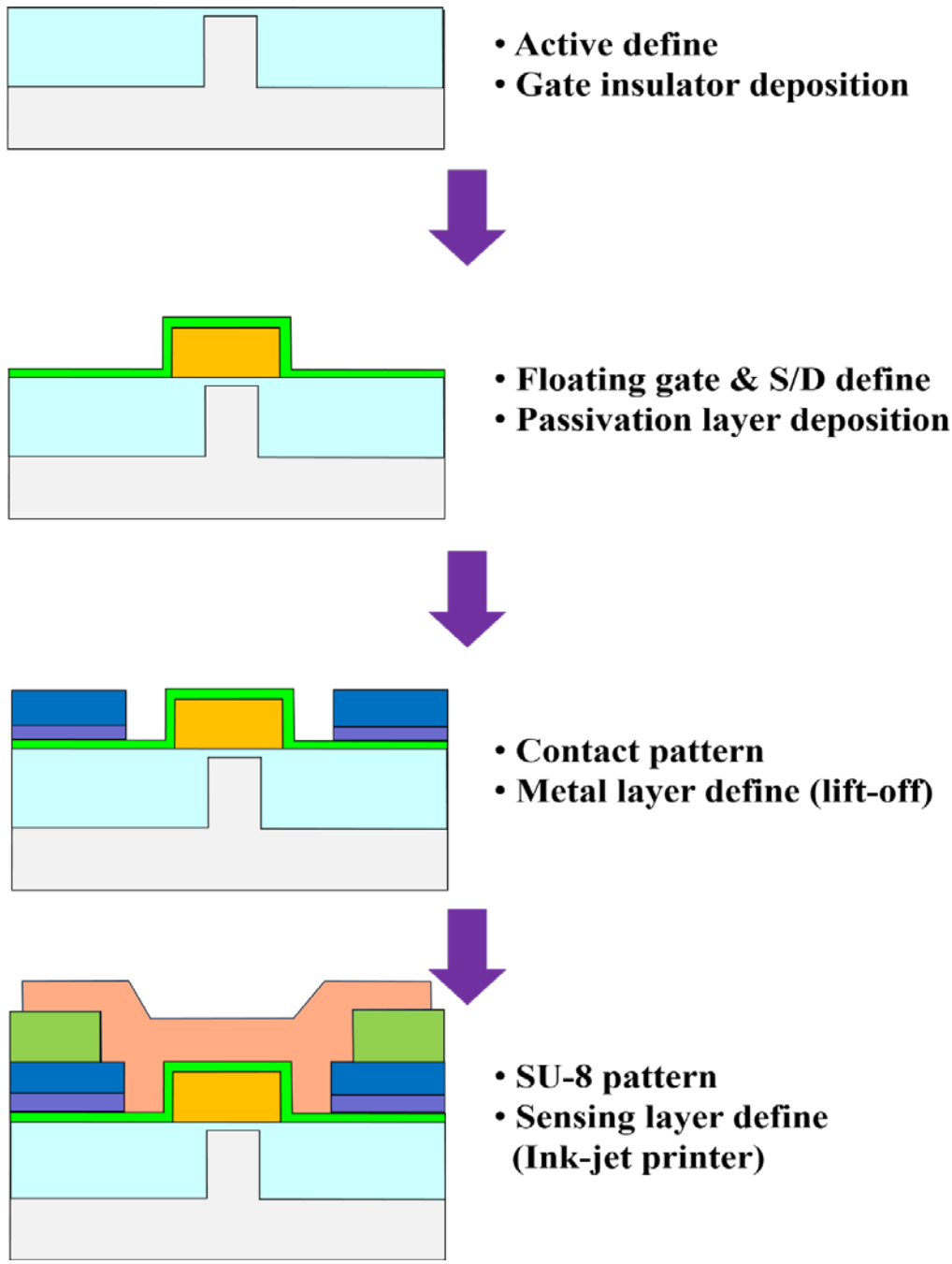

Fig.3-27. Fabrication process flow and steps of the fabricated gas sensor with CNT sensing layer.

Fig. 3-28 (a) and (b) show transfer curves of the fabricated gas sensor as a parameter of NO_2 concentration. An I_D of the gas sensor increases when the device is exposed to NO_2. Transient response of the fabricated gas sensor by changing chamber ambient (air and 50 ppm NO_2) at 180 ^oC. The applied V_{CGS} and V_{DS} are fixed at -1.0 V and -0.5 V, respectively. As shown in Fig. 3-28 (b), the I_D increases from 0.1 μA in the air to 0.69 μA in the NO_2 ambient. Response and recovery times of the gas sensor are about 20 s and 60 s, respectively. The NO_2 is an acceptor-type gas on the CNT [32]. The WF of the sensing layer increases when the layer is exposed to NO_2. The increased WF shifts threshold voltage of the gas sensor into the positive bias direction and increases sensing current.

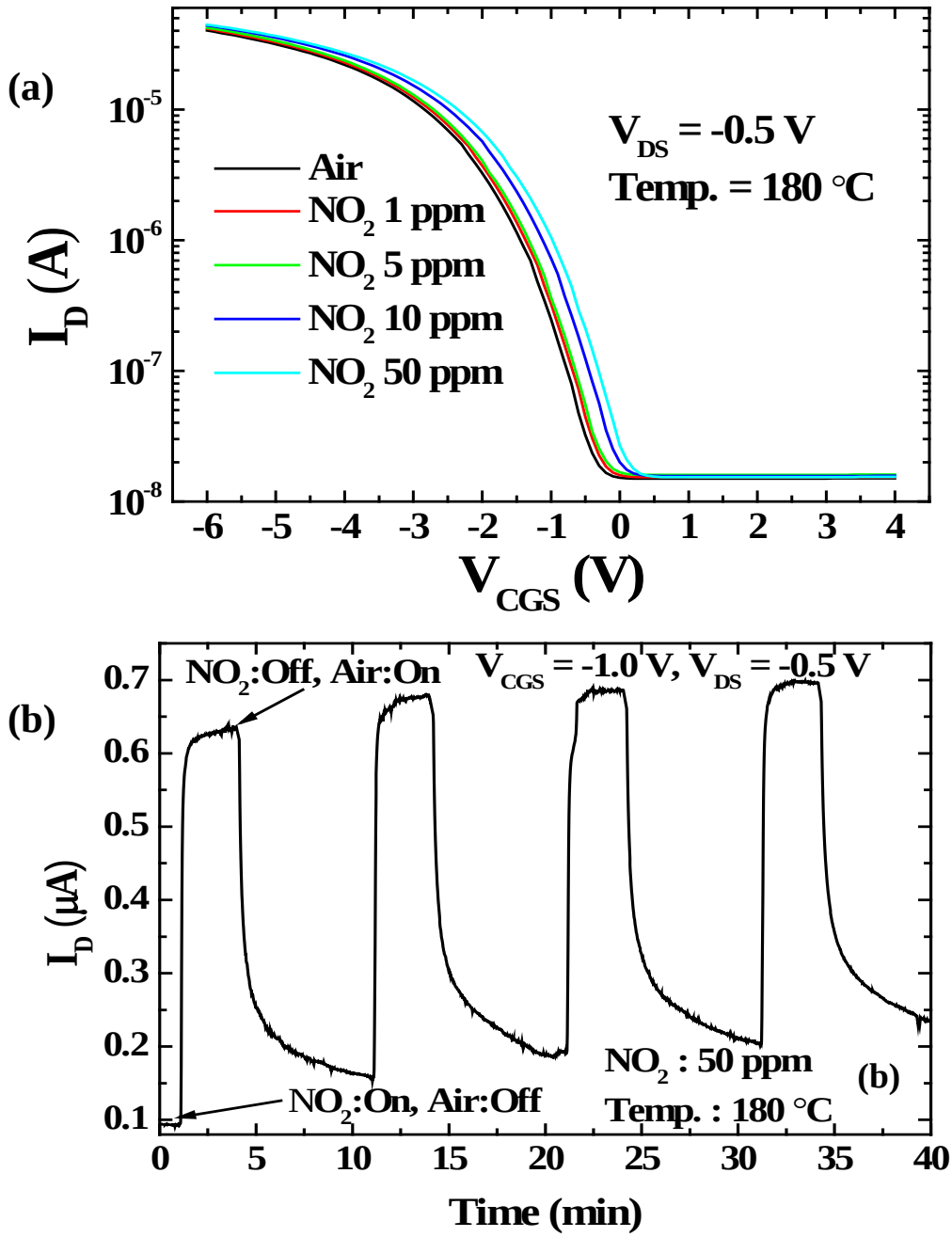

Fig. 3-28. (a) transfer and (b) transient curves for the fabricated gas sensor exposed to air and 50 ppm NO_2.

Fig. 3-29 shows the Langmuir relationship between NO_2 concentration and the threshold voltage change of the gas sensor where the sensing layer is the CNT. The ΔV_{max} and α of the gas sensor are 0.57 V and 0.085 ppm^{-1}, respectively.

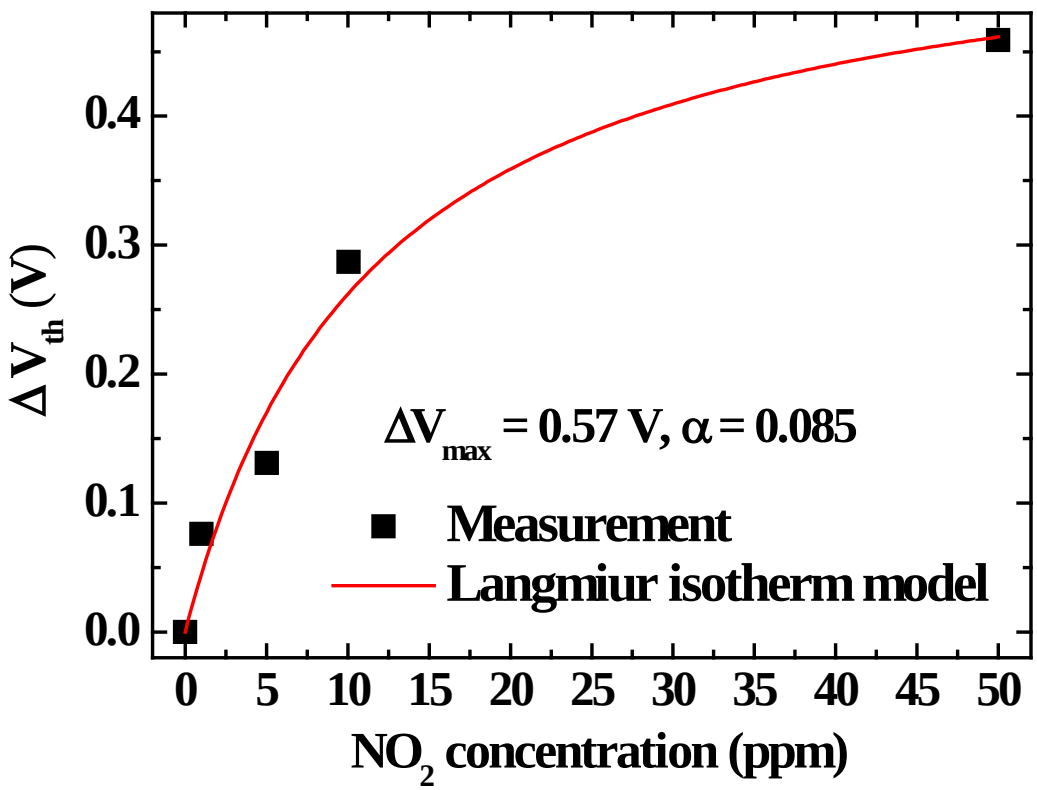

Fig. 3-29. The Langmuir relationship of the gas sensor by using CNT as a sensing layer at NO_2 (ΔV_{max} = 0.57 V and α = 0.085 ppm^{-1}).

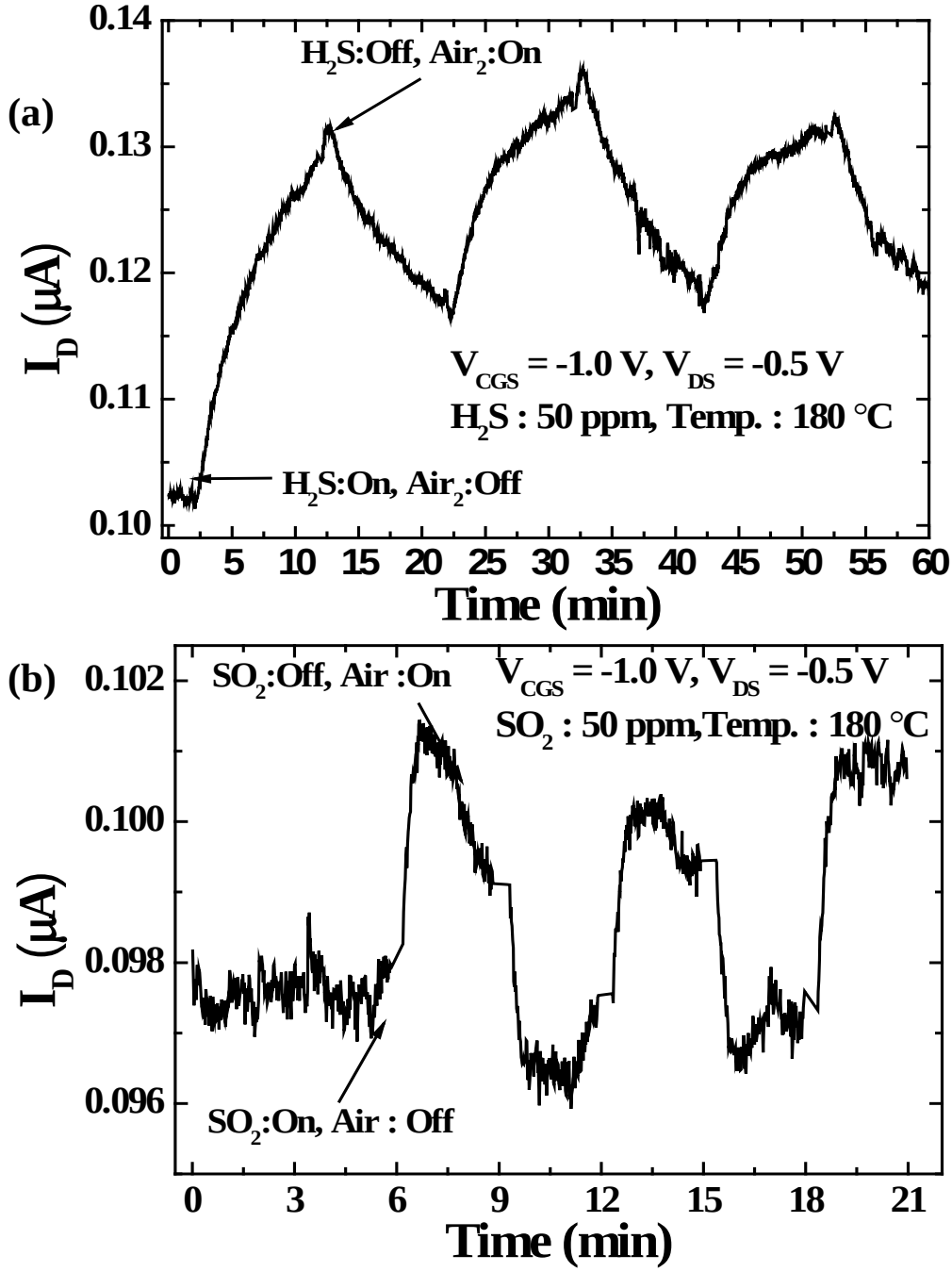

Fig. 3-30. Transient curves for the fabricated gas sensor exposed to air, (a) 50 ppm H_2S and (b) 50 ppm SO_2.

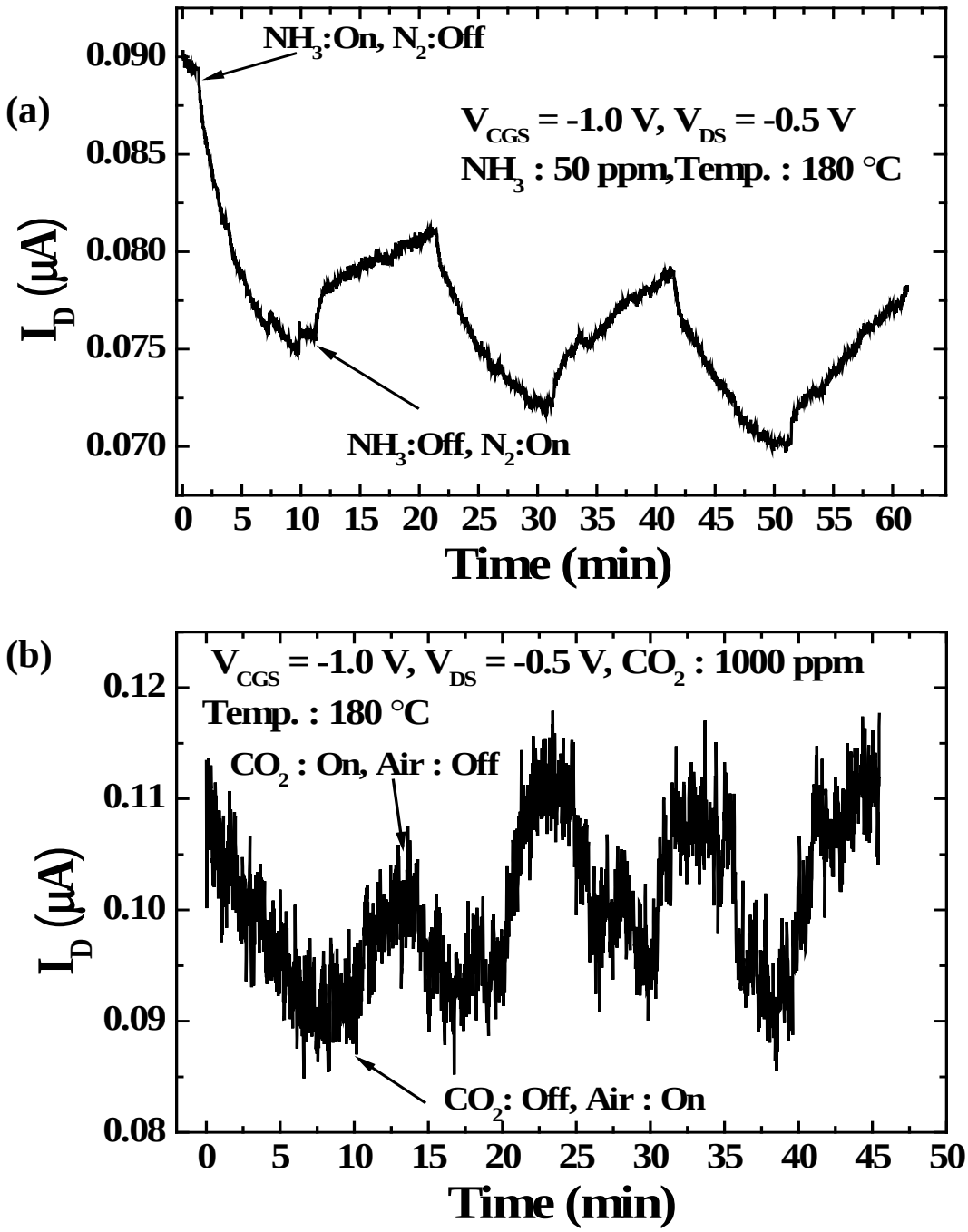

Fig. 3-31. Transient curves for the fabricated gas sensor exposed to air, (a) 50 ppm NH_3 and (b) 1000 ppm CO_2.

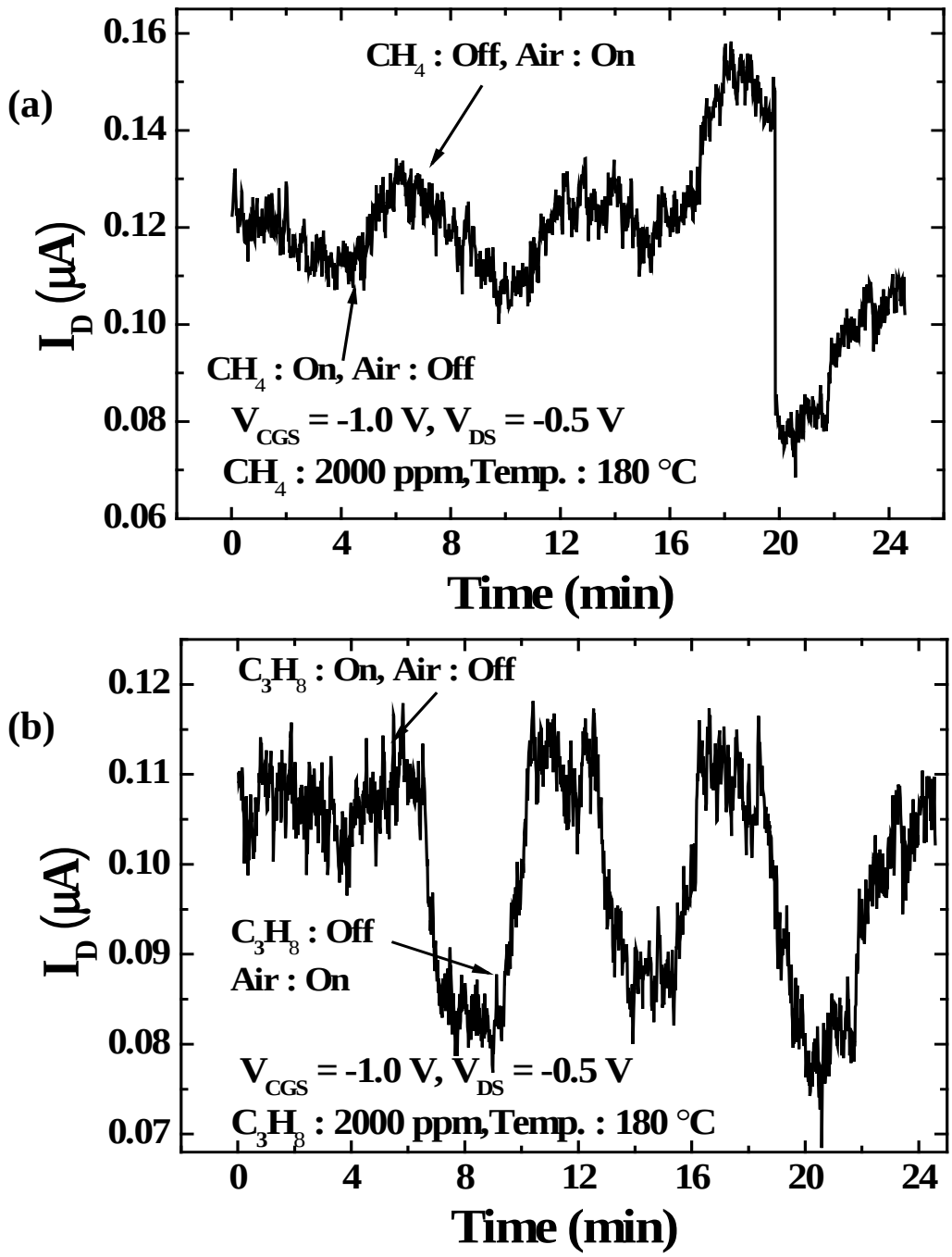

Fig. 3-32. Transient curves for the fabricated gas sensor exposed to air, (a) 2000 ppm CH_4 and (b) 2000 ppm C_3H_8.

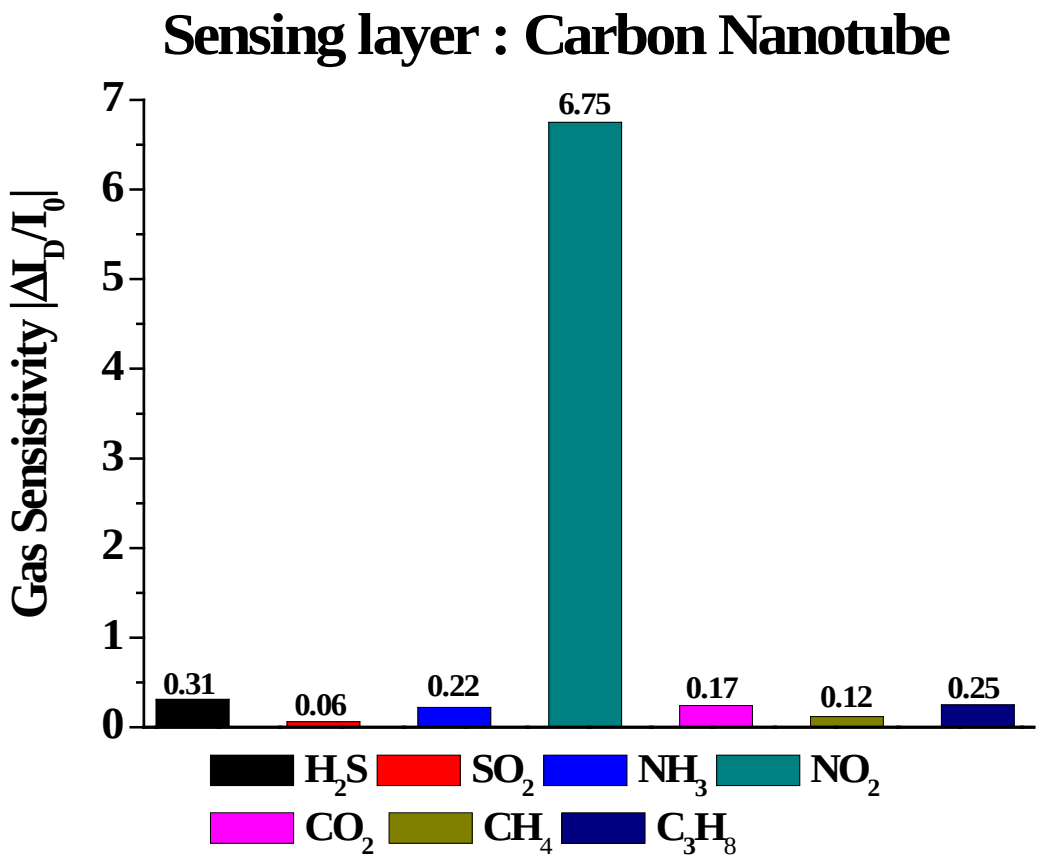

Fig. 3-33. Gas selectivity of the fabricated gas sensor for various gases.

We also investigate gas selectivity of the gas sensor having CNT as a sensing layer. Fig. 3-30, 3-31, 3-32 and 3-33 show transient curves and gas selectivity of the gas sensor for various gases. The gas sensor has higher sensitivity for NO_2 than the others (H_2S, NH_3, SO_2, CO_2, CH_4 and C_3H_8) as shown in Fig. 3-33.

3.5 Sensor calibration

After device fabrication processing, The FET gas sensor show that V_{th} distribution of the device is widened [33]. It is difficult to obtain high yield for the gas senor and become low cost device. To solve the problem, we apply program/erase (P/E) scheme [34] to the fabricated gas sensor. Fig. 3-34 show programming and erasing characteristics of the fabricated gas senor device at 180 °C. We adjust threshold voltage and drain current (sensing current) level by the control gate bias. Transfer curves of the gas sensor are measured at initial and P/E state (@ 180 ºC), respectively. From the transfer curves, we extract threshold voltage (V_{th}) of the gas sensor by using trans-conductance (g_m) - linear - extrapolation method [35]. A control gate voltage pulse of 12 V for 6 s (program) and -14 V for 10 s (erase) cause about a shift of 1.24 V and 0.96 V from the curve at the initial state at 180 ºC ($V_D = V_S = V_B = 0$ V) as shown in Fig 3-34. Fig. 3-35 (a) and (b) show retention characteristics of the fabricated gas senor for P/E state at 180 °C. We extract threshold voltage change (ΔV_{th}) of the gas sensor each P/E state. In this work, threshold voltage change is defined as

$$\Delta V_{th} = |V_{th} - V_{th0}| \qquad (7)$$

where V_{th} and V_{th0} are threshold voltage of the gas sensor at P/E state and initial. As shown in Fig. 3-35, ΔV_{th}s at program and erase state are 0.034 V and 0.025 V for 10000 s, respectively.

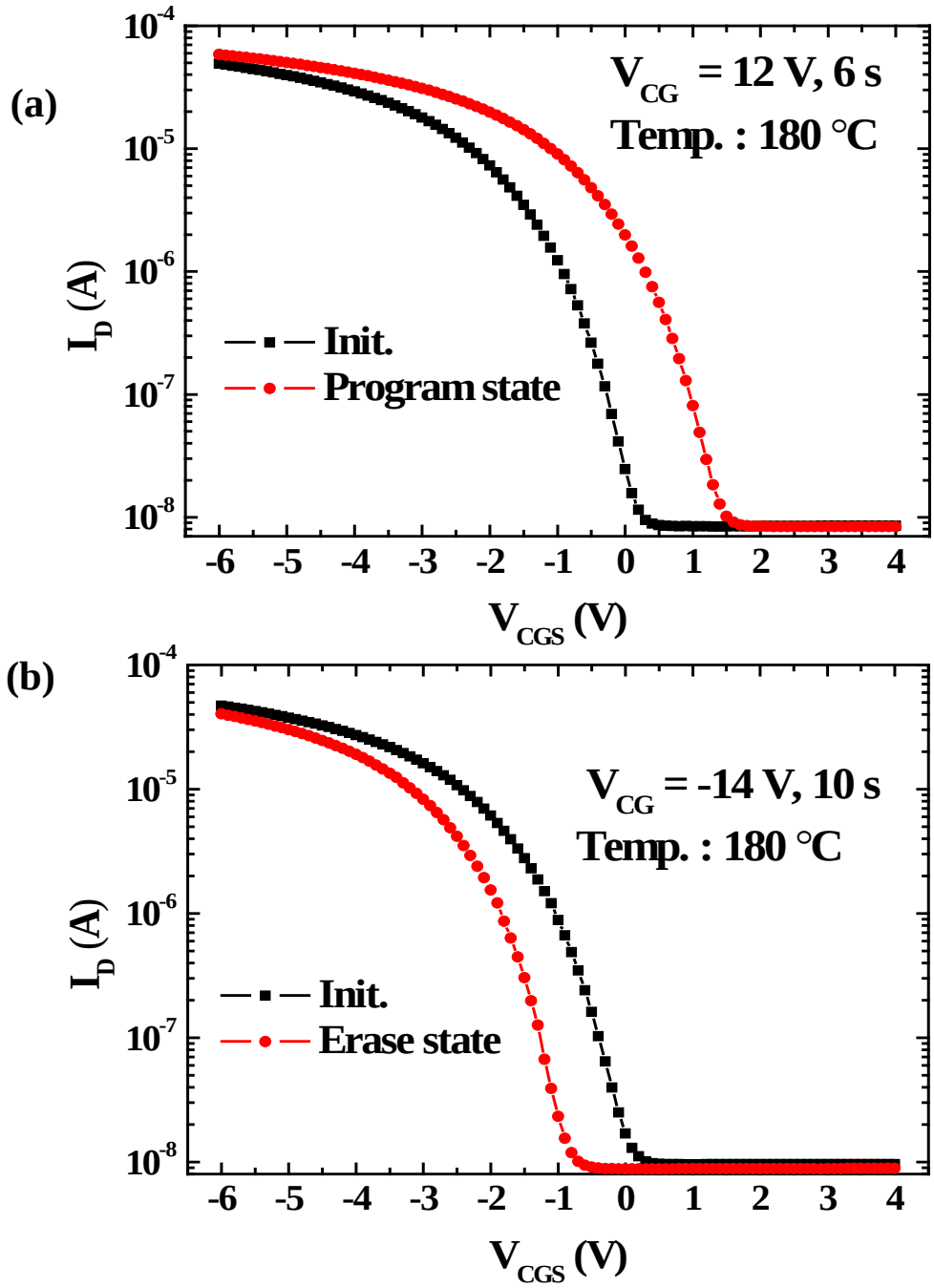

Fig. 3-34. Program and erase characteristics of the fabricated gas senor device at 180 °C

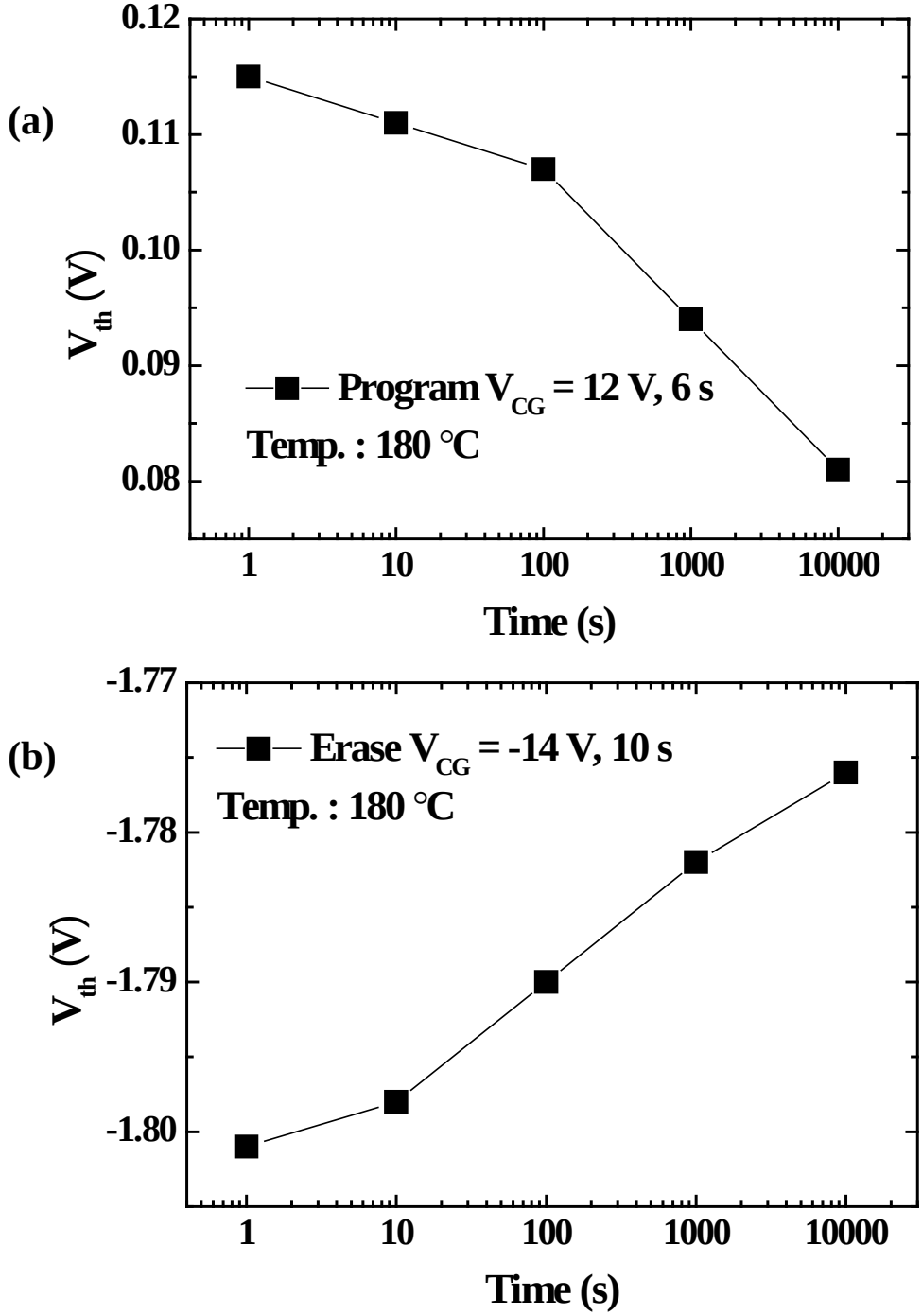

Fig. 3-35. Retention characteristics of the fabricated gas senor device at 180 °C

3.6 Conclusion

We have proposed a new MOSFET gas sensor based on silicon MOSFET and fabricated the gas sensor based on pMOSFET. Since the control-gate is formed in the sides of floating-gate, various kinds of sensing material can be used in this basic sensing structure. In this work, SnO_x, ZnO and CNT sensing layer were adopted to sense a NO_2. In our experiment, drain current increase with increasing NO_2 concentration because of increasing work-function at the sensing layers. However, the I_D decreases with the increase in H_2S due to decrease in WF of the sensing layer at SnO_x and ZnO. We also investigate gas selectivity. The fabricated gas sensor have high sensitivity for NO_2 at the sensing layers. The gas sensor which use SnO_x and ZnO as a sensing layer can also detect H_2S. We also investigate the Langmuir relationship between the target gases and threshold voltage change and response characteristics of the gas sensor. Measured response and recovery times of the gas sensor when exposed to air and 50 ppm NO_2 alternatively, are 50 s and 300 s at SnOx, respectively. We show that the gas sensor can adjusts drain current level of the device by control gate bias and obtain high yield for gas sensor. It means that the proposed gas sensor is low cost gas sensor by using the sensor calibration. These results confirm that proposed gas sensor can be useful and a key component in an electronic nose system.

Chapter 4

AlGaN/GaN MISFET Gas Sensor Having a Horizontal Floating Gate

4.1 Introduction

Recently, there has been a growing interest in gas sensors which operate at high temperature (T > 300 °C) to detect exhaust gases from automobile. A promising FET type gas sensor based on Si MOSFET having a lateral floating gate (FG) has been proposed to achieve high reliability, and small size. The gas sensor uses a metal oxide sensing layer which has a wide range of working temperature [36]. However, Si MOSFET type gas sensor has a maximum working temperature of 250 °C because the junction leakage in Si MOSFET degrades sensing property at a temperature higher than 250 °C [37]. Thus, it becomes increasingly important to develop a FET type gas sensor to work at a high temperature [38]. In this work, we propose an AlGaN/GaN MISFET (Metal Insulator Semiconductor Field Effect Transistor) gas sensor having a horizontal FG and show gas sensing characteristics of the device by using SnO_x and NO_2 as a sensing layer and a target gas, respectively.

4.2 Device structure and fabrication

Fig. 4-1 (a) and (b) show the top and 2D cross sectional views of the fabricated gas sensor, respectively. The device reads out work-function (WF) change in the sensing layer butted to the control gate (CG), when the device is exposed to a target gas.

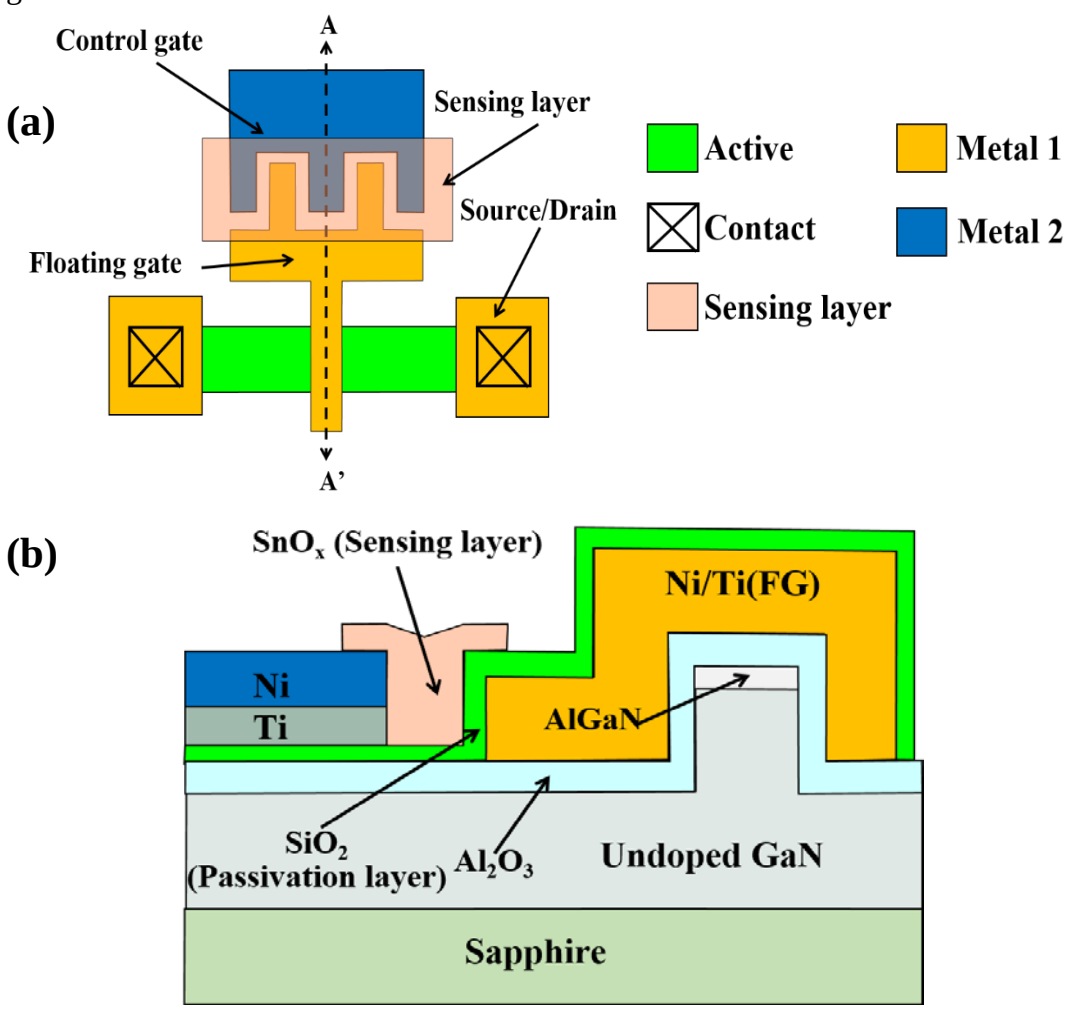

Fig. 4-1. (a) Top and (b) 2D cross sectional views of the fabricated gas sensor cut along A–A'.

Key fabrication process steps of the device are shown in Fig 4-2 and explained as follows. An AlGaN/GaN hetero-structure is grown by metal organic chemical vapor deposition (MOCVD) on a sapphire wafer. After photolithography process for active patterns, the layers are etched. Then, a 30 nm thick Al2O3 layer is deposited by atomic layer deposition (ALD) to form a gate insulator. The layer is etched by wet etch process after photolithography process for contact pattern. Then, a titanium (Ti) and nickel (Ni) are patterned by lift-off process to form a source, drain and FG. A 50 nm thick SiO2 layer is deposited by plasma enhancement chemical vapor deposition (PECVD) to be used for a passivation layer. Then, the CG (Ni/Ti) and sensing layer (n-type SnO_x) are formed by e-beam evaporation and sputtering processes, respectively. They are patterned by lift-off process. Thicknesses of SnO_x, Ni and Ti to be used for the CG and FG are 100 nm, 70 nm and 30 nm, respectively.

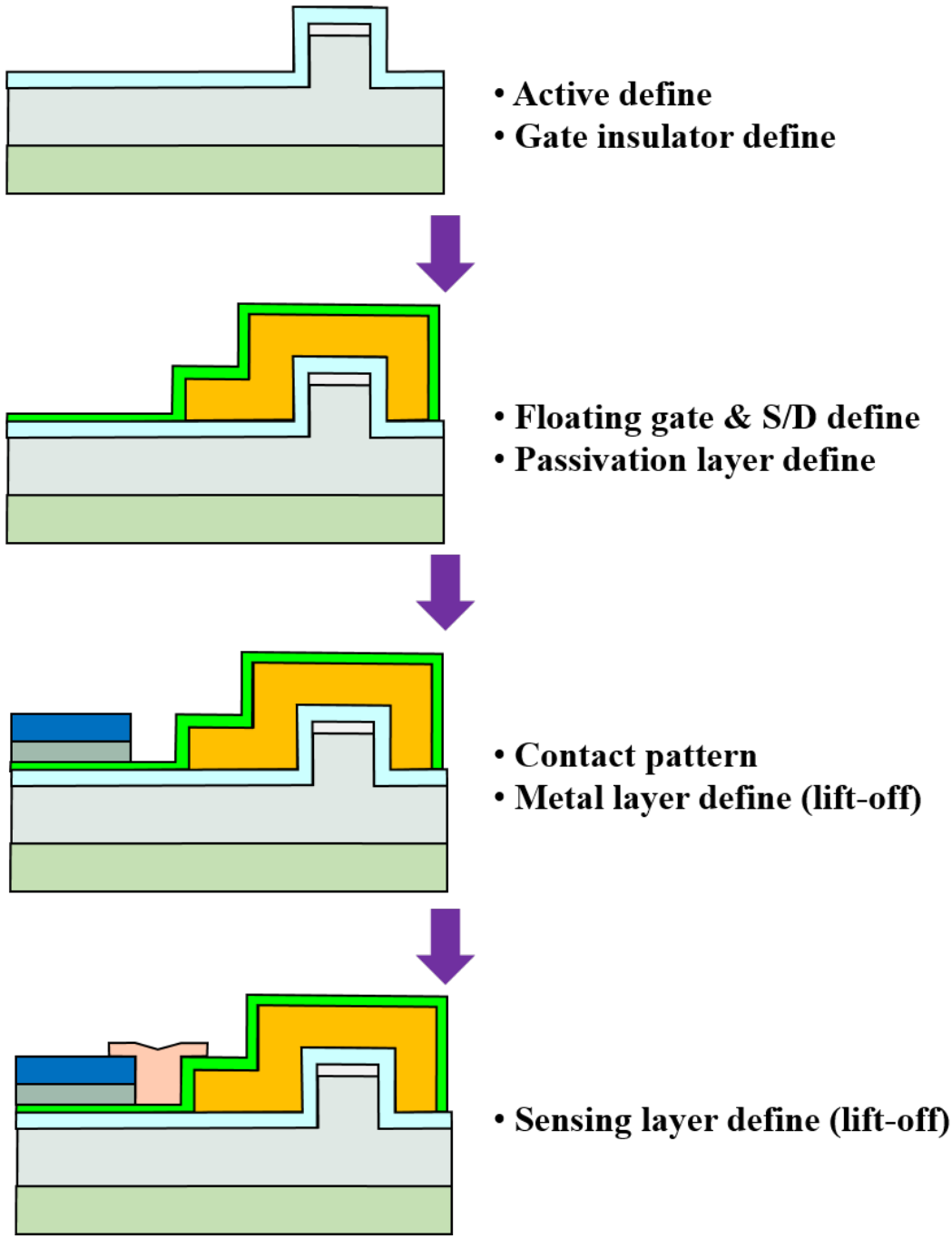

Fig. 4-2. Process flow of the fabricated gas sensor based on AlGaN/GaN substrate

4.3 Electrical and gas sensing characteristics

Fig. 4-3 shows I_D-V_{GS} curve of the fabricated gas sensor based on n-type MISFET at 25 °C. Both of the channel length and width of the device are 5 μm, respectively. The gas sensor reads out WF change in the sensing layer butted to the CG, when the device is exposed to a target gas. The SnO_x in our work is a semiconductor.

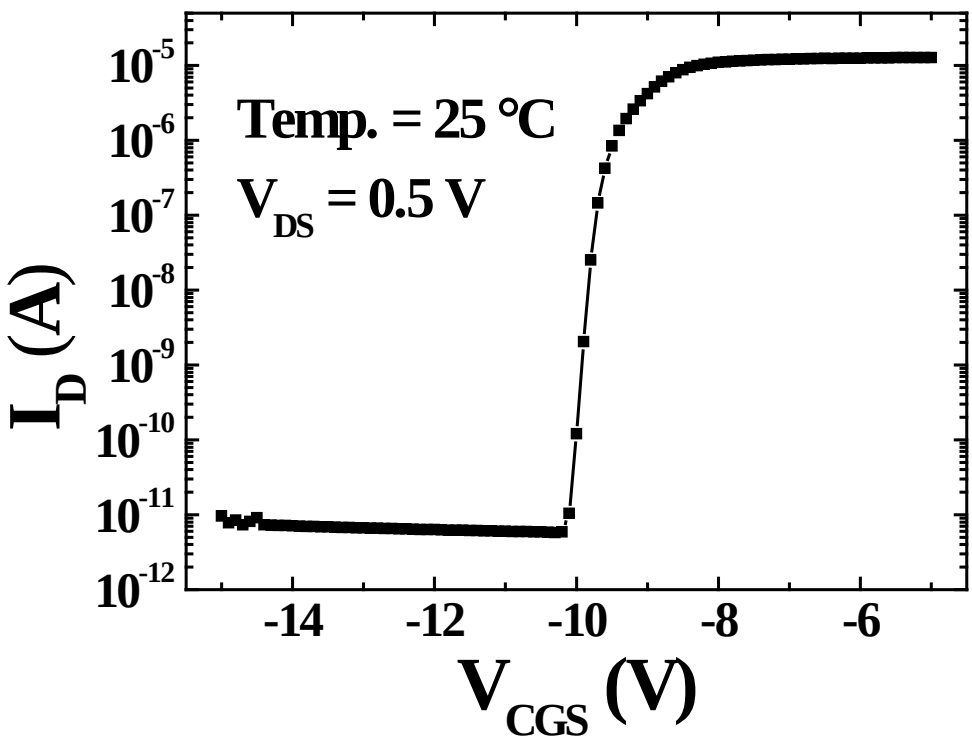

Fig.4-3. Transfer (I_D-V_{CGS}) curve of the fabricated gas sensor based on n-type MISFET at 25 °C.

Fig. 4-4 (a) shows I_D-V_{CGS} curve for the fabricated gas sensor exposed to N_2 and NO_2 at 300 °C. An I_D of the gas sensor decreases when the device is exposed to NO_2. Transient characteristic of the device is measured by changing chamber ambient (N_2 and 50 ppm NO_2) alternately at 300 °C as shown in Fig. 4-4 (b). Response and recovery times of the device are about 35 s and 60 s at V_{GS} = -13.5 V, V_{DS} = 0.5 V, respectively. In this work, the NO_2 is an acceptor type gas on the SnO_x [12]. When the gas sensor is exposed to NO_2 gases, the gases diffusing through the SnO_x extract electrons from the SnO_x and become negatively charged ions at surface of SnO_x. It creates a positive space charge (depletion) region in the SnO_x. The region increases WF of the SnO_x. The increased WF shifts threshold voltage of the gas sensor into the positive bias direction and decreases sensing current [11].

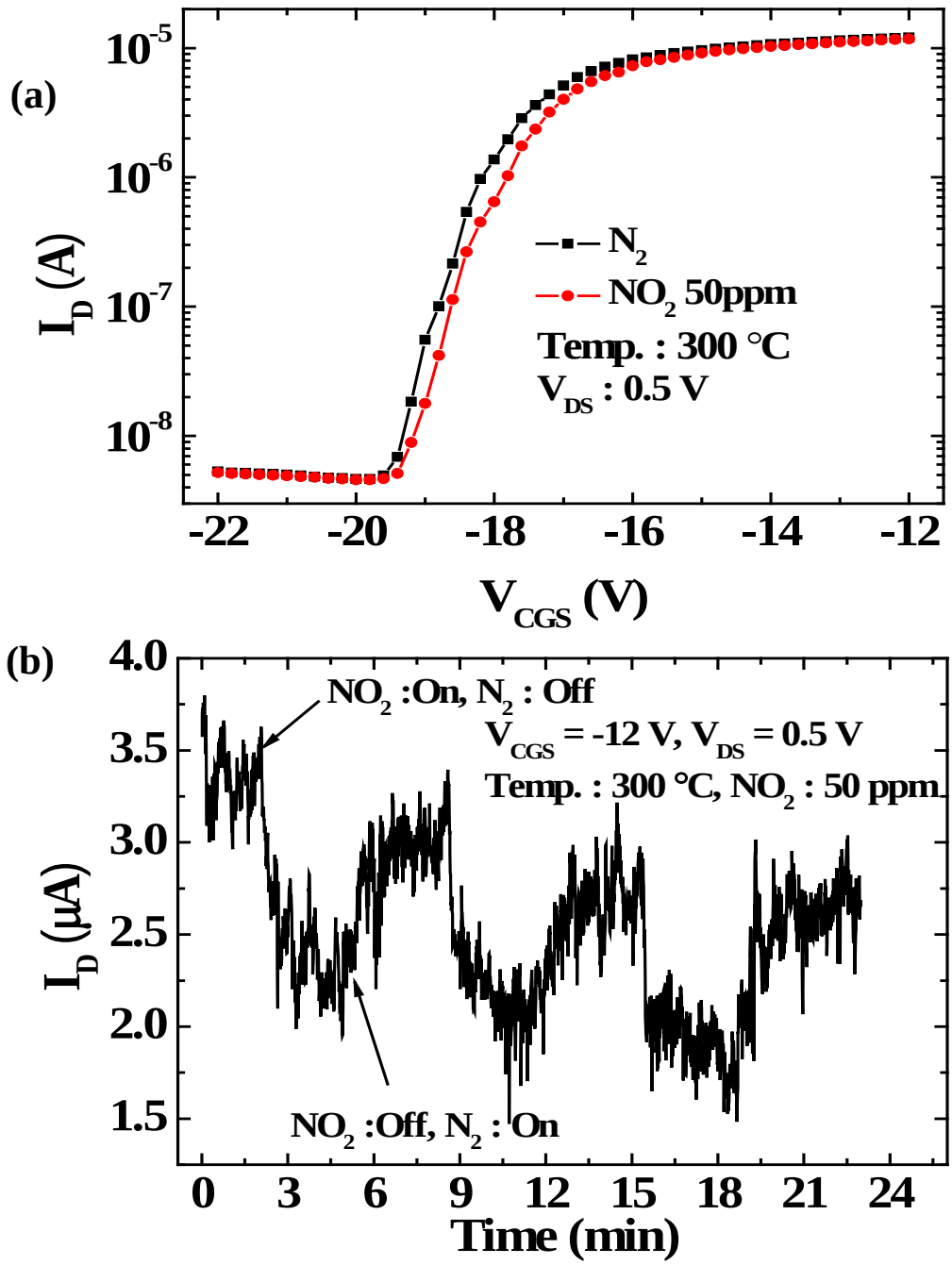

Fig.4-4. (a) transfer and (b) transient curves for the fabricated gas sensor exposed to N_2 and 50 ppm NO_2

4.4 Conclusion

We have proposed an AlGaN/GaN MISFET gas sensor having a horizontal floating gate which is able to work at high temperature. In this work, a SnO_x sensing layer was adopted to sense NO_2. The threshold voltage move to positive bias direction and sensing current (drain current) of the gas sensor exposed to NO_2 decreases due to increasing WF of the sensing layer. We also response characteristics of the fabricated gas sensor. Measured response and recovery times of the gas sensor when exposed to N_2 and 50 ppm NO_2 alternately, are about 35 s and 60 s, respectively.

Conclusion

In this dissertation, we propose a new MOSFET type gas sensor having a horizontal floating-gate (FG). The structure and fabrication process of the device is introduced. We also investigate gas sensitivity, selectivity and response characteristics of the proposed gas sensor by using SnO_x, ZnO and CNT as a sensing layer and control gate of the proposed MOSFET gas sensor. The work-function (WF) of the sensing layer is changed when the layer is exposed to target gas. The changed WF determine drain current level. Next, we investigate gas sensing characteristics by measuring transfer and transient curves of the gas sensor. In our experiment, drain current increase with increasing NO_2 concentration because of increasing work-function at all of the sensing layers. However, the I_D decreases with the increase in H_2S due to decrease in WF of the sensing layer at SnO_x and ZnO. The high sensitivity for NO_2 is shown in the fabricated gas sensor. The gas sensor adopted to SnO_x and ZnO can detect H_2S. Measured response and recovery times of the gas sensor (@ SnO_x) are 50 s and 300 at NO_2. In case of H_2S, the times are 75 s and 400 s. The proposed gas sensor guarantee high yield by device calibration function based on program erase operation. Finally, we have proposed an AlGaN/GaN MISFET gas sensor to work at high temperature. We also evaluate performance of the fabricated gas sensor based on GaN. It means that the proposed gas sensor platform can be applied to various FET devices.

Bibliography

[1] *PERES - Smart way to protect you from food.* [Online]. Available: http://www.myfoodsniffer.com

[2] Korotcenkov and Ghenadii, *Handbook of Gas Sensor Materials*. New York: Springer. Presss, 2013.

[3] Electrochemical type gas sensor. [Online]. Available: http://archive.sensorsmag.com/articles/0102/34/main.shtml

[4] Electrical type gas sensor. [Online]. Available: http://www.figaro.co.jp/en/technicalinfo/principle/mos-type.html

[5] Pengcheng Xu, Xinxin Li, Haitao Yu and Tiegang Xu, “Advanced Nanoporous Materials for Micro-Gravimetric Sensing to Trace-Level Bio/Chemical Molecules”, *Sensors*, vol. 14, no. 10, pp. 19023-19056, Oct. 2014.

[6] Magnetic type gas sensor. [Online]. Available: http://www.illinoisth.com/_m/index.php

[7] Jane Hodgkinson and Ralph P Tatam, “Optical gas sensing: a review”, *Measurement Science and Technology*, vol. 24, no. 1, pp. 1-59, Nov. 2012.

[8] Thermometric type gas sensor. [Online]. Available: http://www.e2v.com/products-and-services/instrumentation-solutions/gas-sensors/our-gas-sensor-technology/pellistors-catalytic-bead/

[9] *Sensor Technology – Gas Sensors*: Siemens Global Website, 2004 [Online]. Available:http://www.siemens.com/innovation/en/publikationen/publications_pof/pof_fall_2004/sensors_articles/gas_sensors.htm.

[10] K.I. Lundström, M.S. Shivaraman and C.M. Svenson, "A hydrogen- sensitive Pd-gate MOS transistor", *J. Appl. Phys. Lett.*, vol. 46, no. 9, pp. 3876-3881, Sep. 1975.

[11] Alexandru Oprea, Nicolae Bârsan and Udo Weimar, "Work function changes in gas sensitive materials: Fundamentals and applications", *Sensors and Actuators B*, vol. 142, no. 2, pp. 470-493, Nov. 2009

[12] I. Eisele, T. Doll and M. Burgmair, "Low Power Gas Detection with FET sensors", *Sensors and Actuators B*, vol. 78, no. 1, pp. 19-25, Aug. 2001.

[13] A.lexandru Oprea, Heinz-Peter Frerichs, Christoph Wilbertz, Mirko Lehmann and Udo Weimar, "Hybrid gas sensor platform based on capacitive coupled field effect transistors: Ammonia and nitrogen dioxide detection", *Sensors and Actuators B*, vol. 127, no. 2, pp. 161-167, Aug. 2007.

[14] G. Halek, I.D. Baikie, H. Teterycz, P. Halek, P. Suchorska and K. Wiśniewski, "Work Function Analysis of Gas Sensitive WO_3 Layers with Pt Doping", *IMCS 2012 - The 14th International Meeting on Chemical Sensors*, pp. 331- 334, 2012.

[15] I.D. Baikie, S. MacKenzie, P.J.Z. Estrup and J.A.Meyer, "Noise and the Kelvin method", *Review of Scientific Instruments* vol. 62, pp. 1326-1332. 1991.

[16] Scanning Kelvin probe system (Model: SKP 5050) [Online]. Available:

www.kptechnology.com

[17] United State Environmental Protection Agency (EPA). [Online]. Available: http://www.epa.gov 2010.

[18] Chang-Hee Kim, In-Tak Cho, Jong-Min Shin, Kyu-Bong Choi, Jung-Kyu Lee and Jong-Ho Lee, "A New Gas Sensor Based on MOSFET Having a Horizontal Floating-Gate", *IEEE Electron Device Letters*, vol. 35, no. 2, pp.265-267, Feb. 2014.

[19] Kenneth K., Namkyu Park, and Dong-Jun Yang. "1/f noise of NMOS and PMOS transistors and their implications to design of voltage controlled oscillators", *Radio Frequency Integrated Circuits (RFIC) Symposium*, 2002, pp. 59-62.

[20] R. Pohlea, O. von Sicarda, M. Fleischera, H.-P. Frerichsb, Ch. Wilbertzb and I. Freundb, "Gate pulsed readout of floating gate FET gas sensors", *Procedia Engineering*, vol. 5, no. 1, 2010, pp. 13-16, Sep. 2010.

[21] M. C. Horrillo, P. Serrini, J. Santos, and L. Manes, "Influence of the Deposition Conditions of SnO_2 Thin Films by Reactive Sputtering on the Sensitivity to Urban Pollutants", *Sensors and Actuators B*, vol. 45, no. 3 pp. 193–198, Dec. 1997.

[22] Y. Taur and T. H. Ning, *fundamentals of Modern VLSI Devices*. New York: Cambridge Univ. Presss, 1998.

[23] Susheel Sharma, SS Rajput and SS Jamuar, "Floating-gate MOS Structures

and Applications", *IETE Technical Review*, vol. 25, no. 1, pp. 338-345, Feb. 2009.

[24] Shih-Chia Chang, "Thin-film semiconductor NO_x sensor", *IEEE Transactions on Electron Devices*, vol. 26, no. 12, pp. 1875-1880, Dec. 1979.

[25] Rafael Rios, Narain D. Arora, and Cheng-Liang Huang, "An analytic polysilicon depletion effect model for MOSFETs", *IEEE Electron Device Lett*, vol. 15, no. 4, pp. 129-131, Apr. 1994.

[26] V.V. Malyshev and A.V. Pislyakov, "SnO_2-based thick-film-resistive sensor for H_2S detection in the concentration range of 1–10 mg m^{-3}", *Sensors and Actuators B*, vol. 47, no. 3 pp. 181-188, Apr. 1998.

[27] PUZZOVIO Delia, "Surface interaction mechanisms in metal-oxide semiconductors for alkane detection", PhD Thesis. Università degli studi di Ferrara, 2009.

[28] Yasuhiro Morita, Ken-ichi Nakamura and Chol Kim, "Langmuir analysis on hydrogen gas response of palladium-gate FET", *Sensors and Actuators B*, vol. 1, no. 33 pp. 96–99, July 1996.

[29] Toshihiro Yoshida, Naoyuki Ogawa, and Tomonori Takahashi, "Influence of NO and NO_2 Composition on Resistivity Changes of SnO_2", *Journal of The Electrochemical Society*, vol.146, no. 3, pp. 1106 - 1110, 1999

[30] Abu Z. Sadek, Supab Choopun, Wojtek Wlodarski, Samuel J. Ippolito and Kourosh Kalantar-zadeh, "Characterization of ZnO Nanobelt-Based Gas Sensor

forH$_2$,NO$_2$and Hydrocarbon Sensing", *IEEE SENSORS JOURNAL*, vol. 7, no. 6, pp.919-924, June 2007.

[31] Niranjan S. Ramgir, Preetam K. Sharma, N. Datta, M. Kaur, A.K. Debnath, D.K. Aswal and S.K. Gupta, "Room temperature H_2S sensor based on Au modified ZnO nanowires", *Sensors and Actuators B*, vol. 186, no. 3, pp. 718-726, Sep. 2013.

[32] Muhammad Qazi, and Goutam Koley, "NO_2 Detection Using Micro-cantilever Based Potentiometry", *Sensors*, vol. 8, no. 11, pp. 7144-71566, July 2008.

[33] R. Shirota, and H. Watanabe, "Analysis of the Scaling Effect on NAND Flash Memory Cell Operation", *ECS Transactions*, vol. 50, no. 34, pp.27-35, 2013.

[34] Roberto Bez, Emilio Camerlenghi, Alberto Modelli and Angelo Visconti, "Introduction to flash memory", *Proceedings of the IEEE*, vol. 91, no. 4, APR. 2003.

[35] Hon-Sum Wong, Marvin H. White, Thomas J. Krutsick and Richard V. Booth, "Modeling of transconductance degradation and extraction of threshold voltage in thin oxide MOSFET's", *Solid-State Electronics*, vol. 30, no. 9, pp. 953-968, Sep. 1987.

[36] G. Eranna, B. C. Joshi, D. P. Runthala, and R. P. Gupta, "Oxide Materials for Development of Integrated Gas Sensors—A Comprehensive Review", *Critical Reviews in Solid State and Materials Sciences*, vol. 29, no. 3, pp. 111-188, Aug.

2004.

[37] Ingemar Lundström, Thomas Ederth, Hans Kariis, Hans Sundgren, Anita Spetz, Fredrik and Winquist, “Recent developments in field-effect gas sensors”, *Sensors and Actuators B*, vol. 23, no. 2, pp. 127-133, Feb. 1995.

[38] D. Donoval, M. Florovič, J. Kováč, and P. Kordoš, “High temperature performance of AlGaN/GaN HFETs and MOSHFETs”, *Microelectronics Reliability*, vol. 48, no. 10, pp. 1669-1672, Oct. 2008.

초 록

오늘날 다양한 산업에서 사용하고 있는 많은 종류의 가스들이 존재한다. 하지만 산업 과정에서 호흡기관련 질병을 발생시키는 해로운 가스들이 발생한다. 그러므로 이런 유해한 가스들을 검출할 수 있는 가스센서의 수요가 증가할 것으로 예상된다. 특히, 스마트 기기에 적용 가능한 휴대용, 저가격형, 고신뢰성, 저전력형 가스센서의 관심이 크게 증가하고 있다. 현재까지 많은 연구자들에 의해서 다양한 종류의 가스센서들이 개발되어 왔다. 대표적인 예로 전기화학식 (electrochemical), 전기식 (electrical), 질량 감지식 (mass sensitive), 자기식 (magnetic), 광학식 (optical) 및 열전식 (thermometric) 가스센서들이 있다. 이 가스센서들 중에서 전계 효과 트랜지스터 (FET: Field Effect Transistor) 가스센서가 스마트 기기에 적용 가능한 가장 진보된 가스센서로 간주되었다. 하지만 기존의 FET형 가스센서는 많은 단점들을 가지고 있다.

본 논문에서는 앞에서 언급한 기존의 FET형 가스센서에서 나타나는 문제점들을 개선하기 위해 수평형 플로팅 게이트 (floating gate) 를 갖는 FET 가스센서 플랫폼을 제안한다. 먼저 제안된 소자의 구조 및 공정 과정을 소개한다. 제안된 소자는 금속 산화막 반도체 전계 효과 트랜지스터 (MOSFET: Metal Oxide Semiconductor Field Effect Transistor) 구조를 기반으로 수평형 플로팅 게이트를 가지며, 가스 감지층을 컨트롤 게이트와 플로팅 게이트의 표면에 형성되어 있는 보호 절연막 사이에 형성되어 있다. 제안된 가스센서는 가스 반응시 가스센서에 형성된 감지물질의 일함수(work function) 변화를 이용한다. 본 연구에서 가스 감지물질은 반도체 (Semiconductor) 혹은 반금속 (semi

metal)를 사용하였다. 제작된 가스센서에 여러 가스 감지 물질 및 다양한 가스들을 이용하여 가스센서의 가스감지 특성을 분석하였다. 이를 위해 감지 센서의 감지 가스에 대한 트랜스퍼 (transfer) 및 트랜지언트 (transient) 특성을 측정하고, 측정 데이터로부터 가스센서의 동작 원리를 설명하였고, 또한 가스 민감도 (sensitivity), 선택성 (selectivity), 반응 (response), 원복(recovery) 특성 및 Langmuir relationship을 각각 보인다. 또한, 가스센서에 여러 감지물질들을 적용하기 위해나 공정 방법을 소개하였다. 이번 연구에서는 주석산화물 (Tin Oxide), 아연산화물 (Zinc Oxide) 및 탄소나노섬유 (Carbon Nanotube)들을 스퍼터링 (sputtering) 방식, 원자층 증착 방식 (ALD: Atomic Layer Deposition) 및 잉크젯 프린팅 (Ink-jet printing) 방식 등을 이용하여 감지물질들을 형성한 가스센서들을 보인다. 그 다음 가스센서의 컨트롤 게이트에 전압을 인가하여 센서 보정하는 방법을 보인다. 마지막으로 제안된 수평형 플로팅 게이트 기반의 FET 가스센서를 고온에서 동작하기 (Temp. > 300 °C) 위해 넓은 밴드갭 (band gap)을 갖는 GaN 기판을 이용하여 가스센서를 제작하였고, 가스 반응 특성을 분석하였다.

제안된 가스센서 플랫폼은 다양한 FET형 소자 (TFT: Thin Film Transistor, TFET: Tunneling Field Effect Transistor)에 적용할 수 있고, 또한 제안된 가스센서 플랫폼은 전자코 시스템에 유용하게 사용될 수 있다.

주요어: 가스 센서, 전계 효과 트랜지스터, 수평형, 플로팅 게이트, 플랫폼, 일함수, 감지물질, 감지 특성, 센서 보정

학번: 2012-30932